MECHANISMS FOR ENABLING CLOSED-LOOP UPPER LIMB SENSORIMOTOR PROSTHETIC CONTROL

BY

AADEEL AKHTAR

DISSERTATION

Submitted in partial fulfillment of the requirements
for the degree of Doctor of Philosophy in Neuroscience
in the Graduate College of the
University of Illinois at Urbana-Champaign, 2016

Urbana, Illinois

Doctoral Committee:

Associate Professor Timothy Bretl, Chair
Associate Professor Levi Hargrove, Northwestern University
Professor Elizabeth T. Hsiao-Wecksler
Professor Mark Nelson

ABSTRACT

Myoelectric upper limb prostheses are limited in their ability to provide sensory feedback to a user. The lack of sensory feedback forces prosthesis users to rely on visual feedback alone in manipulating objects, and often leads to abandonment of the prosthesis in favor of the user's unimpaired arm. Consequently, there is a critical need to develop mechanisms that enable people with upper limb amputations to be able to receive sensory feedback from the environment.

The goal of this dissertation is to describe the development and evaluation of various mechanisms that enable simultaneous myoelectric control of hand prostheses with proprioceptive and touch/pressure feedback. Sensory feedback is enabled through the use of a passive skin stretch mechanism for proprioception (Chapter 2), an epidermal electronic device that can provide electrotactile stimulation (Chapter 3), and a custom-built prosthetic hand that relays contact and pressure information from the fingertips (Chapter 4). In each of these chapters, motor control is simultaneously enabled through the use of electromyographic sensors. The remainder of the dissertation focuses on a method of enabling long-term wear of electrotactile stimulation electrodes by modeling (Chapter 5) and controlling (Chapter 6) sensation intensity in response to changes in the impedance of the electrode-skin interface. The techniques described in this dissertation have the potential to improve prosthesis embodiment for a person with an upper limb amputation, with the ultimate goal of reducing prosthesis abandonment and improving quality of life.

To my wife Whitney, my son Zain, and my parents.

ACKNOWLEDGMENTS

In the name of God, the most beneficial, the most merciful.

I'd first like to thank my wife Whitney and my family for getting me to this point. Whitney, thank you for keeping me sane throughout the many years we've been together. None of this would have been possible without your love and support.

To my dissertation committee, thank you for the wonderful guidance you have provided me with over the years. Prof. Bretl, thank you for allowing me to explore my own path and helping me to flourish in ways I would never have dreamed of before entering the program here. Prof. Hargrove, thank you for taking a chance on me in collaborating with the Center for Bionic Medicine with my research. Prof. Hsiao-Wecksler, thank you for letting me continuously borrow your equipment and for the many discussions we've had regarding my research. Prof. Nelson, thank you for providing a neuroscientific-focused lens as I approached my research from my qualifying exam to my final defense.

Sam Beshers, thank you for taking a chance on me in allowing me to join the NSP when things were looking grim.

I would also like to thank Prof. John Rogers for also taking the time to collaborate with our group on our research. Hong Yeo, Baoxing Xu, and Howard Liu, it has been a great pleasure working with you all and thank you for teaching me how to increase the impact of my work.

Prof. Cliff Shin, thank you for providing your funding and design input to the projects in our group. Our group has benefited greatly in our collaboration with you.

Dave Rotter, what can I say—you are the world's greatest prosthetist. I can't thank you enough for your generosity and willingness to push the boundaries of what's possible with upper limb prostheses. I look forward to continuing to work with you in the near future.

To my ROMP family: David Krupa, I can't wait for my next visit to Ecuador so

you, Pat Mathay and Diana Svea can all check out our latest prosthesis advancements.

To Juan Suquillo and Garrett Anderson—this work would not be possible without the sacrifices you both made for your countries. Thank you for your service and for your many hours dedicated to helping us make the next best prostheses.

To the Ph.D. graduates from the Bretl Research Group that came before me: Aaron Becker, Abdullah Akce, Miles Johnson, Dennis Matthews, and Navid Aghasadeghi. You all have shown me the way. Jamie Norton and Matt Petrucci, it's hard to believe we've come this far after that fated NSP interview day 6 years ago. Jamie, you're up next! Joe DeGol, thank you for the many conversations and venting sessions in the office. Andy Borum, thank you for helping me edit this dissertation and for your sharp humor. Dave Hanley and Xinke Deng, be persistent—your hard work will eventually pay off.

To my prosthetics crew, without whom this work would not have been possible. To those there from the start: Mary Nguyen, Brandon Boyce, Logan Wan, Pat Slade, Michael Fatina, Edward Wu, Sam Goldfinger, and Joseph Sombeck—I can't believe the amount of progress we had made in just the last three years in all the iterations we've made on the hand, the electronics, and the sensory feedback. Mary, thank you for the energy you brought. Pat, thank you for transforming the way our group approaches research—you started a brand new culture of building our own robots in the lab. That is no small feat. Michael and Ed, it has been great to see your ECE skills increase exponentially over the years. I have been able to learn so much from you two. Brandon and Joe, I am so deeply, deeply indebted to all the work you two had put into electrotactile feedback. Brandon, you helped me start this entire line of work from scratch with no guidance at all. Joe, your dedication has allowed us to take the technology to the next level—actually implementing it in our prosthetic hands. I cannot overstate the importance you guys have had to furthering the state-of-the-art in this research. Also, thank you Joe for your help in editing and revising my dissertation.

To Kyung Yun Choi and Jesse Cornman, working with you two has been one of the most fun and rewarding experiences of my life. The amount I have learned mechanically and electrically from you two is astonishing. I can't wait to continue to push the boundaries of prosthetics with you guys.

Hafsa Siddiqui, out of all the family I've tried to get to work in the lab, I last expected the graphic designer to be the one to stick. Your talent for drawing, design, and photography is incredible. I am so glad that I had the chance to work

with you over the last two years.

Finally, I'd like to thank my funding sources over the years, including the NSF IGERT in Neuroengineering (0903622), NSF CAREER-0955088, NIH NRSA-F30HD084201, the Burroughs Wellcome Fund Collaborative Research Training Grant, ISUR, ECE independent study, VentureWell, and the Technology Entrepreneurship Center.

TABLE OF CONTENTS

CHAPTER 1

INTRODUCTION

State-of-the-art upper limb prostheses are limited in their ability to provide sensory feedback to a user. The lack of sensory feedback forces prosthesis users to rely on visual feedback alone in manipulating objects, and often leads to abandonment of the prosthesis in favor of the user's unimpaired arm [1,2]. The loss of arm functionality severely limits a person's ability to do daily tasks, and it is projected that the number of persons in the US with upper limb loss will double by the year 2050 [3]. Therefore, there is a critical need to develop mechanisms that enable people with upper limb amputations to be able to receive sensory feedback from their environment while operating their prosthesis [1,2].

In order to enable closed-loop sensorimotor prosthetic control, we describe in this dissertation the development and evaluation of sensory feedback mechanisms and devices that provide proprioception and touch/force feedback to users of myoelectric prostheses. We then focus on a particular mechanism of sensory feedback, electrotactile stimulation, and detail a method for enabling long-term use of this type of stimulation when performing activities of daily living.

1.1 Enabling proprioception with myoelectric control of a prosthesis

The loss of proprioception, the body's internal representation of joint kinematics and dynamics, is one of the key causes of prosthesis abandonment in people with upper limb amputations [2]. Prosthesis users have to rely almost exclusively on visual feedback in order to know the position and orientation of the joints in their prosthesis, which quickly becomes cumbersome, leading them to favor their intact arm in the case of unilateral amputation. In Chapter 2, we describe the development and evaluation of a method of passive linear skin stretch that proportionally relays prosthesis joint angle and velocity information to the user. In Chapter 3, we

provide proprioception through the use of electrotactile stimulation electrodes. In each case, we evaluate the usefulness of the feedback in various myoelectric control tasks and show that the incorporation of our mechanisms for proprioception in myoelectric control tasks help reduce errors in targeting specific joint angles.

1.2 Enabling touch/force feedback with myoelectric control of a prosthesis

In addition to proprioception, the ability to detect contact and forces on the prosthesis was important to users of prostheses [2]. In Chapter 3, we describe the design of a device that can simultaneously record electromyography (EMG) for myoelectric control and provide electrotactile stimulation for touch/force feedback from a prosthesis. We demonstrate the utility of the device in using EMG to control the grip aperture of a robot arm to grasp a bottle of water without crushing it. In Chapter 4 we describe the development of a hand with custom pressure sensors that relays touch/force information to a subject with a transradial amputation via electrotactile stimulation. With the stimulation feedback, he is able to grasp egg shells and fragile cups of water without crushing them.

1.3 Enabling long-term wear of stimulation electrodes for sensory feedback

When a person wearing electrotactile stimulation electrodes sweats or if the electrodes begin to lose contact, the sensation the person feels changes due to changes in the electrode-skin interface impedeance. Consequently, there is a critical need to be able to modulate stimulation parameters so that sensation intensity can be controlled when the impedance of the electrode-skin interface changes. In Chapter 5, we present a model for electrotactile stimulation that describes the relationship between peak pulse energy, phase charge, and impedance—specifically, that at a constant perceived sensation intensity, there is a linear relationship between the peak energy of the pulse and the impedance of the electrode-skin interface, as well as the phase charge of the pulse and the impedance. By imposing these relationships when impedance changes by modulating current amplitude and pulse duration, we can keep sensation intensity constant. We implement and evaluate a

controller based on this model in Chapter 6, validating our results on ten subjects, including a subject with a transradial amputation performing activities of daily living while wearing the myoelectric prosthesis with sensory feedback described in Chapter 4.

1.4 Overview

Chapters 2-6 address these topics, containing background information, relevant literature review, as well as the methods and results used for evaluating our mechanisms for enabling closed-loop sensorimotor control. Chapter 7 provides a summary of the work presented in this dissertation as well as potential future studies that are now possible as a result of this work.

CHAPTER 2

PASSIVE MECHANICAL SKIN STRETCH FOR MULTIPLE DEGREE-OF-FREEDOM PROPRIOCEPTION IN A HAND PROSTHESIS[1]

In this chapter, we present a passive linear skin stretch device that can provide proprioceptive feedback for multiple degrees of freedom (DOF) in a prosthetic hand. In a 1-DOF virtual targeting task, subjects performed as well with our device as with a vibrotactile array, and significantly better ($p < 0.05$) than having no feedback at all. In a 3-DOF grip recognition task, subjects were able to classify six different grips with 88.0% accuracy. Training took 6 minutes and the average time to classification was 5.2 seconds. Subjects were also able to match a set of target grip apertures with 11.1% error on average.

2.1 Introduction

While major advancements have been made in the functionality of upper limb myoelectric prostheses, commercial devices still lack the ability to provide users with proprioceptive feedback. As a result, users have had to rely primarily on vision to know the position and orientation of their prosthesis. Surveys have reported that this over-dependence on vision is one of the largest contributors to prosthesis abandonment [2]. Various sensory substitution techniques have been used by research groups in order to provide proprioceptive feedback for use with upper limb myoelectric prostheses. Witteveen et al. [5] used a vibrotactile array on the forearm to relay grip aperture to unimpaired subjects controlling a single degree-of-freedom (DOF) virtual hand with a mouse wheel. Wheeler et al. [6] developed a rotational skin stretch device that provided elbow angle feedback to unimpaired subjects controlling a single-DOF virtual arm with electromyography (EMG). While these devices were effective in improving accuracy when controlling a single-DOF virtual prosthesis, most users perform tasks which require

[1] This work includes material published in [4].

controlling multiple DOFs on their prostheses, for example, in selecting between different grips for a specific task [7]. Furthermore, a large amount of surface area is required by both the vibrotactile array and the rotational skin stretch device. In addition, the rotational skin stretch device consumes a great deal of power and adds a considerable amount of weight (see Sec. 2.4.3).

Initial work to relay multiple DOF information was done by Cheng et al. [8], who used vibrotactile patterns presented on a belt around the waist to convey the configuration of a virtual hand performing various grips. While they achieved 79.7% accuracy in grip recognition, these results were marred by a long training time (30 min) and slow average time to classification (29.4 s).

To alleviate power, weight, and space issues, as well as easily provide multiple-DOF proprioceptive feedback for a prosthetic hand, we developed a passive mechanical linear skin stretch device (Fig. 2.1). The device cost less than $2 in raw materials. We compared our skin stretch device to a vibrotactile array and to a case where no feedback was given in a single-DOF virtual finger targeting task with myoelectric control. Extending our experiment to three DOFs, we also assessed how well the user could recognize grips involving different configurations of the thumb, index, and middle fingers.

2.2 Methods

Five unimpaired subjects, four male, one female (ages: 19-27), volunteered for these experiments. The subjects were asked to participate in two experiments, one testing single-DOF proprioception, and the other testing multiple-DOF proprioception. During each experiment, six surface electromyography (EMG) electrodes were placed over the finger flexor and extensor muscle groups located radially around the right forearm, with three electrodes being placed over each muscle group. A 16-channel Delsys Bagnoli system (Delsys, Inc., Natick, MA) was used to record the EMG signals measured across these muscles. All data were collected and processed using the MATLAB DAQ Toolbox (Mathworks, Natick, MA).

2.2.1 Single-DOF Virtual Finger Task

In the first experiment, subjects were asked to move an onscreen virtual finger in a single-DOF task (Fig. 2.2a) based on [6] and [9]. The virtual finger was con-

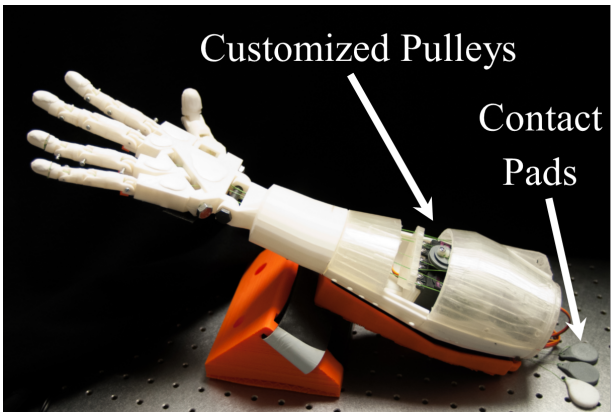

(a)

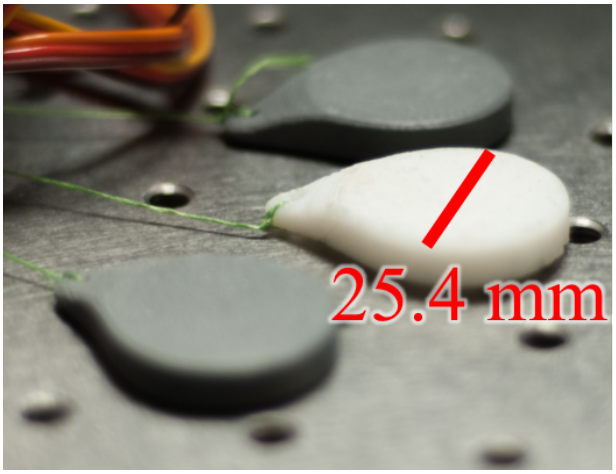

(b)

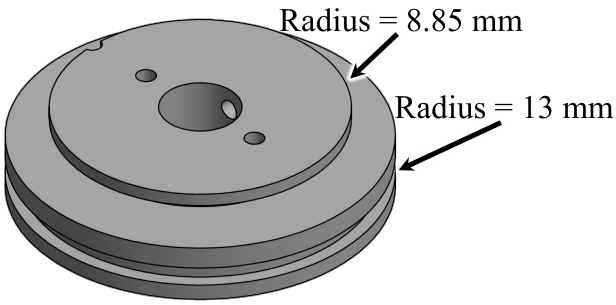

(c)

Figure 2.1: Passive linear skin stretch device attached to prosthesis. The InMoov hand used in our study (a) had custom pulleys pulling both the tendons driving the fingers and the lines to the contact pads (b). A schematic of one of the pulleys is shown in (c). The two different radii of the pulley grooves are for the two tendons used to actuate the fingers and the contact pads adhered to the skin.

strained to move between 0-90°. Meanwhile, the subject's metacarpophalangeal (MCP) joints on the right hand were restrained to 45° in order to remove any of the subject's own proprioceptive cues in controlling the arm. Flexing or extending the MCP joints against the restraint (Fig. 2.2b) would generate EMG signals. Linear discriminant analysis was used to classify these EMG signals to virtual finger movements every 0.1 s, following the procedure outlined in [10]. In order to have subjects rely more on feedback than timing-based open loop control strategies [5], we varied the angular velocity of the MCP joint according to a random walk bounded between 5-20°/s with a random initial velocity unknown to the user. Three feedback conditions were tested during the Virtual Finger Task: vibrotactile feedback, passive linear skin stretch feedback, and no feedback.

Vibrotactile Array

We used a vibrotactile array based on [5] to provide proprioceptive feedback of the angle of the virtual finger. It consisted of eight standard eccentric rotating mass vibration motors (310-103, Precision Microdrives, London, UK) placed longitudinally along the forearm, with each tactor spaced 29 mm apart (Fig. 2.2b). The joint angle range of the virtual finger (θ in Fig. 2.2a) was divided into eight intervals, each successively mapped to one of the vibrotactile motors.

Passive Linear Skin Stretch

To use passive skin stretch to provide proprioceptive feedback, we constructed a prosthetic hand that pulled contact pads adhered to the forearm. The hand was modified from InMoov, an open source 3D-printed robotics project [11]. Five servo motors (MG946R, TowerPro, Taiwan) mounted in the forearm of the prosthesis drove the tendon-actuated fingers. We seated the hand in a rigid plastic interface, which was then attached to a wrist brace. Guide holes at the proximal end of the interface kept the lines to the contact pads as horizontal as possible to maximize shear forces on the skin. For the single-DOF task, we adhered only the white contact pad to the skin (Fig. 2.2c).

We designed custom 3D-printed pulleys and mounted them onto the servos for the thumb, index, and middle fingers. A pulley had one channel to pull a tendon actuating a finger and a second to pull the line to a contact pad on the subject's arm. We set the ratio of the radii of these channels so that the displacement of the

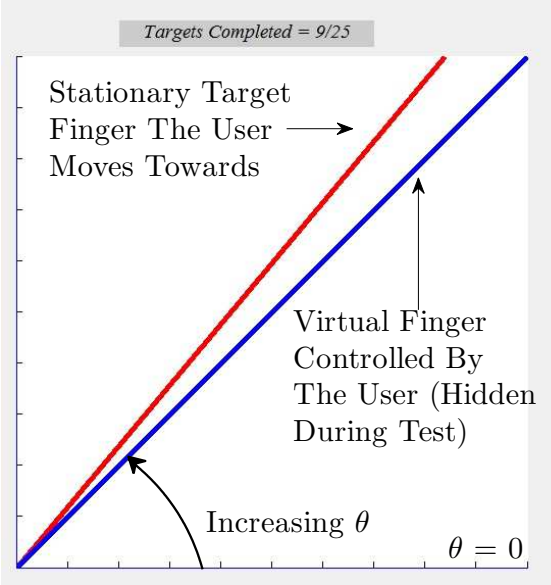

(a)

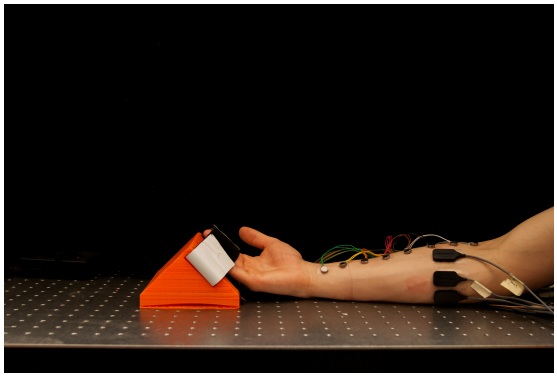

(b)

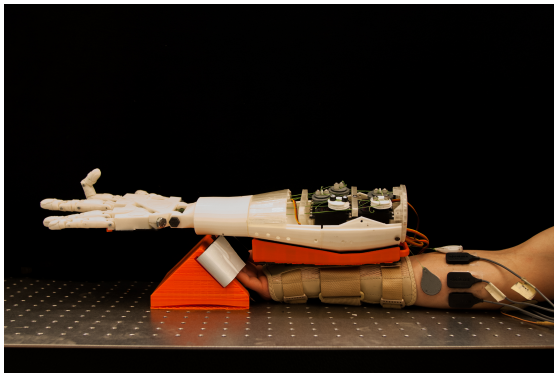

(c)

Figure 2.2: (a) MATLAB GUI used for the single-DOF virtual finger task. (b) Vibrotactile array placement. (c) Passive linear skin stretch setup. A third contact pad was adhered to the skin on the radial side of the forearm. The orange triangular block restrained the subjects' hand in order to remove intrinsic proprioceptive cues.

contact pad was 13 mm with respect to the finger's range of motion (Fig. 2.1c). In addition, we 3D-printed each contact pad to have a circular contact area of 507 mm^2 and a hole to connect to the line from the pulley (Fig. 2.1b). Contact pads were adhered to the skin using BMTT-A adhesives (Garland Beauty Products, Hawthorne, CA) with roughly 1.5 N of initial tension.

Training and Evaluation

A trial consisted of a training and evaluation phase for a particular feedback condition. During training, each subject used EMG to freely control the virtual finger for 60 s. Next, the subject was given five practice target angles from the evaluation phase. They were asked to move the virtual finger, now invisible, until it matched a series of displayed targets (Fig. 2.2a). Once the subject believed he was at the target angle, he would press a button and would be shown the actual angle to which he moved. Following the five practice angles, the subject was evaluated using 20 more targets. The mean absolute error between the target angle and the subject's estimate were recorded.

Subjects participated in two sessions consisting of a trial for each of the three feedback conditions, with each condition presented in a random order for each session. Two sessions were conducted in order to evaluate whether performance improved over time. To help ensure subjects relied only on the feedback method under consideration, they wore headphones playing pink noise throughout the experiment. Additionally, when evaluating linear skin stretch, the prosthesis and contact pads were occluded from view.

2.2.2 Multiple-DOF Tasks

To extend the single-DOF skin stretch feedback to multiple-DOFs, we introduced two additional contact pads to either side of the right forearm. We placed a contact pad on the ulnar side for the middle finger, the middle for the index finger as before, and the radial side for the thumb (Fig. 2.2c). Two tasks were performed with skin stretch feedback: a grip recognition task and a grip aperture targeting task. For the grip aperture targeting task, subjects were also evaluated with no feedback. As before, subjects listened to pink noise through headphones and the prosthesis and contact pads were hidden from view during evaluation.

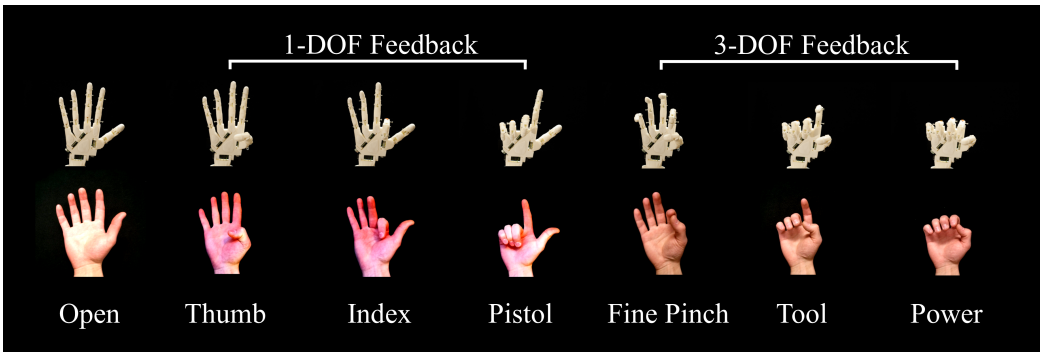

Figure 2.3: Grips used for multiple-DOF experiments. The thumb, index, and pistol grips displace one contact pad; while the power, tool, and fine pinch grips displace multiple contact pads. The 1- and 3-DOF grips are shown at 100% grip aperture.

The multiple-DOF tasks involved six grips plus a starting reference configuration (open hand) (Fig. 2.3). To examine whether single-DOF grips could be distinguished from multiple-DOF grips, half of the grips chosen displaced a single contact pad: the thumb, index, and pistol grips. The other three grips displaced multiple contact pads simultaneously: power, fine pinch, and tool grips. The amount of skin stretch per contact pad was proportional to each corresponding joint angle for each grip. These specific multiple-DOF grips were chosen because they are commonly implemented in upper limb myoelectric prostheses [7].

Grip Recognition Task

This task was modified from [8]. In this task, grips were presented starting from the open hand reference configuration, transitioning over about 4 s to the completed grip. During the first of two training periods, subjects were shown an image of the grip while also being provided with the appropriate skin stretch feedback. Once the grip had completed moving, it was held for 3 s. The hand then transitioned back to the open hand reference configuration over another 4 s, followed by a 3 s pause before continuing to the next grip. The order of the grips were randomized and each grip occurred twice. In the second training period, subjects were asked to identify grips within 3 s after grip completion and were told the actual grip. Again, the order of the grips was randomized, except each grip occurred three times. The combined total training time across both periods took 6 min.

During evaluation, subjects had to identify a series of 30 grips, with each grip

being presented five times in random order. This time, subjects were not told the correct grip after their selection. No time limit was imposed on the subjects when selecting a grip, and they were allowed to select a grip before the 4 s it took for the grip to reach completion. The proportion of correct selections and the time from grip onset to selection was recorded.

Grip Aperture Targeting Task

This task extended the single-DOF virtual finger task to incorporate the six grips from the grip recognition task. The aperture of each grip was normalized from 0% (open hand) to 100% (completed grip). Subjects had to match target apertures at 25%, 50%, and 75% grip completion using EMG control.

To decouple EMG pattern recognition from matching a percent aperture for a grip, the grips were pre-selected. Subjects flexed or extended the same muscles from the single-DOF task to control the aperture for all grips. During training, the subject was prompted to close a grip to within $\pm 5\%$ of a target percent aperture and stay in the zone for 2 s. We repeated this process for each of the six grips at each of the three target apertures, presented in a randomized order. We use percent aperture instead of angle since different fingers will be at different angles throughout the grips.

Evaluation consisted of 30 random targets in which the subject tried to match percent aperture after starting from a random percentage between 0-100%. In order to reduce the completion time of the experiment, a random subset of all the combinations of grip and percent aperture were presented to each subject. Subjects repeated the task twice for both no feedback and skin stretch feedback conditions, with the order of conditions randomized for each repetition of the task for each subject. The mean absolute error between the target percent aperture and subject's estimate was recorded.

2.3 Results

For the single-DOF virtual finger task, the no feedback, vibrotactile, and skin stretch conditions had ($17.75 \pm 5.17^\circ$), ($8.58 \pm 2.12^\circ$), and ($9.79 \pm 2.68^\circ$) of mean absolute error, respectively. We ran a two-way repeated measures ANOVA, where the within-subject factors were session number and feedback condition.

We found a significant difference between the no feedback and vibrotactile conditions ($p < 0.01$) as well as the no feedback and skin stretch conditions ($p < 0.05$) (Fig. 2.4a). However, there were no significant differences between skin stretch and vibrotactile or between sessions for any feedback condition.

Over the course of the multiple-DOF grip recognition task, subjects correctly selected 88.0 $\pm$ 5.6% of the presented grips on average. Figure 2.4b shows the confusion matrix, which depicts the absolute number of correct and incorrect selections for a presented grip. The average time for grip selection was 5.2 $\pm$ 0.6 s, where time was measured from the start of when the reference began moving toward the closed grip. For the multiple-DOF grip aperture task, Fig. 2.4c shows that the error in percent aperture for the skin stretch condition ($11.1 \pm 1.5\%$) was significantly lower ($p < 0.05$) than the no feedback condition ($18.7 \pm 5.1\%$).

2.4 Discussion

2.4.1 Single-DOF Virtual Finger Task

In the single-DOF virtual finger task, subjects had lower average error when given either linear skin stretch or vibrotactile feedback than when they were given no feedback. There was no significant difference between either form of feedback. However, users of prostheses have reported that vibrotactile feedback becomes distracting after prolonged periods of time [12], though constant proprioceptive feedback may be desired. Subjects in this study reported skin stretch remained comfortable throughout the experiments, which could make it more desirable than vibrotactile stimulation at providing proprioceptive feedback, but studies assessing the long-term comfortability of skin stretch need to be performed.

2.4.2 Multiple-DOF Tasks

Grip Recognition Task

Subjects in this study distinguished between six different grips in an average of 5.2 s with 88.0% accuracy across subjects, while those in Cheng et al. [8] distinguished between five different grips in an average of 29.4 s with 79.7% accuracy.

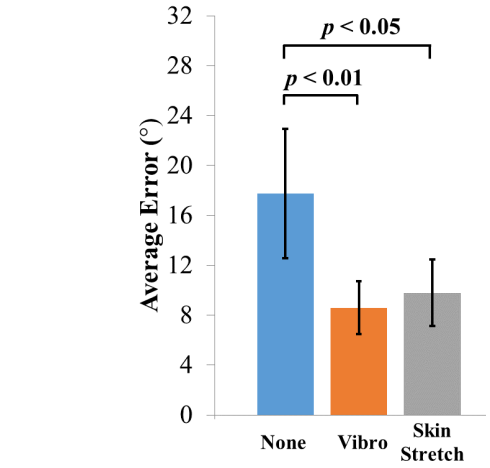

(a)

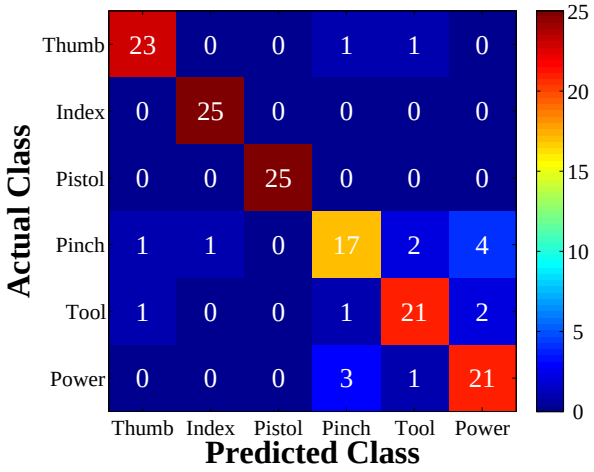

(b)

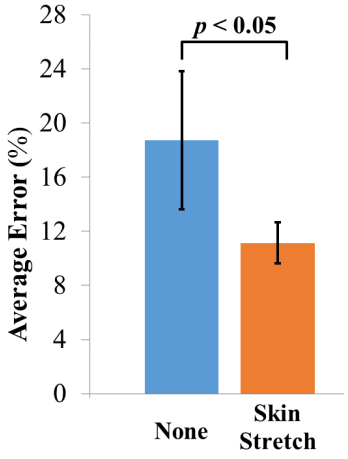

(c)

Figure 2.4: (a) Average mean absolute error for the single-DOF virtual finger task. (b) Confusion matrix for grip recognition task. (c) Average percent grip aperture error for the grip aperture targeting task.

Though the grips used in this study differ from those used by Cheng et al., the similar success rates suggest that our passive linear skin stretch device is a viable system to use for multiple-DOF tasks.

Refinements will be made to the linear skin stretch system to further improve grip recognition accuracy. One possible improvement to the system would involve creating maximally distinct contact pad trajectories for each grip.

Grip Aperture Targeting Task

In the grip aperture task, subjects performed better with skin stretch feedback than without, regardless of the grip. In later studies, we would like to determine whether subjects attend to all three contact pads or simply the one with the maximum range of stretch for a particular grip.

2.4.3 Power, Weight, and Surface Area Comparisons

During prosthesis design, power and weight must be considered. For feedback devices, the available skin area and size of the tactors are additional concerns, especially when competing for area with the prosthesis' sensors. First, for a single-DOF assuming a 7.4 V, 2400 mA h battery, the vibrotactile array used in this study would decrease battery life by 2%, while the 3.2W motor for the rotational skin stretch device by Wheeler et al. [6] would decrease it by 9% if the device ran constantly. Our passive skin stretch mechanism decreases the battery life by 1% due to the additional current needed to supply enough torque to actuate both the fingers and the contact pad. Our device would be even more efficient in prostheses with motors that produce more torque. Second, our device, the vibrotactile array, and Wheeler et al.'s device would add 2g, 6g, and 82g to the prosthesis, respectively. Compared to the weight of commercially available prostheses, our device and the vibrotactile array were negligibly light. Finally, the area used by our device over the full range of stretch was 975 mm^2, while vibrotactile used 2380 mm^2, and Wheeler et al.'s device used 2800 mm^2. Thus, our passive skin stretch device used the least surface area of these three devices, drains little power, and is lightweight.

2.5 Conclusion

We have shown that for a single-DOF virtual finger targeting task, linear skin stretch is comparable to vibrotactile feedback and better than no feedback. In the multiple-DOF grip recognition task, our results are comparable to those attained in a previous study [8] that used a vibrotactile array. However, subjects in our study were able to achieve similar classification accuracy (88.0% vs. 79.7%) after a shorter training period (6 min vs. 30 min) and required less time to make classifications (5.2 s vs. 30 s). In the grip aperture targeting task, subjects matched target grip apertures with 11.1% error on average. Finally, the simplicity, low cost, low power consumption, light weight, small contact area, and overall comfort make our passive linear skin stretch device well-suited for multiple-DOF proprioceptive tasks. Supplementary Video 2.1 shows a demonstration of the device and experiments.

CHAPTER 3

AN EPIDERMAL STIMULATION AND SENSING PLATFORM FOR SENSORIMOTOR PROSTHETIC CONTROL[1]

We report the design of an ultra-thin, conformal epidermal electronic device that integrates electrotactile stimulation with simultaneous electromyography, temperature, and strain sensing on a single substrate. The focus of this chapter will be on the simultaneous function of electromyography and electrotactile stimulation on the device. We validate the simultaneous use of these functions in sensorimotor control of a robot arm. Subjects were asked to perform a force modulation task in order to myoelectrically control a robot to grip a bottle of water without crushing it while receiving force feedback through electrotactile stimulation. Additionally, as well as a virtual arm targeting task to assess simultaneous myoelectric control while receiving proprioceptive feedback through electrotactile stimulation. Our results show that for the force modulation task, when stimulation was present, a user could stop the closing of a robot gripper in order to prevent maximum deformation of the bottle. For the virtual arm targeting task, there was a significant difference ($p < 0.05$) between feedback and no feedback conditions, and there was no significant difference between the epidermal electronic device and conventional electrodes.

3.1 Introduction

Skin-mounted sensors of physiological signals are useful in areas ranging from clinical diagnostics to human-machine interfaces [10, 14–18]. The recent development of concepts in "skin-like" semiconductor technologies, sometimes referred to as epidermal electronics, create important opportunities in long-term, non-invasive, conformal interfaces to the body [19–25]. These systems offer advantages in device mechanics and user mobility over traditional technologies for healthcare monitoring and disease diagnostics, with demonstrated capabilities in

[1] This work includes material published in [13].

precision measurement of hydration [26], strain [27–29], pressure [30, 31], temperature [32] and others parameters of interest. Additional recent work shows that similar platforms designed for the fingertips can offer advanced capabilities in electrotactile stimulation [33]. Combining these functions in a single, simple device platform designed for operation on the trunk or limbs of the body could be attractive in applications such as neuromuscular electrical stimulation [34], neuromodulation rehabilitation therapy [35], pain mitigation and prevention [36], human-machine interfaces [10], and sensorimotor control in prosthetic and orthotic devices [37], where electromyography (EMG) and electro-stimulation could serve as sensing and actuating platforms. Here, we present systems of this type, where multiple transcutaneous electrical stimulation electrodes co-integrate on a common substrate with electromyography, temperature and mechanical strain sensors. The ability to simultaneously record physiological data and deliver neural stimulation provides valuable functionality, as illustrated in examples of sensorimotor prosthetic control.

The integration of sensory feedback and myoelectric control has been demonstrated in previous studies [37, 38]. In 2010, Antfolk et al. demonstrated the use of five vibrotactile feedback elements that responded to five force sensors embedded in the fingertips of a myoelectrically controlled prosthetic hand. The subject expressed that the ability to feel the prosthetic hand when controlling it was an "amazing feeling" [39]. While these initial results were successful in enabling the subject to feel his prosthetic hand, vibrotactile elements have the disadvantage of being bulky and only capable of producing a single sensation (vibration). Kim et al., designed haptic devices for upper extremity prosthetics to display vibration, pressure, shear, or temperature sensations on the skin. However, these devices are also large—the size of the tactor heads are between 11-14 mm, much larger than the point localization threshold of reinnervated patients, which is 1-2.8 mm [40, 41]. On the other hand, by changing the frequency, amplitude, pulse duration and overall shape of electrotactile stimulation waveforms, it is possible to elicit different sensations, such as vibration, tingling, pins and needles, itching, pain, and others [42]. Furthermore, due to the small size of the electrodes used in electrotactile stimulation—Kajimoto et al., have used electrodes as small as 2.54 mm in diameter with $<$1 mm interelectrode spacing in a 512-electrode array—it is possible to create practical high-density arrays of electrotactile stimulation electrodes [43].

Simultaneous electrical stimulation and EMG recording is most common in

Functional Electrical Stimulation (FES) literature [34, 44]. In FES applications, a goal is to determine the amount of voluntary muscle contraction through EMG in the presence of signal artifact from muscle stimulation. Frigo et al. used 16.67 Hz, 40 mA, constant current monophasic square waves in order to stimulate the rectus femoris muscle. Subjects were also asked to simultaneously contract the muscle voluntarily. In order to filter out the stimulation artifact, Frigo et al. used a combination of blanking (zeroing the signal at the onset of a stimulation) and a comb filter (a filter that attenuates the power of a specific frequency and its harmonics). As a result, Frigo et al. was able to recover the EMG from the voluntary muscle contraction, while removing the stimulation artifact. We apply the same technique to successfully remove stimulation artifacts in our study.

3.2 Methods

Figure 3.1a provides an optical micrograph of a multifunctional epidermal device constructed from patterned metal traces and polymer dielectric materials on a thin layer of silicone elastomer (thickness: 60 μm, Young's modulus: $\sim$60 kPa, Smooth-On, USA), supported by a temporary, water-soluble substrate of polyvinyl alcohol (PVA, Aicello, Japan). The layout includes electrodes for electrotactile stimulation and the measurement of EMG, temperature and strain, as shown in the schematic illustration of Fig. 3.1b. The simplicity of the construction is a key feature of the design. In particular, the active parts of the entire system involve only two layers of metal thinfilm with patterned interlayer dielectrics semiconductor materials are not required. The EMG sensor uses the same metal layers, patterned in a different geometry, for the reference, measurement, and ground electrodes. Each of these electrodes (2 mm width and 12 mm length; 24 mm^2 sensor area) consist of 20 μm-wide traces in an interwoven serpentine morphology to maximize mechanical stretchability, and have a spacing of 10 mm between electrodes to optimize signal quality [45]. Each stimulation electrode is coaxial, consisting of an inner disk with a radius of 1.0 mm, an outer ring with a radius of 2.0 mm, separated by a 0.5 mm space. The EMG and stimulation electrodes remain exposed to the skin. All sensors connect to peripheral contact pads that allow interfaces to external power supplies and data acquisition hardware. Mounting the epidermal device on the skin involves washing away a water-soluble backing layer of poly(vinyl alcohol) (PVA), using procedures described previously [19]. Figure 3.1c illustrates

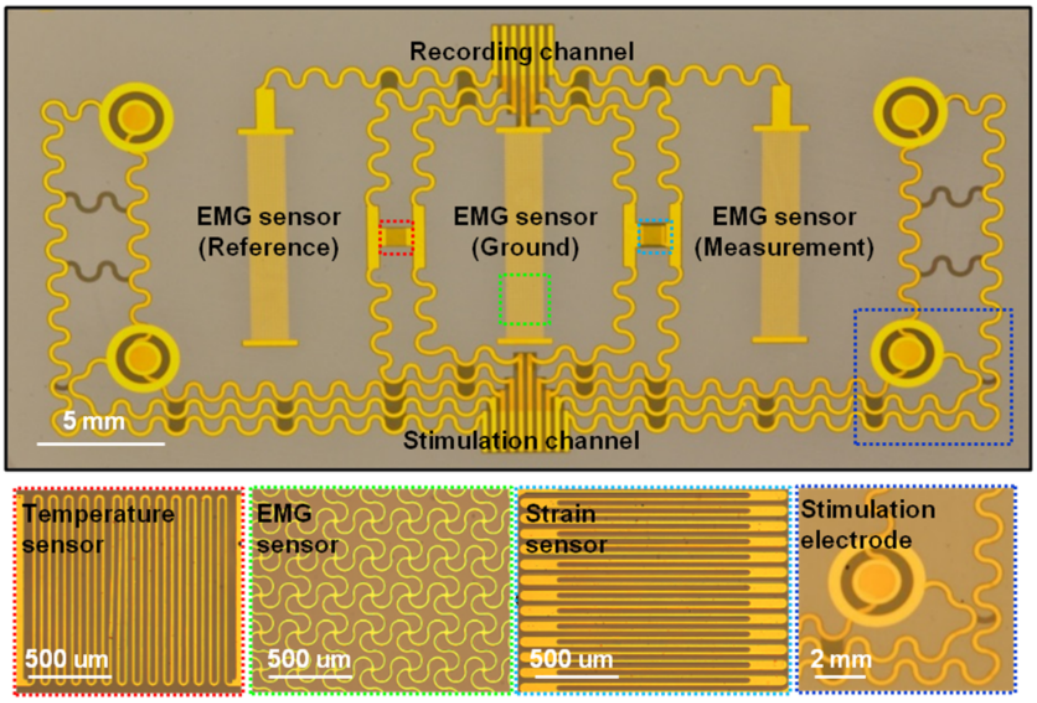

(a)

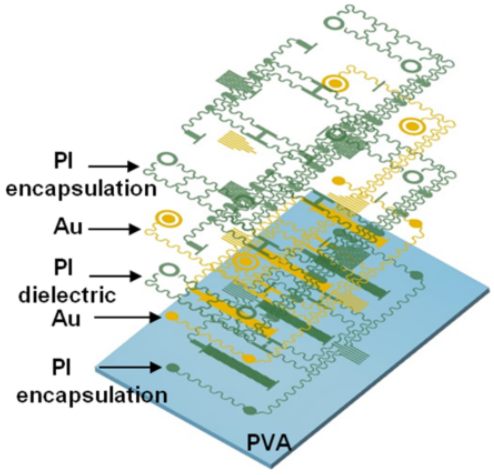

(b)

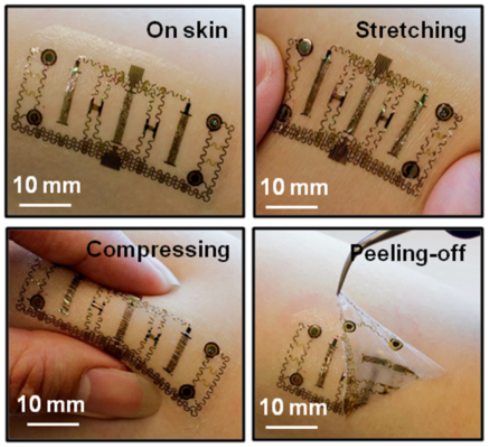

(c)

Figure 3.1: Images and design features of a simple, multifunctional device with skin-like physical characteristics and capabilities in both sensing and stimulation. (a) Planar view optical micrograph of a representative device. The insets highlight various active regions. (b) Exploded-view schematic illustration of the multilayer construction, comprised only of patterns of metals and dielectrics. (c) Images of a device mounted on the forearm, with examples under stretching, compressing and peeling-off.

the way in which the thin, soft construction of the device allows it to conform and adhere to the surface of the skin, based on van der Waals interactions alone. The low elastic modulus of the device substrate avoids any significant constraint on the natural motion of the skin. The advantages of using this type of device compared to conventional gel-based electrodes for electrical stimulation or EMG measurements are summarized in Table 3.1 [46, 47]. Furthermore, conventional gel-based electrodes and other previously reported work [10, 15, 19–21, 26, 32, 33, 47] do not offer the type of multifunctional operation in the device described here.

Table 3.1: Comparison of conventional gel-based single electrode and multifunctional epidermal device.

	Gel-based electrode*	Multifunctional epidermal device
Functionality	EMG, Stimulation	EMG, Stimulation, Temperature, Strain
Modulus	∼200-300 kPa	∼69 kPa
Thickness	∼1 mm	∼20 μm
Scalability	Separate electrode pairs per EMG/stimulation channel	Integrated electrodes and sensors on a single substrate
Materials	Ag/AgCl hydrogel	Silicone elastomer

*Based on AMBU Neuroline 710 electrodes

3.3 Results & Discussion

3.3.1 Circuit model and analysis of electrode on the skin

The stimulation electrodes add an important functional capability to the epidermal device. Current injected into the skin through these electrodes stimulates sensory nerve fibers to elicit sensations that resemble tingling, vibration, light touch, or pressure [42]. All procedures and equipment were approved by the Institutional Review Board of the University of Illinois at Urbana-Champaign (#13920). A constant-current monophasic square pulse (3 mA amplitude, 0.2 ms pulse duration, 20 Hz frequency) applied to the skin through one of the stimulation

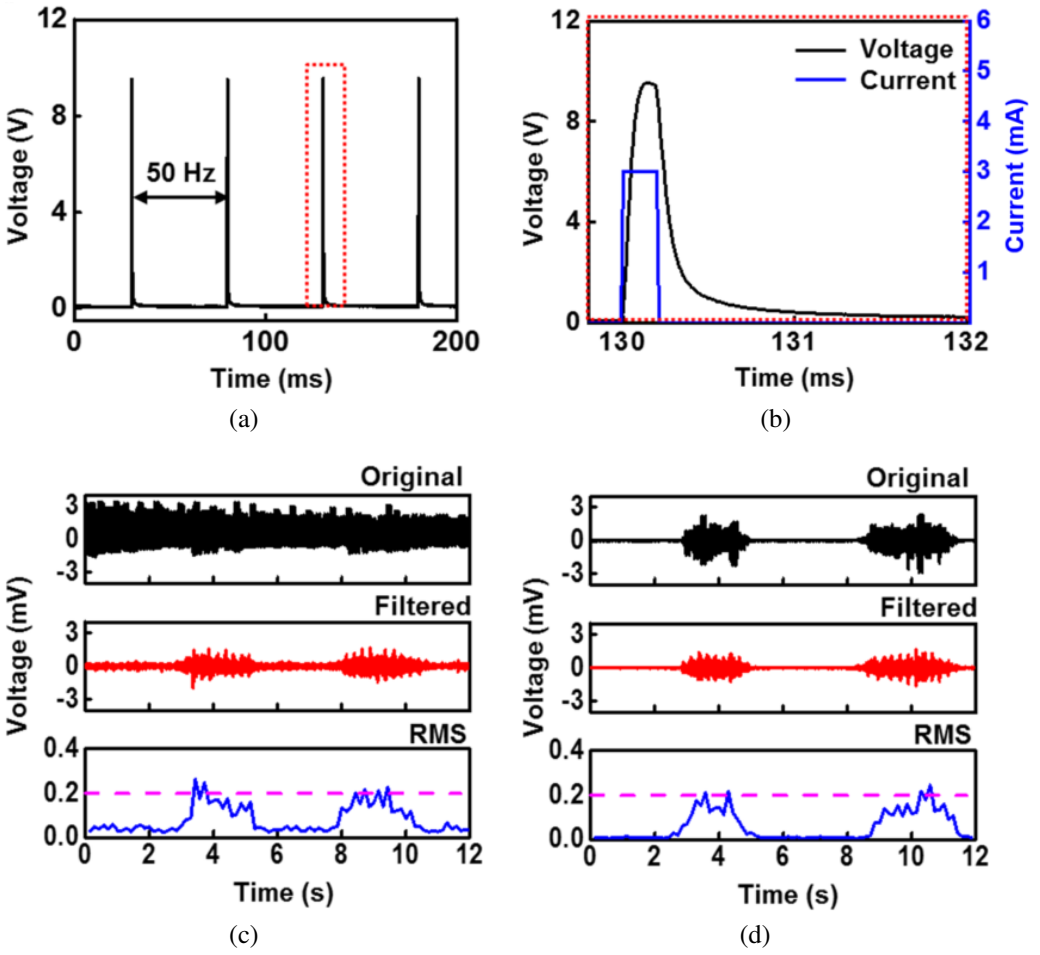

Figure 3.2: Summary of functional attributes in sensing and stimulation. (a) Voltage recorded between the two coaxial electrodes associated with an electrotactile stimulator during 20 Hz operation at 3 mA. (b) Magnified view of the recorded voltage over one period of stimulation (black), with applied stimulation current signal (blue) (c) EMG signals collected from the forearm (original, filtered, and root mean square (RMS)) during simultaneous stimulation from the top two electrodes (Fig. 3.1a). The raw recorded data includes signals that arise from the stimulation, masking the EMG response. Digital filters can remove the effects of stimulation, to yield EMG data that correspond well to recordings performed without stimulation, shown in (d).

electrodes using a computer-controlled linear isolated stimulator (STMISOLA, BIOPAC, Inc., CA) yields typical voltage responses [42], shown in Fig. 3.2a. The voltage response of a single pulse from the epidermal device is shown in Fig. 3.2b. We can model this voltage response across the anode and cathode of the stimulation electrodes (Fig. 3.3) and characterize the resistive and capacitive electrical properties by using a circuit model that represents the electrodes, electrode-skin

interface, the underlying skin, and tissue [42, 48].

The contact between electrode and skin can be described as a resistor and a capacitor in parallel. Figure 3.3a shows the equivalent circuit model, where R_{es} and C_{es} are the effective resistance and capacitance of the electrode-skin interface, respectively. When a constant current is supplied, a typical resistorcapacitor voltage step response curve is measured using both conventional electrodes and the epidermal device. Here, we take the charging phase for analysis [42, 49]. The applied current was a 0.2 mA positive monophasic square pulse at 20 Hz with a 10 ms pulse duration. A 10ms pulse duration was used to allow enough time for the voltage response to reach steady state in order to estimate it accurately. While impedance is affected by the amount of applied current, 0.2 mA was applied to both conventional and epidermal electrodes at a level that was comfortable to the user. Using the equation for capacitive charging, we can estimate the steady-state voltage, RC time constant, and the DC offset.

$$V(t) = (V_s - V_0) * (1 - e^{-\frac{t}{\tau}}) + V_0$$

Where V_s is the steady-state voltage, V_0 is the DC offset and τ is the time constant for the charging phase. The resistive part of the impedance can be computed by taking the steady-state voltage (V_s), subtracting it from the DC offset (V_0), and then dividing it by the stimulation current amplitude [42, 49]. To account for the different sizes of electrodes, the resistance is normalized by multiplying the area of the electrode [42]:

$$R_{norm} = \frac{V_s - V_0}{I} * area_{electrode}$$

The capacitive part can then be computed by dividing the resistance value from the estimate of τ. To account for the different sizes of the electrodes, the capacitance is normalized by dividing by the area of the anode [42]:

$$C_{norm} = \frac{\tau}{R} * \frac{1}{area_{electrode}}$$

The area of the conventional electrode was 263 mm^2 and the area of the epidermal stimulation electrode was 3.14 mm^2. The values of R_{es} and C_{es} depend on the contact areas of the electrodes, their constituent materials, the thickness and electrical properties of the skin, and the waveform being sent [42]. Upon stimulating the skin superficial to the left flexor carpi radialis and normalizing to the size of

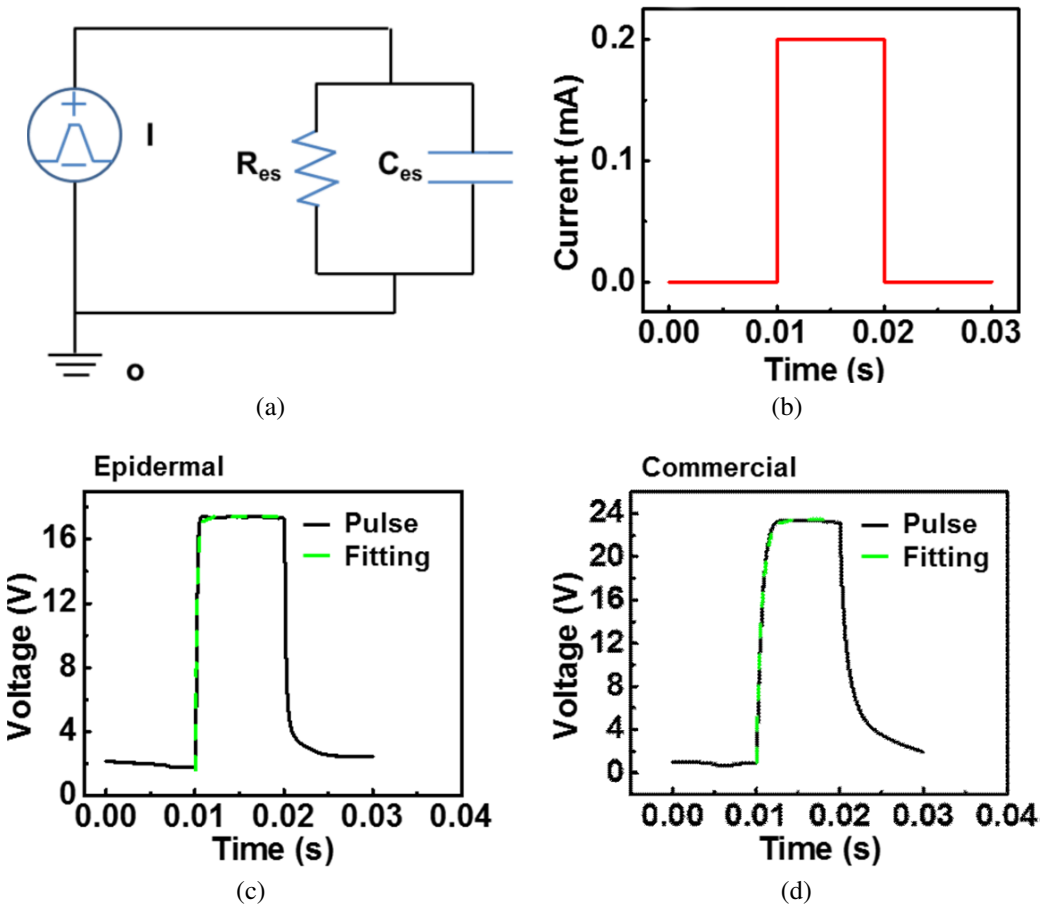

Figure 3.3: (a) Simplified electrical model for the electrode-skin impedance with R_{es} and C_{es}. (b) Current stimulation profile used in stimulation of both epidermal and commercial hydrogel electrode. The measured voltage waveform is shown in (c) for the the concentric epidermal electrode with an area of 3.14 mm^2 and in (d) for the commercial hydrogel electrode with an area of 263 mm^2.

the electrode, we obtain values of 273.5 $k\Omega\,mm^2$ and 75.13 nF/mm^2 for R_{es} and C_{es}, respectively, for the epidermal device; and 30.79 $M\Omega\,mm^2$ and 20.84 pF/mm^2 for the conventional electrodes. Consequently, because the epidermal device has a lower normalized resistance, current can flow more freely through the skin, reducing the occurrence of local high density current areas which can cause painful stimluation [42, 49].

3.3.2 Simultaneous function of EMG and electrotactile electrodes on the epidermal device

Due to the use of a common, compact device platform, the stimulation electrodes can cause artifacts in the EMG recordings, as shown in Fig. 3.2c for the case of stimulation (20 Hz, 200 μs positive monophasic square pulse across two stimulation electrodes with an amplitude of 1.6 mA) on the left flexor carpi radialis muscle of a 21-year-old unimpaired female subject during EMG recording while flexing the left wrist for 2 s, resting for 3 s, and then making a clenched fist for 2 s, each to maximum voluntary contraction (MVC). Figure 3.2c shows the EMG signal collected without electrical stimulation. Such data are similar to those obtained using conventional electrodes (Neuroline 710, Ambu A/S, Denmark), as in Fig. 3.4. A comb filter can attenuate responses at frequencies at 20 Hz and its harmonics [34], to eliminate the stimulation artifact without significantly altering the EMG data, as illustrated in Fig. 3.2c. Additional experiments show that the stimulation frequency, magnitude, number and position of the electrodes do not affect the EMG measurements (Fig. 3.4).

3.3.3 Force Feedback - Bottle Grasp Task

Advanced surgical techniques such as targeted reinnervation provide patients with upper limb amputations the ability to control a prosthetic limb using intuitive muscle commands that map to their missing limb, and to experience sensations perceived as originating from their missing limb [7, 50]. Here, nerves that originally supplied the missing limb are rerouted to intact muscle and skin elsewhere in the body. Because the reinnervated muscle and skin sites often overlap with or are in close proximity to one another, existing bulk electrode technologies cannot simultaneously record EMG and electrically stimulate the overlying skin for force and proprioceptive feedback [1,2]. The devices introduced here, where sensors and actuators can be located closely adjacent to one another, with lithographic precision, create opportunities in this context. A simple demonstration involves devices applied to the right flexor carpi radialis and the extensor carpi radialis muscle groups of a 22-year-old unimpaired male subject. The root mean square (RMS) value of the EMG signal is used for proportional control of the grip aperture of a humanoid robot (Baxter, Rethink Robotics, MA). The gripper applies force to a plastic bottle filled with water (Fig. 3.5a), measured from a sensor (25 lb Flexiforce, Tekscan,

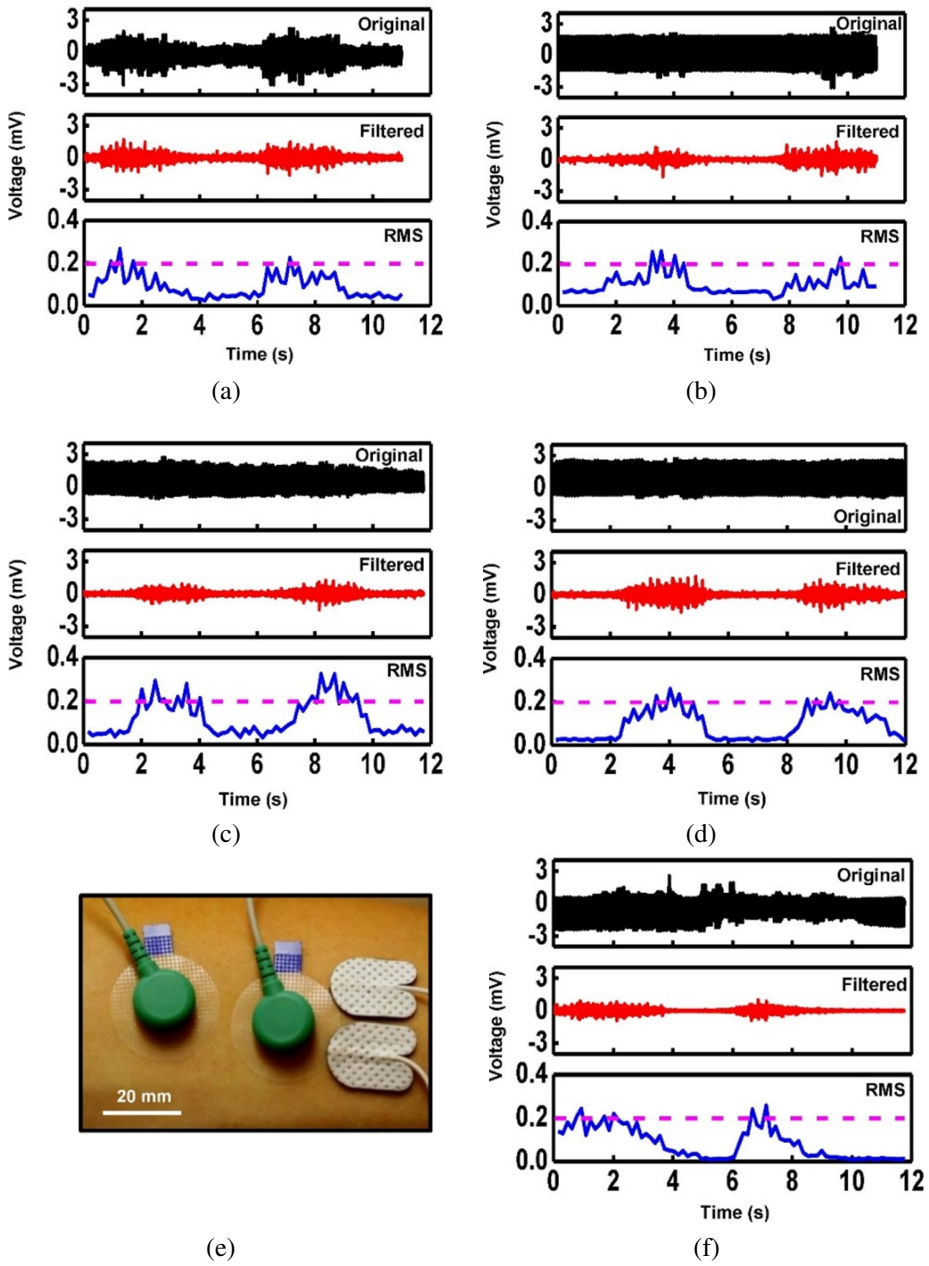

Figure 3.4: Effects of stimulation on EMG measurements taken simultaneously through the epidermal device and conventional electrodes. (a) EMG recorded on the epidermal device during 20 Hz constant current stimulation at electrode 1, (b) 20 Hz stimulation at electrode 2, (c) 50 Hz stimulation at electrode 1, and (d) 10 Hz stimulation at electrode 1. (e) Image of simultaneous electrotactile stimulation and EMG recording using conventional stimulation electrodes (white) and conventional EMG sensors (green). (f) EMG recorded from conventional EMG sensors during 20 Hz stimulation using conventional stimulation electrodes.

Inc., MA) mounted on the inside of gripper (Fig. 3.6a). In evaluations, the subject, blindfolded and acoustically shielded, attempts to grip the bottle, both with and without stimulation. With stimulation, the subject receives sensory input at a level proportional to the force measured by the sensor. The maximum stimulation, 2 mA, in this case, corresponds to 27 N, the maximum force available to the gripper. Figure 3.5b shows that, without feedback, the subject cannot consistently close the gripper without causing the bottle to collapse. With force feedback, the subject can successfully stop the grip at any desired level of gentle touch. Similar capabilities are possible with a wooden block used in place of the bottle (Fig. 3.6).

3.3.4 Proprioceptive Feedback - Virtual Arm Task

Stimulation can also provide proprioceptive feedback, as demonstrated in the control of virtual arms presented on a computer screen as well as physical robotic arms. Here, two separate devices are mounted over the long head of the biceps brachii and the lateral head of the triceps brachii muscles (Fig. 3.5c). In the virtual arm targeting task, a 22-year old unimpaired male subject attempts to flex and extend the elbow of a single degree-of-freedom virtual arm to match the orientation of a target virtual arm presented onscreen [4, 6]. The virtual arm can move between -60° to 60°. During experiments, the subject grips a vertical handle and maintains his elbow in a fixed position at 90°with respect to the humerus to remove any natural proprioceptive cues. Flexing or extending the elbow joint against the handle generates EMG signals (Fig. 3.5d). Linear discriminant analysis classifies these signals to virtual arm movements every 0.1 s, according to previously reported procedures [4, 10]. Evaluations involve four conditions: EMG control with conventional electrodes and no feedback; EMG control with conventional electrodes and stimulation feedback; EMG control with the epidermal device and no feedback; and EMG control with the epidermal device and electrotactile feedback. The feedback activates stimulation with electrodes 1 and 2, that maps, using the tactile funneling illusion [51], the virtual arm angular range (-60° to 60°) to different current levels (Fig. 3.5e). In the tactile funneling illusion, when two stimulation electrodes are simultaneously active, a single sensation is perceived between the two electrodes. By modulating the stimulation current amplitudes, the location of the perceived sensation can be adjusted to any point between the two electrodes. As a result, any virtual arm angle can be mapped to a unique

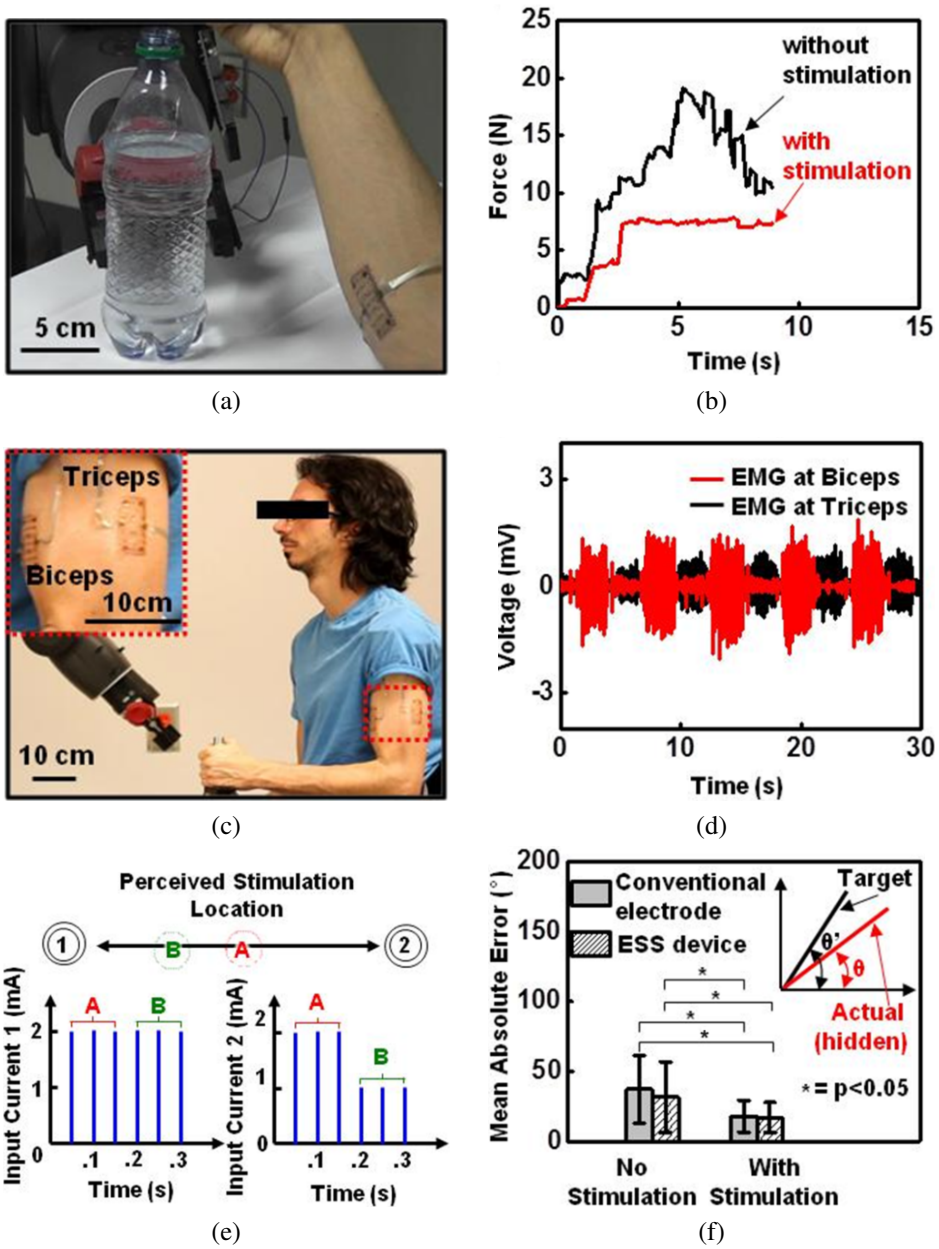

Figure 3.5: Sensorimotor control of a robot arm. (a) The device on the forearm while controlling a robot arm to grip a bottle filled with water. (b) Gripping force with and without stimulation feedback. When feedback is present, the subject can grip the bottle in a controlled manner, to prevent collapse. (c) Devices on the bicep and tricep (inset) during control of the elbow angle of a robot arm. (d) EMG signals from two devices when alternating between flexion and extension of the robot arm's elbow. (e) Example stimulation waveforms used to produce the tactile funneling illusion. (f) Accuracies in virtual arm targeting task comparing performance with and without stimulation using both conventional electrodes and the device ($p < 0.05$, Two-Way ANOVA, Tukey post-hoc).

(a)

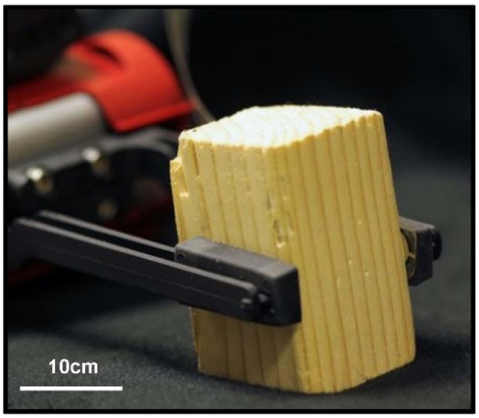

(b)

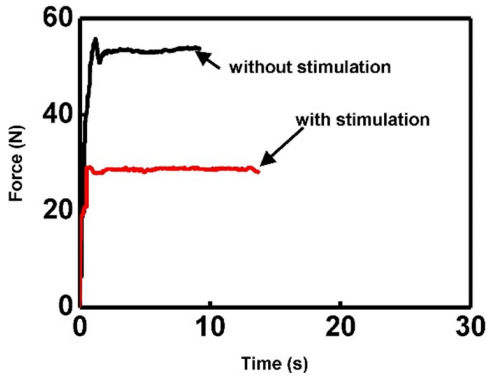

(c)

Figure 3.6: Control of robot gripping a block of wood while receiving electrotactile force feedback. (a) Image of robot gripper with force sensor (inset, magnified view). (b) Image of the block of wood being gripped. (c) Corresponding recorded gripping force.

stimulation location perceived between the two electrodes. In turn, the subject interprets this stimulation location as the joint angle of the virtual arm.

A block diagram explaining the virtual arm task can be found in Fig. 3.7. The training phase involves free control of the virtual arm for 60 s, and then a presentation of five hidden target angles to match. After each attempt, the subject presses a button to reveal the actual angle of the virtual arm. Performance tests based on 25 random targets appear in Fig. 3.5f, which shows a schematic illustration of

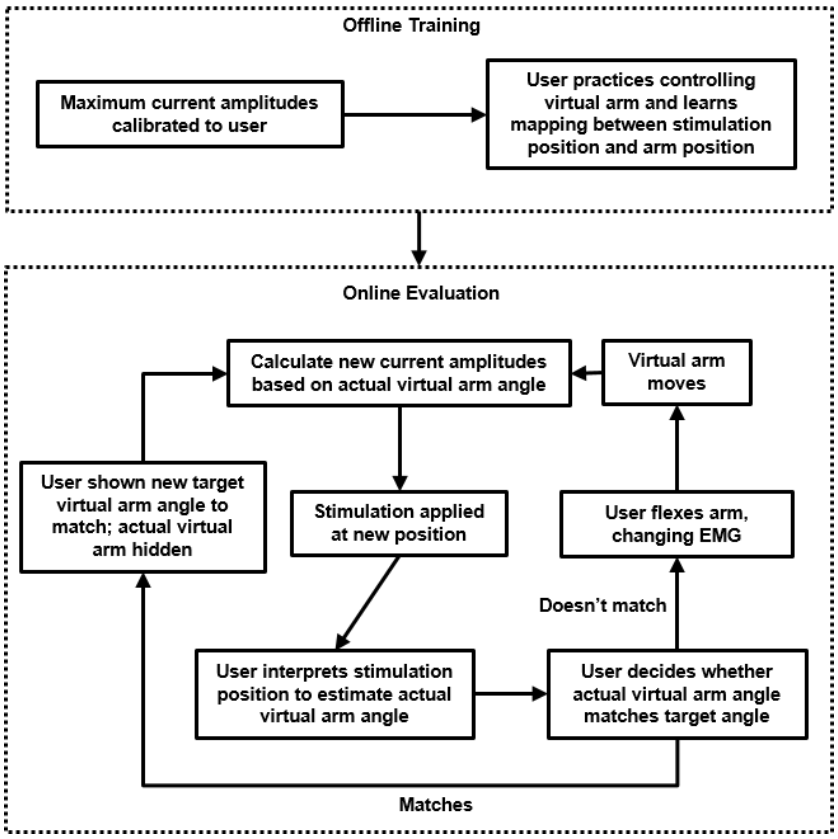

Figure 3.7: Block diagram detailing the experimental protocol used in the virtual arm targeting task.

the virtual arm, as well as the errors between the target angle and the subject's estimate for each of the four conditions. Feedback yields statistically significant improvements in performance (Two-Way ANOVA, Tukey post-hoc, $p < 0.05$). In particular, the mean absolute errors for conditions without feedback are 37.2° and 31.6° with conventional and epidermal electrodes, respectively. With feedback, the errors decrease significantly to 17.8° and 16.9° with conventional electrodes and epidermal electrodes, respectively. These performance gains are similar to those found in other studies using sensory substitution (electrotactile, vibrotactile, or skin stretch) for proprioceptive feedback in modulating upper limb joint angles [4–6]. While the performance with the epidermal electronics offers lower error both with and without feedback compared to the conventional electrodes, no statistically significant difference was found. Nevertheless, the ability to provide multiple points of stimulation while simultaneously recording EMG in a single device, as opposed to the multiple sets of conventional electrodes needed to enable

sensorimotor control, represents a significant advantage.

These collective capabilities allow for efficient prosthetic control, as demonstrated by control of the elbow joint of a robot, using EMG recorded from devices on the upper arm (Supplementary Video 3.1). The control involves gripping a bottle, lifting it, and placing it back down on a table while blindfolded and acoustically shielded. Here, electrotactile stimulation provides touch and proprioceptive feedback.

3.4 Conclusion

In conclusion, the conformal, multifunctional, epidermal device reported here seamlessly integrates sensors for electromyography with electrical stimulation electrodes, in a simple architecture that incorporates only metal traces and dielectric layers. Demonstrated application possibilities include prosthetic control with sensory feedback. Future work will investigate long-term application in clinical settings, with a focus on patients with upper limb amputations to simultaneously control and feel from their prosthetic device. In such cases, means for accommodating variations in stimulation parameters that occur with changes in the impedance of the electrode-skin interface over time will be important [52], which we explore in Chapters 5 and 6.

CHAPTER 4

A LOW-COST, OPEN-SOURCE, COMPLIANT HAND FOR ENABLING SENSORIMOTOR CONTROL FOR PEOPLE WITH TRANSRADIAL AMPUTATIONS[1]

In this chapter, we describe the design and implementation of a low-cost, open-source prosthetic hand that enables both motor control and sensory feedback for people with transradial amputations. We integrate electromyographic pattern recognition for motor control along with contact reflexes and sensory substitution to provide feedback to the user. Compliant joints allow for robustness to impacts. The entire hand can be built for around $550. This low cost makes research and development of sensorimotor prosthetic hands more accessible to researchers worldwide, while also being affordable for people with amputations in developing nations. We evaluate the sensorimotor capabilities of our hand with a subject with a transradial amputation. We show that using contact reflexes and sensory substitution, when compared to standard myoelectric prostheses that lack these features, improves grasping of delicate objects like an eggshell and a cup of water both with and without visual feedback. Our hand is easily integrated into standard sockets, facilitating long-term testing of sensorimotor capabilities.

4.1 Introduction

The vast majority of open source hands focus only on mechanical design of the hands rather than the complete integration of motor control and sensory feedback systems [54]. Many of these hands involve hardware that require external power sources, housing, or custom sockets that are not practical for widespread usage. Much of this stems from the lack of development along side clinicians who design sockets to be used with commercial myoelectric systems. In this paper, we describe the design and implementation of a low-cost, open-source hand that can easily be integrated into standard sockets made by clinicians. Further-

[1] This work includes material published in [53]

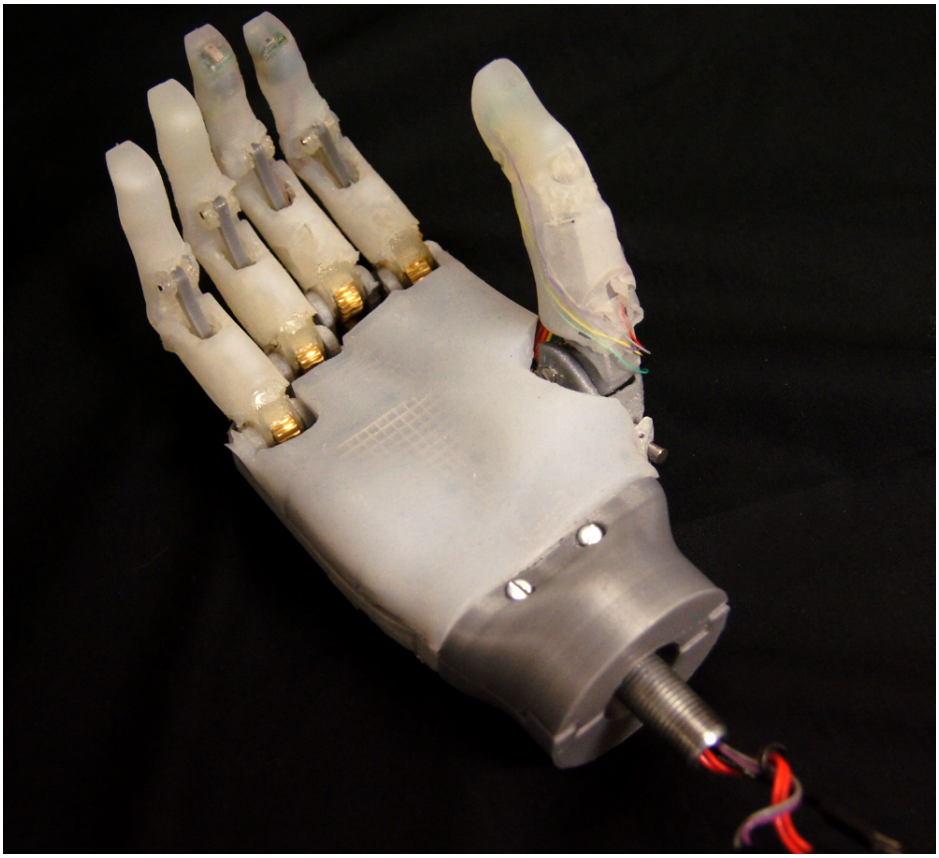

Figure 4.1: The open-source prosthetic hand with EMG pattern recognition, contact reflexes, and sensory substitution capabilities. All files, designs, materials, and source code can be found on our website[2].

more, our hand integrates both motor control through electromyographic (EMG) pattern recognition and sensory feedback through contact reflexes and electrotactile stimulation.

The low-cost is especially important given that 80% of people with amputations are in developing nations, while less than 3% of them have access to affordable rehabilitative care [55,56]. Additionally, the high cost of state-of-the-art myoelectric devices hinders researchers in evaluating effectiveness of new motor control and sensory feedback strategies. The prosthetic hand we present in this paper (Fig. 4.1) can be used for evaluating sensorimotor control and can be built for around $550. Furthermore, since this hand can be readily integrated into standard sockets, it facilitates long-term studies regarding motor control and sensory feedback in upper limb prostheses.

The chapter is organized as follows—in Section 4.2, we discuss the design of

[2]http://bretl.csl.illinois.edu/prosthetics

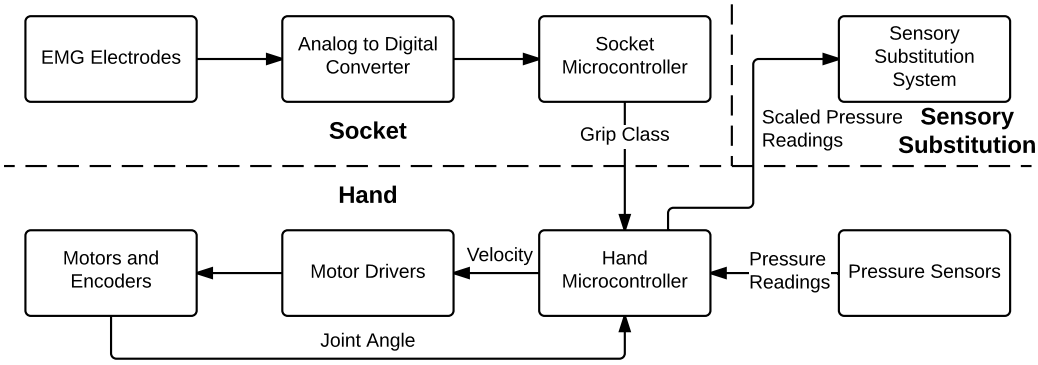

Figure 4.2: Hardware Block Diagram

the hand, and the components used to enable EMG pattern recognition, contact reflexes through pressure sensors in the fingers, and sensory substitution. We also describe a set of experiments we performed on a subject with a transradial amputation to evaluate the performance of the contact reflexes and sensory substitution when using pattern recognition to grasp objects such as an eggshell or a cup of water. We compare these results to those from a standard OttoBock myoelectric prosthesis. In Section 4.3, we describe and discuss the results of these experiments and their implications for further studies, followed by our conclusion in Section 4.4.

4.2 Methods

A block diagram of the hardware is given in Fig. 4.2. The hardware was compartmentalized into three subsystems: 1) the socket, 2) the hand, and 3) the sensory substitution system. The socket collects and filters electromyography (EMG) data from the residual limb of the user, and runs the pattern recognition classifier used to associate EMG signals with one of five different grasping classes (rest, open, power, three-jaw chuck, fine pinch). The hand requests the classified grasp from the socket, and actuates up to six motors to perform the grasp. The six motors control flexion/extension in all five digits, as well as thumb opposition. In addition, the hand receives pressure readings from the three pairs of pressure sensors located in the fingertips of the thumb, middle, and index fingers. The sensory substitution system receives information from the hand about the pressure applied to the fingertips, and can give the user appropriate feedback regarding contact forces at the fingertips. In this paper, we used an electrotactile stimulation system to

provide feedback to the user about contact forces.

4.2.1 Mechanical Design

Materials and costs required for building the hardware are listed on Table 4.1. Compared to our previous work [54], the entire hand has been mechanically redesigned to be smaller, more robust through the use of compliant materials, and energy efficient through the use of non-backdrivable worm gears. The dimensions of the hand are at 50th percentile female anthropometry (Fig. 4.3). Both PLA and ABS were used for 3D printing molds for silicone casting along with all structural components. Brass sprocket and worm gears were used for proximal joints due to their exposure to large loads and impacts. The fingers and palm are cast out of silicone to achieve compliance in the finger joints, providing human-skin like texture to the prosthesis. The compliant joints were developed by building a composite structure made of silicone (Dragon Skin 20, Smooth-On, Macungie, PA) and 3D-printed flexible material (SemiFlex, NinjaTek, Mannheim, PA). By using a flexible bone inside of a silicone outer structure, compliance in the distal and proximal joints was achieved (Fig. 4.4). The joint compliance allows shock absorption from either flexion or extension directions. Non-backdrivable worm gears decrease power consumption when gripping objects with constant high torque. Although the worm gear set and motors are susceptible to environmental shock, the compliant joints prevent damage to the gears.

4.2.2 Motor Control and Sensory Feedback

EMG & Pattern Recognition

EMG was used to control actuation in the hand (Fig. 4.5a). To save costs in electrodes, up to eight pairs of nickel-plated copper rivets can be used to record EMG signals from the residual limb of a person with an amputation, with an extra rivet being used as a ground electrode. Each rivet costs $0.23 and can be easily integrated into a socket, while standard stainless steel dome electrodes typically cost around $40 per electrode. Future work will compare the performance of the rivets to standard commercial stainless steel dome electrodes. The eight EMG channels and ground were connected to a custom board we fabricated using the TI

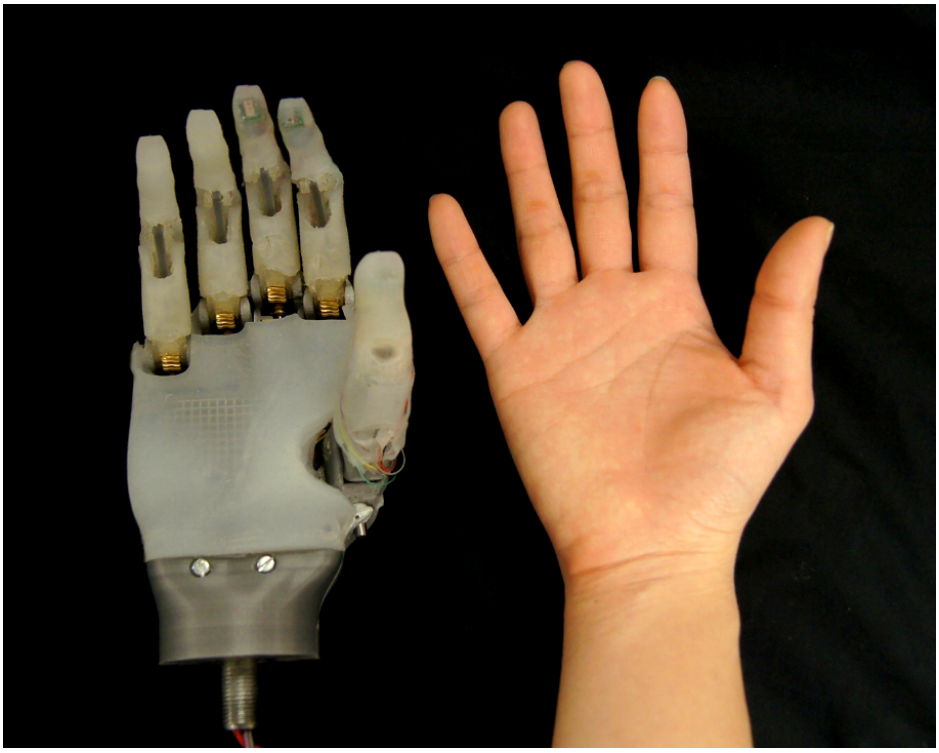

Figure 4.3: The dimensions of the hand are at 50th percentile female anthropometry.

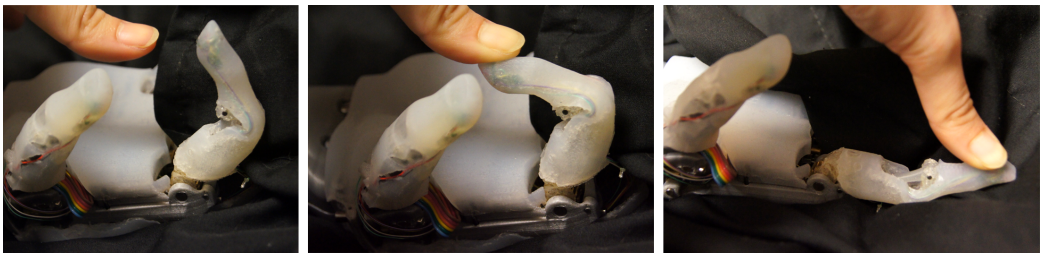

Figure 4.4: Demonstration of compliant joints.

ADS1298 (Texas Instruments, Dallas, TX) 24-bit analog-to-digital converter. The EMG signals were digitally filtered with a bandpass filter with cutoffs of 30 Hz to 450 Hz, and convolved with a notch filter at 60 Hz. All signal processing was performed on a Teensy 3.1 microcontroller (PJRC, Sherwood, OR) in the socket.

We implemented Linear Discriminant Analysis (LDA) with proportional velocity control on the socket microcontroller as our pattern recognition algorithm [57]. In this paradigm, users undergo a $\sim$2 min training period where they are asked to hold each of the five grasping classes for 25 s. LDA is then used to classify the user's desired grip every 75 ms using a sliding window of the past 200 ms of EMG signals. Proportional velocity control is implemented using the mean ab-

Table 4.1: Cost of materials for building a single hand. Sources and prices for individual items can be found on our website[2].

Items	Cost
Microcontrollers	$39.60
Integrated Circuits	$89.59
Printed Circuit Boards	$12.58
Electronic Passives	$11.13
Electrical Power	$63.35
Motors	$128.55
Mechanical Components	$126.28
3D Printing Materials	$81.98
Total	$553.06

solute value of the most active EMG channels for the desired grasp, as described by Scheme, et al. [57]. A Teensy 3.1 microcontroller in the hand uses the classified grasp and proportional velocity to control the velocity of the motors used to achieve the desired grasp.

Pressure Sensing & Contact Reflexes

The hand microcontroller polls three pairs of MPL115A2 barometric pressure sensors (Freescale, Austin, TX) located in the finger tip and finger pad of the thumb, index, and middle distal phalanges (Fig. 4.5b). Using the low-cost method described by Tenzer, et al. [58], we cast the sensors in silicone (Dragon Skin 20, Smooth-On, Macungie, PA) to turn them into highly sensitive touch sensors when depressing the silicone. The pressure readings from each sensor are scaled to a value between 0 and 1, and we detect contact when the pressure value exceeds a threshold of 0.2. If contact is detected in any of the six pressure sensors, a contact reflex takes place in which the speed of the hand is reduced to 30% of its current speed in order to provide the user with finer control in manipulating the contacted object without damaging it [59].

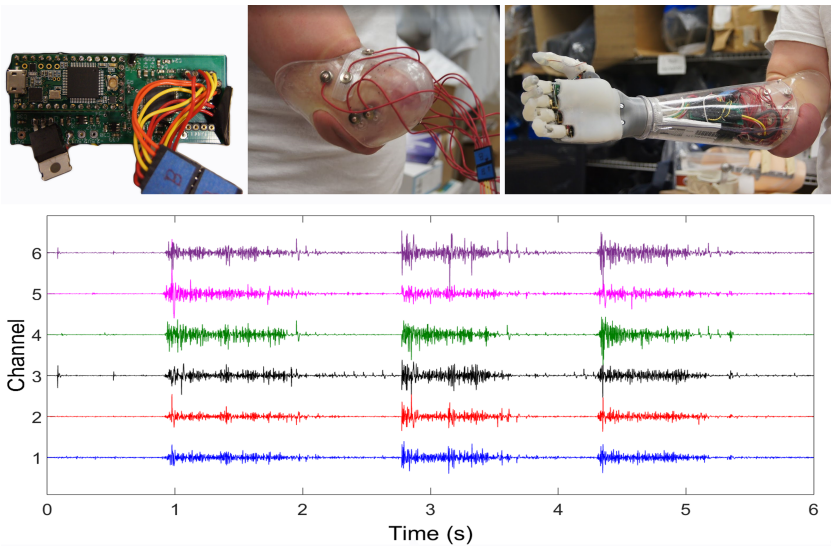

(a)

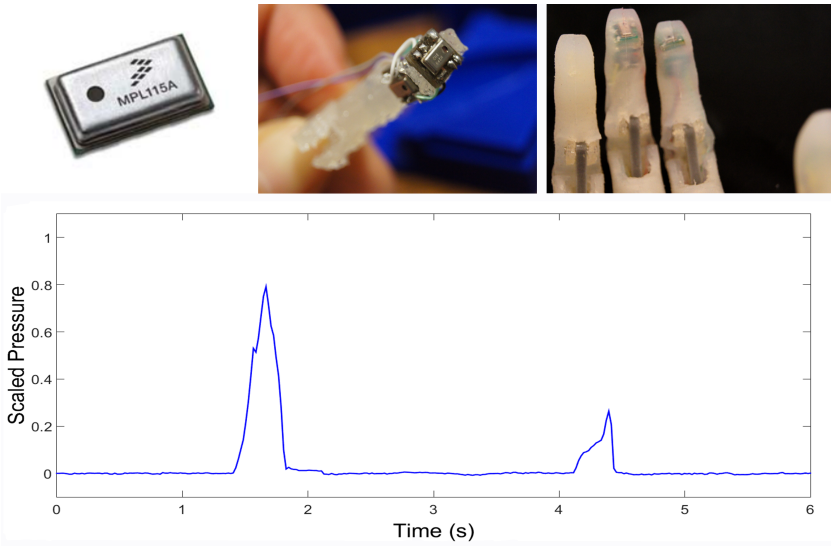

(b)

Figure 4.5: (a) EMG board based on the ADS1298 chip on the top left. Nickel-plated copper rivets used in the socket as electrodes in the top middle, followed by all the electronics fitted into the hand/socket on the top right. Six channels of EMG are displayed in the plot below the images, corresponding to 3 hand open movements. (b) The MPL115A2 barometric pressure sensor in the top left image is embedded into a bone structure of a finger in the top middle image. The top right image shows the final finger with the pressure sensors embedded inside. Below the images is a plot of the pressure reading from a single sensor showing a strong pinch followed by a weak pinch.

Sensory Substitution

In addition to providing contact reflexes, information from the pressure sensors can be delivered to the user via sensory substitution. In particular, we use electrotactile stimulation to provide this feedback, though any sensory substitution system, such as vibrotactile stimulation or skin stretch, can be used. Previous studies have shown that electrotactile stimulation can be effective in delivering information about contact to a user [13, 60]. The hand microcontroller communicates with a Teensy 3.1 microcontroller connected to a Biopac linear isolated stimulator (STMISOLA, Biopac, Goleta, CA). When contact is detected from any of the pressure sensors a 50 Hz, 200 μs constant current biphasic square pulse is delivered to the user at a predetermined current amplitude perceived to be a strong and comfortable sensation. We can also vary the amplitude of the stimulation proportionally to the amount of pressure detected by the sensors in the hand. Eventually, this system will be enhanced by adding more stimulation channels corresponding to each of the three digits with pressure sensors, and will be miniaturized to a form factor that can fit within the socket.

4.2.3 Experiments with Subject with Transradial Amputation

In order to evaluate the effectiveness of our motor control and sensory feedback systems, we performed two experiments with a 39-year-old male with a right traumatic transradial amputation. The two experiments performed involved 1) grasping an eggshell without cracking it, and 2) grasping a cup partially filled with water. The subject performed each experiment with his OttoBock two-channel myoelectric hand, as well as the new hand we developed. To interface with our hand, a socket housing six EMG electrode pairs was fabricated to fit the subject's residual limb, and a pair of stimulation electrodes were placed at the distal end of the biceps. When the pressure sensors in the new hand detected contact, the subject received 50 Hz, 200 μs constant current biphasic square pulses of electrotactile stimulation at 1 mA. Each experiment was done under visual feedback and no visual feedback conditions. Visual feedback was removed with the use of a blindfold. In the eggshell grasping task, the subject attempted to grasp a hollow egg held in his unimpaired left hand with his prosthesis ten times. The number of times the eggshell cracked upon grasping was recorded. The goal was to crack as few eggshells as possible out of the ten trials. In the water cup grasping task,

the subject was asked to grasp a 26 mL cup filled with 120 mL of water. Upon grasping the cup, the volume of water displaced was measured by marking on the cup the new height to which the water rose. The goal was to displace as little water as possible when grasping the cup.

4.3 Results & Discussion

The results of the eggshell grasping and water cup grasping tasks are shown in Table 4.2. Representative grasps from both experiments are shown in Fig. 4.6.

Table 4.2: Results for eggshell grasping and water cup grasping tasks.

	Visual Feedback	No Visual Feedback
Number of Eggshells Cracked (Original Myoelectric)	6/10	8/10
Number of Eggshells Cracked (New Hand)	0/10	0/10
Volumetric Displacement (Original Myoelectric)	19 mL	73 mL
Volumetric Displacement (New Hand)	12 mL	19 mL

When using his original myoelectric prosthesis, the subject cracked six eggs and eight eggs when visual feedback was available and then removed, respectively. However, when using the new hand, the addition of contact reflexes helped to stop grasp closure upon contact with the egg, and no eggs were cracked in both visual and no visual feedback conditions. The addition of electrotactile stimulation feedback helped the subject during no visual feedback conditions, allowing him to know when he was making contact with the egg. Furthermore, in qualitative observations, the subject was easily able to control his prosthesis to pinch, three-jaw chuck, or power grasp the eggshell using pattern recognition when using the new hand.

In the water cup grasping experiments, the subject displaced 19 mL and 73 mL of water with visual and no visual feedback, respectively. When using the new hand, he only displaced 12 mL and 19 mL under visual and no visual feedback conditions, respectively. The addition of contact reflexes aided in decreasing the

(a) (b)

Figure 4.6: Experiments with (a) the subject's original myoelectric prosthesis showing him crushing the egg and cup. However, when using the new hand as shown in (b), he successfully grasps the egg without cracking it and grips the cup with minimal water displacement.

amount of volumetric displacement of water. The addition of electrotactile stimulation again helped when there was no visual feedback. In fact, when using his original myoelectric prosthesis, the subject experienced difficulty in knowing when he was grasping the cup of water when no visual feedback was present, resulting in him prematurely releasing his grip on the cup before lifting it. In this case, if stimulation feedback was present, he would be aware that he had released

his grip before lifting the cup.

While previous studies [59] have suggested that stimulation feedback alone may not improve the user's reaction time to stop grasping once contact is made with an object, the advantage of stimulation feedback is evident when visual feedback is not available. Furthermore, when coupled with contact reflexes, another advantage of stimulation feedback is the improvement of the embodiment of the prosthesis [61]. This effect may be further enhanced when using multiple stimulation channels corresponding to each pressure sensor in the fingertips. To truly test the effect of embodiment, however, longitudinal studies need to be performed. Furthermore, tests comparing performance when using contact reflexes alone to stimulation alone as well as their combination should be performed to quantify their effectiveness. We have integrated all components into the socket and hand so that we may perform these experiments (though currently the sensory substitution system is not integrated fully in the socket, which we plan to do in future work).

4.4 Conclusion

In this paper we described the design and implementation of a prosthetic hand that enables sensorimotor control for people with transradial amputations. Specifically, this hand integrates EMG pattern recognition with contact reflexes and sensory substitution, that can all be integrated with standard sockets to facilitate long-term testing. This hand can be built for around $550 and we have open-sourced all of the designs and materials so it can be built by those in the research community and in developing nations. We showed that the use of contact reflexes and sensory substitution improves the grasping of delicate objects like eggshells and a cup of water, when compared to standard myoelectric prostheses. Supplementary Video 4.1 shows the hand in action. All files, designs, materials, and source code can be found on our website[2].

CHAPTER 5

THE RELATIONSHIP BETWEEN ENERGY, PHASE CHARGE, IMPEDANCE, AND PERCEIVED SENSATION IN ELECTROTACTILE STIMULATION[1]

Electrotactile stimulation is a common method of sensory substitution and haptic feedback. One problem with this method has been the large variability in perceived sensation that derives from changes in the impedance of the electrode-skin interface. One way to reduce this variability is to modulate stimulation parameters (current amplitude and pulse duration) in response to impedance changes, which are reflected in the time domain by changes in measured peak resistance, R_p. To work well, this approach requires knowing precisely the relationship between stimulation parameters, peak resistance, and perceived sensation. In this chapter, experimental results show that at a constant level of perceived sensation there are linear relationships between R_p and both peak pulse energy, E_p, and phase charge, Q, from which stimulation parameters are easily computed. These linear relationships held across different subjects, sessions, magnitudes of sensation, stimulation locations, and electrode sizes. The average R^2 values for these linear relationships were 0.941 for E_p vs. R_p and 0.925 for Q vs. R_p, indicating a nearly perfect fit.

5.1 Introduction

Electrotactile stimulation is the application of electrical current over the skin to stimulate sensory nerves. The sensations elicited from electrotactile sensation can be felt as vibration, touch, tingling, itching, pinching, pressure, and pain, among others, by varying the waveform, frequency, location, or electrodes [42]. Consequently, electrotactile stimulation is often used in sensory substitution applications, where a user replaces a lost sensory modality with another sense [62]. In the case of electrotactile sensory substitution, the lost sensory modality is replaced

[1]This work includes material published in [52].

Table 5.1: List of notation.

Abbreviation	Meaning
I	Current
T	Pulse Duration
V_p	Peak Voltage
R_p	Peak Resistance
Q	Phase Charge
$\hat{Q}$	Desired Phase Charge
E_p	Peak Pulse Energy
m_Q	Slope of Q vs. R_p constant sensation line
m_E	Slope of E_p vs. R_p constant sensation line
(x^*, y^*)	Point of convergence of Q vs. R_p constant sensation lines

with touch. Electrotactile stimulation is also useful as a method for delivering information via haptic feedback to a user, such as conveying texture in a multitouch display [63], suture tension to a physician teleoperating a surgical robot [64], or touch and proprioception to amputees who wear prostheses [5].

One problem with electrotactile stimulation has been the large variability in perceived sensation that derives from changes in the impedance of the electrode-skin interface. The changes in impedance may be caused by physiological disturbances, such as the accumulation of sweat, or by mechanical disturbances, such as varying contact between the electrode and the skin [42]. The impedance of the electrode-skin interface is usually determined by using a RC circuit model. As the capacitor charges, the voltage across the electrode-skin interface will eventually reach a steady state value. The impedance of the electrode-skin interface is defined as the steady state voltage divided by the applied current amplitude (Fig. 5.1) [42, 65]. However pulse durations used in electrotactile stimulation are typically not long enough for the voltage to reach steady state [42,66]. As a result, researchers use pre-steady state voltage measurements and divide them by the applied current amplitude to obtain a resistance. Like the impedance, this resistance

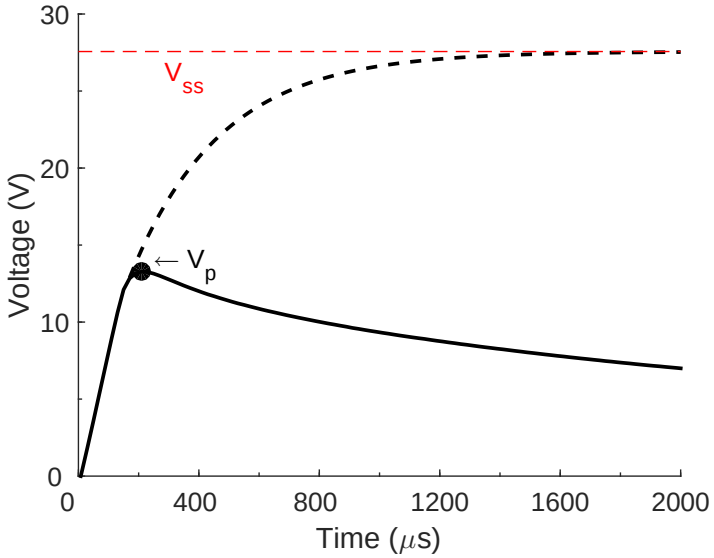

Figure 5.1: Voltage response across two electrodes during a 200 µs monophasic pulse at 2 mA. The impedance is usually defined according to the capacitive charging equation, $V(t) = V_{ss}(1 - e^{-t/RC})$, where V_{ss} is the steady-state voltage, and R and C are the resistive and capacitive components of the impedance, respectively. R is equal to V_{ss} divided by the applied current. Since pulse durations typically used in stimulation end before the voltage reaches steady-state, researchers take the peak voltage (V_p) at the end of the pulse and divide that by the current to obtain a value of resistance, which we refer to as peak resistance (R_p). In this example, the black solid line is the actual measured voltage response, and the black dashed line is the theoretical voltage waveform taken to steady-state when fit with the capacitive charging equation.

also changes in response to external disturbances such as pushing or peeling on the electrodes [62, 66]. As an example, we applied a 3.5 mA, 200 µs, 20 Hz constant current positive monophasic square pulse across the skin superficial to the left flexor carpi radialis in a 21 year-old male subject (Fig. 5.2a). The current passes through the skin across various mechanoreceptors and nerve endings to produce sensation (Fig. 5.2b). If the electrode is peeling off, the current becomes concentrated in a smaller area on the surface of the skin due to poor contact, and can result in a shock. To observe the effect of changing resistance with electrode contact, the subject peeled off the electrode by roughly 25%, 50%, and 75% every five seconds. We measured the peak voltage (V_p) across the electrodes of every pulse and show the mean and standard deviation of the voltage response for a single pulse in Fig. 5.3a. We then obtain the peak resistance (R_p) by dividing each V_p by the current amplitude, I. When the electrode is peeled off, the increase in

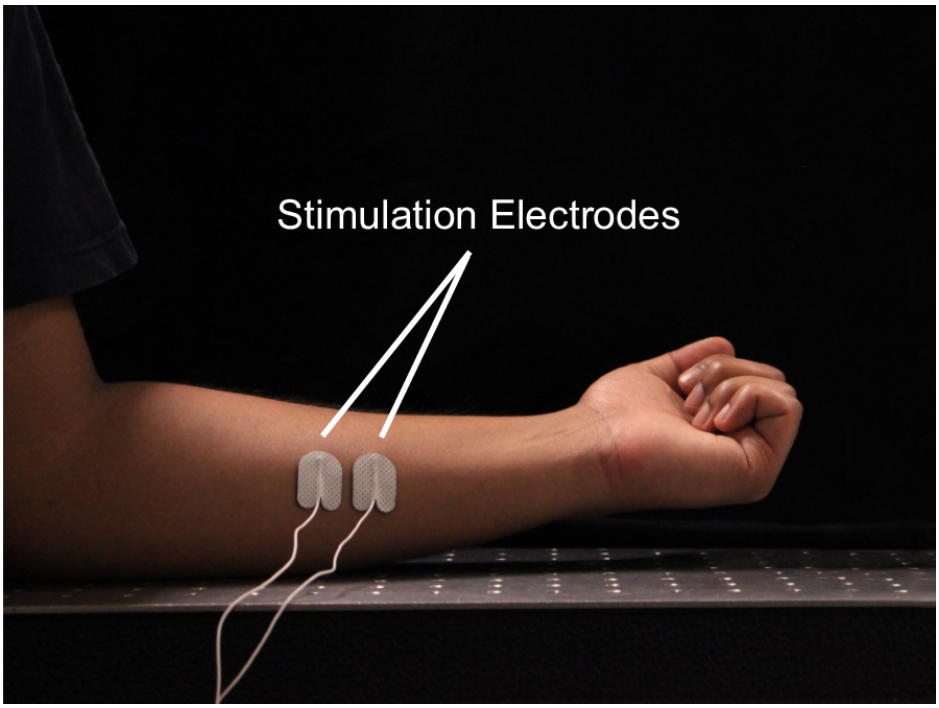

(a)

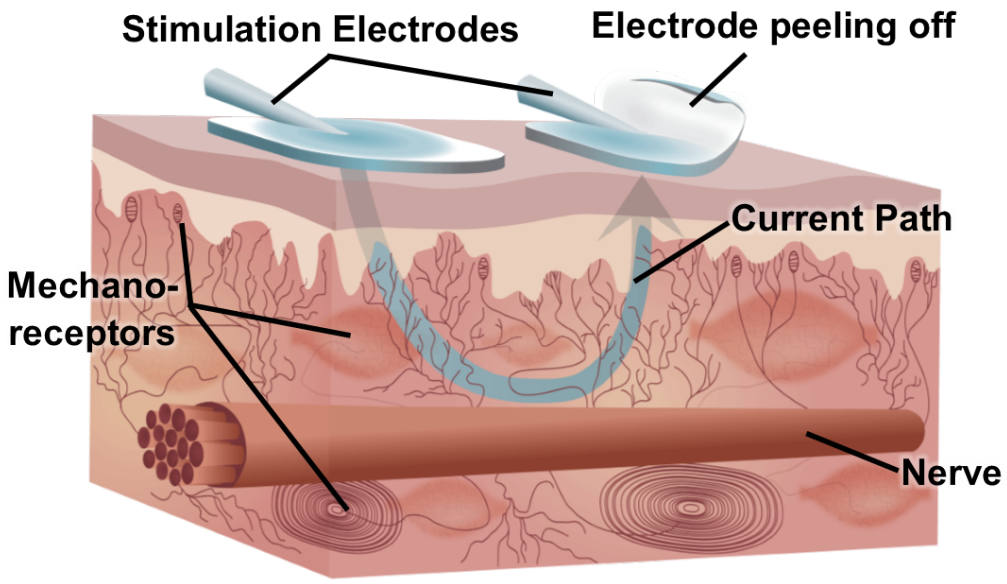

(b)

Figure 5.2: (a) Stimulation electrodes placed over the skin superficial to the left flexor carpi radialis muscle. (b) Current flows across the mechanoreceptors in the skin to produce sensation. When the electrode is peeling off, current density increases, resulting in a stronger sensation.

current density is reflected by a sharp increase in R_p, and the subject experienced increased stimulation intensities to the point of discomfort as the electrode contact area decreased. The mean and standard deviation of the data over five trials are shown in Fig. 5.3b.

Efforts have been made over the past thirty years to reduce variability in perceived sensation by modulating stimulation parameters, specifically current amplitude (I) and pulse duration (T), in response to measurements of impedance. To work well, these approaches require knowing precisely the relationship between stimulation parameters, impedance, and perceived sensation. Existing characterizations of this relationship are able to reduce variability in perceived sensation, but rely on poor models relating sensation intensity to stimulation parameters. For example, seminal work by Tachi et al. [62] equated a constant level of sensation with a constant pulse energy. This work was based upon the assumption that impedance is independent of applied current, an assumption that is known to be false [42, 67]. More recent work by Kajimoto [66] discarded this assumption but relied on a relationship between pulse duration and impedance with a low R^2 value (0.359), suggesting that results may not have been consistent across different subjects, magnitudes of sensation, and locations of stimulation. Kantor et al. [68] observed that phase charge remains nearly constant for constant sensation, but other studies—such as one by Baker and Bowman [69]—provide evidence that phase charge can vary even while perceived sensation remains constant. In this paper, we establish a relationship between stimulation parameters, impedance, and perceived sensation that better matches experimental results.

In particular, we perform an experiment to model the relationship between peak resistance R_p and both peak pulse energy E_p and phase charge Q. We show that at a constant level of perceived sensation these are linear relationships that hold across ten different subjects, two sessions, two magnitudes of sensation, three different stimulation locations, and two electrode sizes. From these linear relationships, we can easily compute stimulation parameters and we implement a controller that modulates current amplitude and pulse width in response to changes in R_p to maintain a constant sensation intensity. We use R^2 to evaluate how well these linear relationships fit the experimental data. In our previous work, we investigated the linear relationships between E_p vs. R_p and Q vs. R_p with only five subjects [52]. Here, we double the number of subjects, further validating our model.

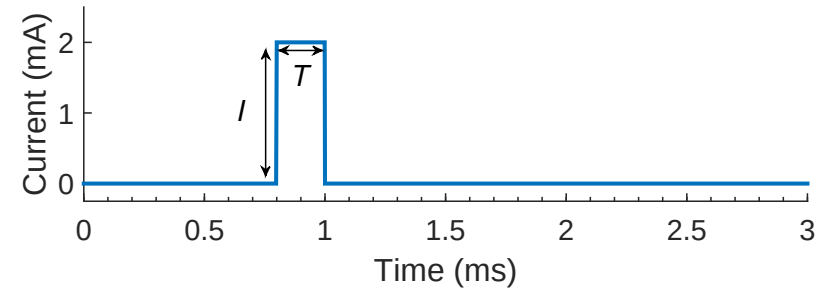

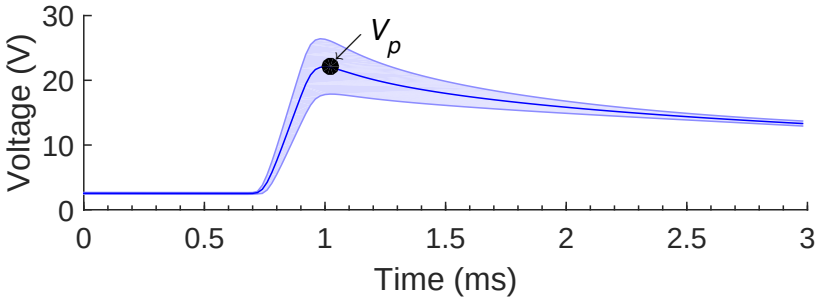

(a)

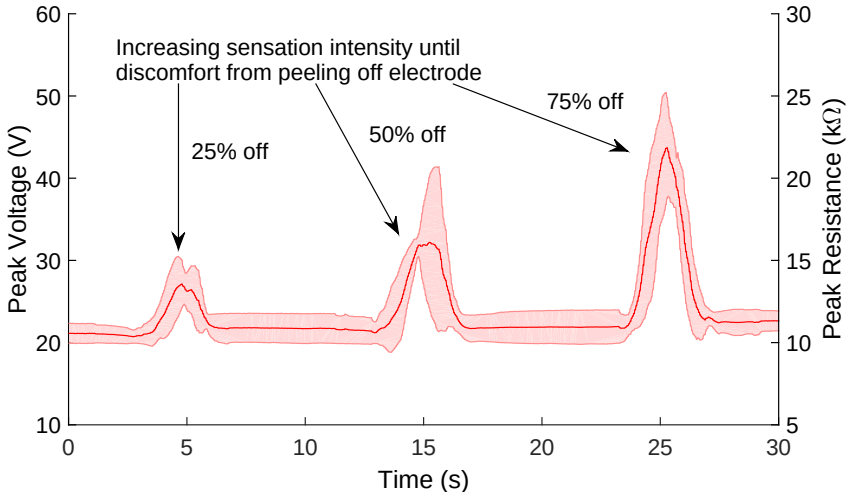

(b)

Figure 5.3: (a) Current stimulation waveform (top) delivered across the skin and the resulting measured voltage waveform (bottom). The mean and standard deviation for an individual pulse are shown as the subject peeled off and reapplied an electrode. The recorded voltage, V_p, is the peak of the voltage waveform. (b) Changes in the peak resistance of the electrode-skin interface due to peeling off and reapplying the electrode. As more of the electrode is peeled off, the sensation gets stronger, leading to discomfort. The mean and standard deviation over five trials are shown.

5.2 Methods

Ten subjects (five male, five female, ages: 20-30) without arm impairment, volunteered for the experiment. Subjects were asked to participate in two sessions held on different days with four trials being held each session, testing eight conditions total. In the first session (Session A), the four conditions tested were 1) weak and 2) strong stimulation using two large 20 x 25 mm electrodes (AMBU Neuroline 710) placed over glabrous skin on the proximal left forearm over the flexor carpi radialis muscle, and 3) weak and 4) strong stimulation using two small 15 x 20 mm electrodes (AMBU Neuroline 700) in the same location. In the second session (Session B), the four conditions tested were again 5) weak and 6) strong stimulation using the larger electrodes on the forearm, and weak stimulation using the larger electrodes on 7) the skin lateral to the long head of the left biceps brachii muscle, and 8) the right lumbar paraspinal area of the back. In all conditions, the center-to-center distance between the electrodes was 3 cm. Monophasic positive square pulses generated by an NI-myDAQ (National Instruments, Austin, TX) data acquisition device were fed to a STMISOLA linear isolated stimulator (BIOPAC Systems, Goleta, CA) that provided a constant current stimulation to the subject. The voltage across the electrodes was also recorded by the NI-myDAQ. All data were collected and processed using the MATLAB DAQ Toolbox (MathWorks, Natick, MA). All procedures and equipment, including the example test described in Sec. 5.1, were approved by the Institutional Review Board of the University of Illinois at Urbana-Champaign (#13920).

In all trials, the method of adjustments was used to match current amplitudes (I) at different pulse durations (T) to a particular magnitude of sensation (Fig. 5.4a). T was varied between 200-700 µs in increments of 50 µs. Two magnitudes of sensation were used, weak and strong. The weak magnitude of sensation was chosen to be around the subjects sensation threshold at 200 µs, and the current amplitude was then increased until it felt like a strong yet comfortable magnitude of sensation. Pulses were delivered at a frequency of 50 Hz. In each trial, eleven data points were collected that had the same perceived magnitude of sensation, consisting of the value of I and the peak voltage (V_p) corresponding to each value of T. V_p was computed as the average of the peak voltages over ten pulses. From this, we derived values for R_p, the peak resistance,

$$R_p = \frac{V_p}{I} \,, \tag{5.1}$$

Q, the phase charge for a monophasic square wave,

$$Q = \int_0^T I \, \mathrm{d}t = IT \ , \tag{5.2}$$

and E_p, the peak pulse energy for a monophasic square wave,

$$E_p = R_p \int_0^T I^2 \, \mathrm{d}t = R_p I^2 T. \tag{5.3}$$

Each trial began by adjusting the current of a waveform with T=200 µs until the sensation intensity for a specified magnitude of sensation was reached. To ensure that each sensation intensity felt the same across all pulse durations, each sensation felt above T=200 µs was compared to the initial reference sensation at T=200 µs. The reference sensation would be presented to the subject for two seconds, followed by a two second period of rest before presenting the new stimulation for two seconds at a higher pulse duration. The subject would then make a decision on whether the new stimulation felt weaker, stronger, or the same as the reference stimulation. The subjects were allowed to repeat the presentation of stimulations as many times as they felt necessary to make a clear decision, typically taking no longer than a minute. In this short amount of time, perceived sensation intensity should not vary for the same stimulation parameters since the impedance of the electrode-skin interface should not vary significantly.

Because a range of current amplitudes may result in the same perceived sensation level, the current was increased just beyond the upper difference limen between the new sensation and the reference sensation. The current amplitude was then reduced just below this threshold to the maximum value at which the two sensations felt the same. The final current amplitude and voltage was recorded. Finally, to validate that the sensation intensity at each pulse duration felt the same, a new reference was set at the stimulation threshold determined at 700 µs, and all current amplitudes and voltages at shorter pulse widths were compared again and adjusted to match the sensation felt. Since skin properties (e.g. hydration) may vary daily, the first two conditions tested in Session A (weak and strong stimulation with larger electrodes on the forearm) were repeated in Session B to observe trends despite different skin conditions. The other four conditions that were tested investigated the effect of changing the size of the electrodes as well as the stimulation location on sensation intensity. For the smaller electrodes, stimulation took place on the forearm at weak and strong magnitudes of sensation. The forearm, bi-

cep, and back locations were chosen since they are commonly chosen stimulation sites in haptic feedback studies [5, 6, 62, 68, 70–72].

5.3 Results

5.3.1 Validation of the relationship between I and T at a constant sensation level

In order to validate that the recorded current amplitudes for a given pulse duration match the recorded values in previous studies, we compared I vs. T across all subjects, sessions, magnitudes of sensation, stimulations locations, and electrode sizes. They follow the logarithmic trend mentioned in [42, 62, 73] (Fig. 5.4a). If we take the average of the slopes of the best fit lines of the log of the data, we obtain a value of -0.497, which very closely matches the -0.5 slope that Tachi et al. reports in [62]. In Fig. 5.4b, we show a subset of the data plotted with their best fit lines that have slopes constrained to -0.5. The average R^2 value of the constrained best fit lines for all subjects and conditions is 0.956, indicating a near perfect fit. Therefore, our results when comparing I and T are validated by their consistency with previous studies.

5.3.2 Results across subjects, sessions, magnitudes of sensation, location, and electrode size

Data showing the relationship between both E_p vs. R_p and Q vs. R_p across two of the ten subjects, both sessions, both magnitudes of sensation, all three stimulation locations, and both electrode sizes are plotted in Figs. 5.5-5.6. The results from all ten subjects are shown in Figs. 5.7-5.8. Each sensation felt at each data point of the same color and marker was equivalent in subjective intensity. All subjects across all conditions showed strong linear trends for both E_p vs. R_p and Q vs. R_p. Furthermore, when fitting best fit lines through the data, all lines tended to originate from a common point. When comparing weak and strong magnitudes of sensation, stronger sensations had higher slopes for the linear trend in every case.

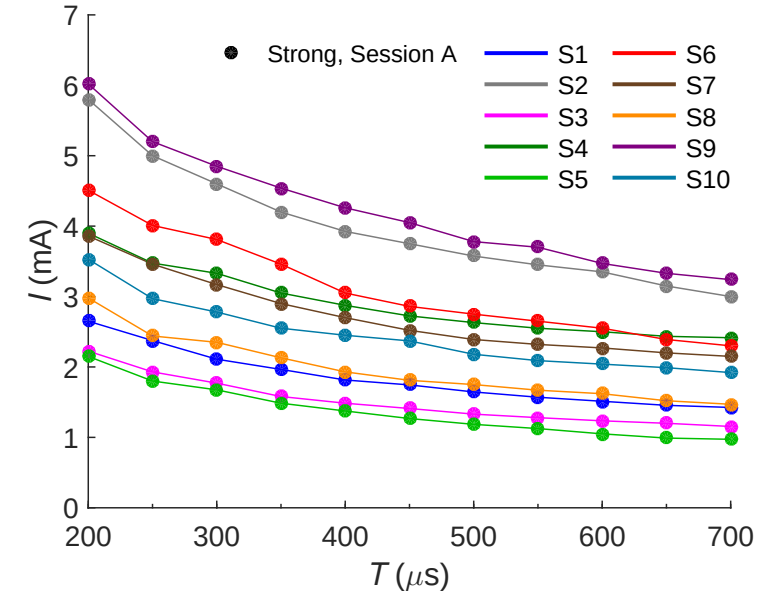

(a)

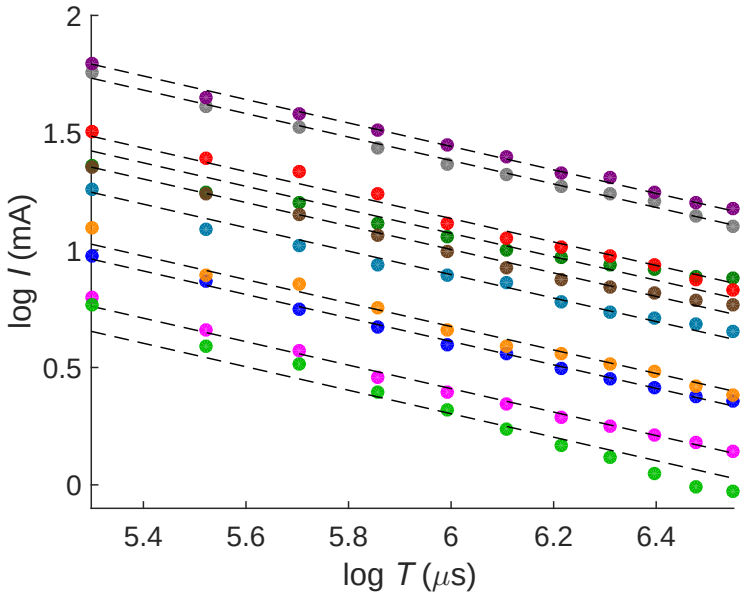

(b)

Figure 5.4: (a) Current (I) vs. pulse duration (T) for 10 subjects. The data points for each subject represent stimulation parameters having the same perceived sensation intensity. For clarity, only the data from Session A at the strong magnitude of sensation are shown. (b) Linear relationships from the same data when plotted on a log-log scale. The best fit lines shown are constrained to a slope of -0.5.

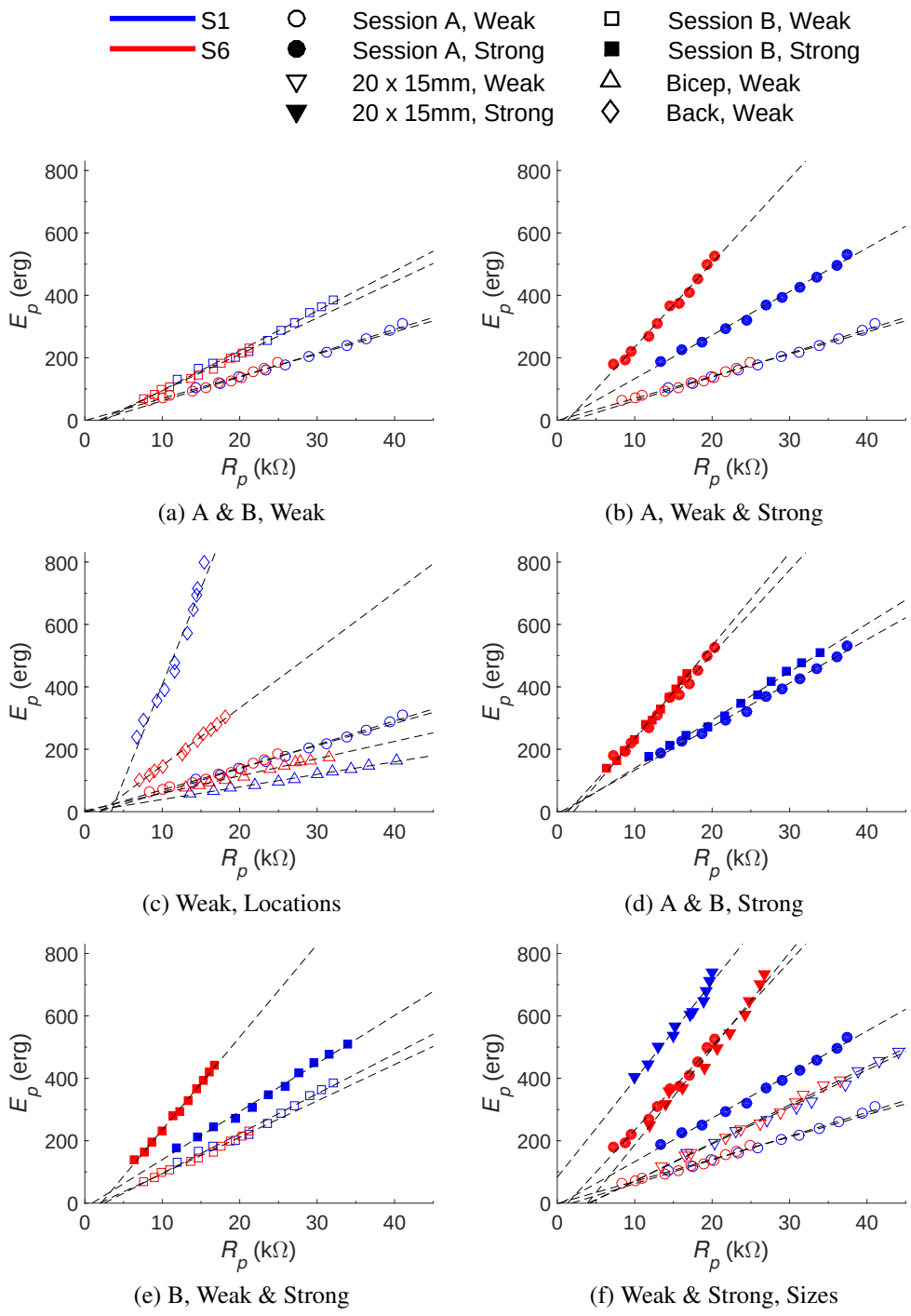

(a) A & B, Weak

(b) A, Weak & Strong

(c) Weak, Locations

(d) A & B, Strong

(e) B, Weak & Strong

(f) Weak & Strong, Sizes

Figure 5.5: Peak pulse energy (E_p) vs. peak resistance (R_p) plots for two subjects showing linear trends across (a) two sessions at weak magnitude, (b) two magnitudes of sensation during Session A, (c) three stimulation locations (forearm, bicep, and back), (d) two sessions at strong magnitude, (e) two magnitudes of sensation during Session B, and (f) two electrode sizes (20 x 25 mm and 20 x 15 mm).

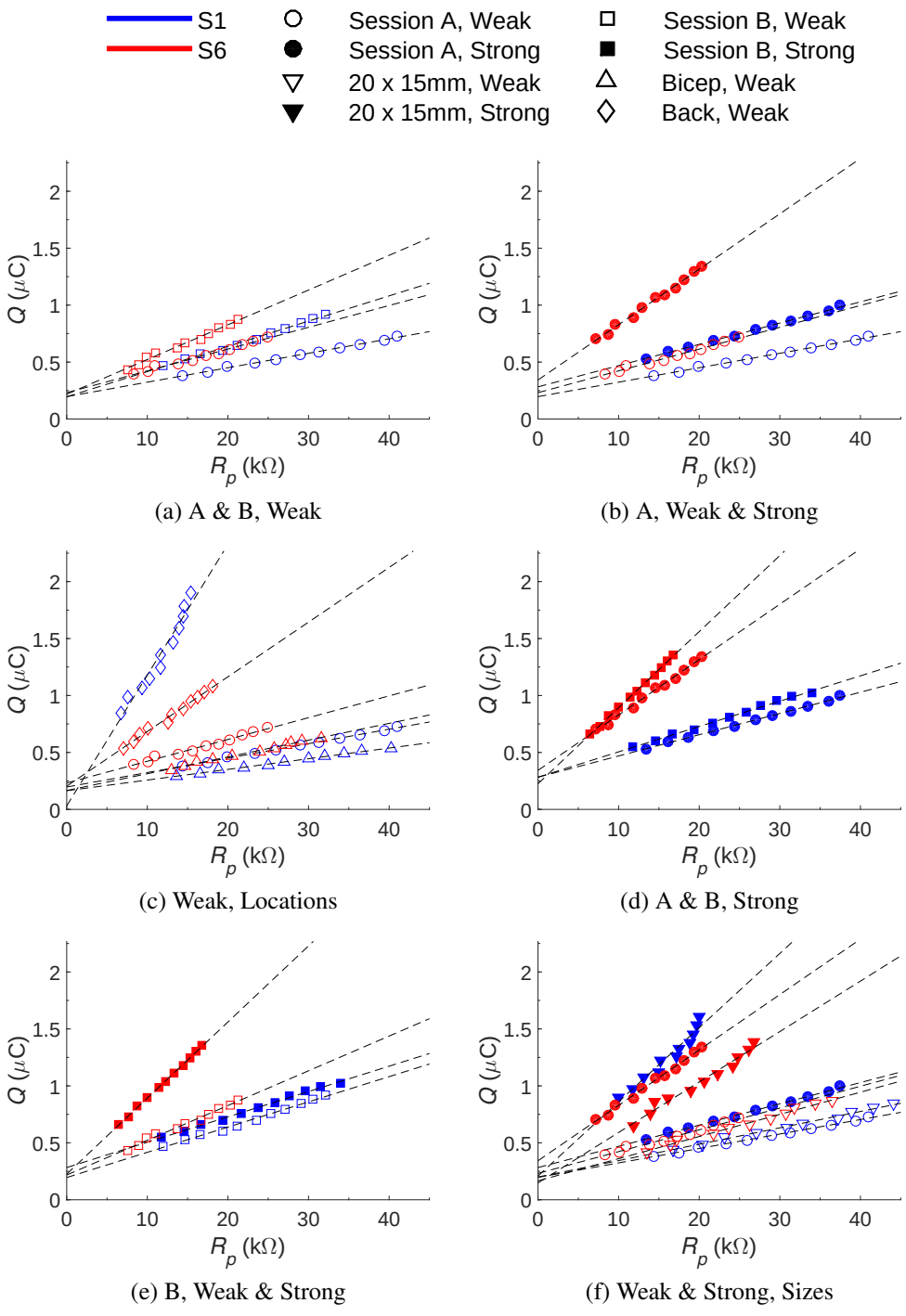

(a) A & B, Weak

(b) A, Weak & Strong

(c) Weak, Locations

(d) A & B, Strong

(e) B, Weak & Strong

(f) Weak & Strong, Sizes

Figure 5.6: Phase charge (Q) vs. peak resistance (R_p) plots for two subjects showing linear trends across (a) two sessions at weak magnitude, (b) two magnitudes of sensation during Session A, (c) three stimulation locations (forearm, bicep, and back), (d) two sessions at strong magnitude, (e) two magnitudes of sensation during Session B, and (f) two electrode sizes (20 x 25 mm and 20 x 15 mm).

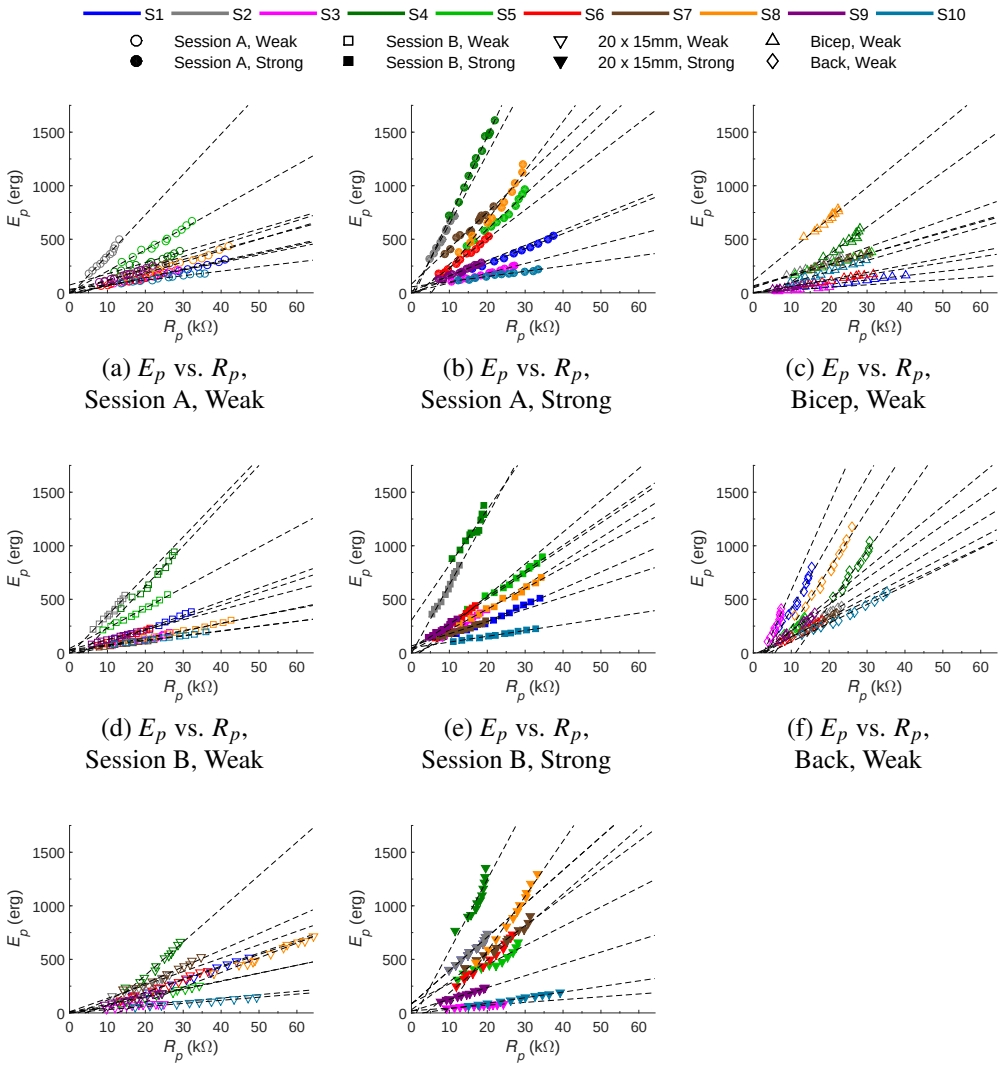

(a) E_p vs. R_p, Session A, Weak

(b) E_p vs. R_p, Session A, Strong

(c) E_p vs. R_p, Bicep, Weak

(d) E_p vs. R_p, Session B, Weak

(e) E_p vs. R_p, Session B, Strong

(f) E_p vs. R_p, Back, Weak

(g) E_p vs. R_p, 20x15mm, Weak

(h) E_p vs. R_p, 20x15mm, Strong

Figure 5.7: Peak energy (E_p) vs. peak resistance (R_p) plots for all ten subjects showing linear trends across each of the eight conditions.

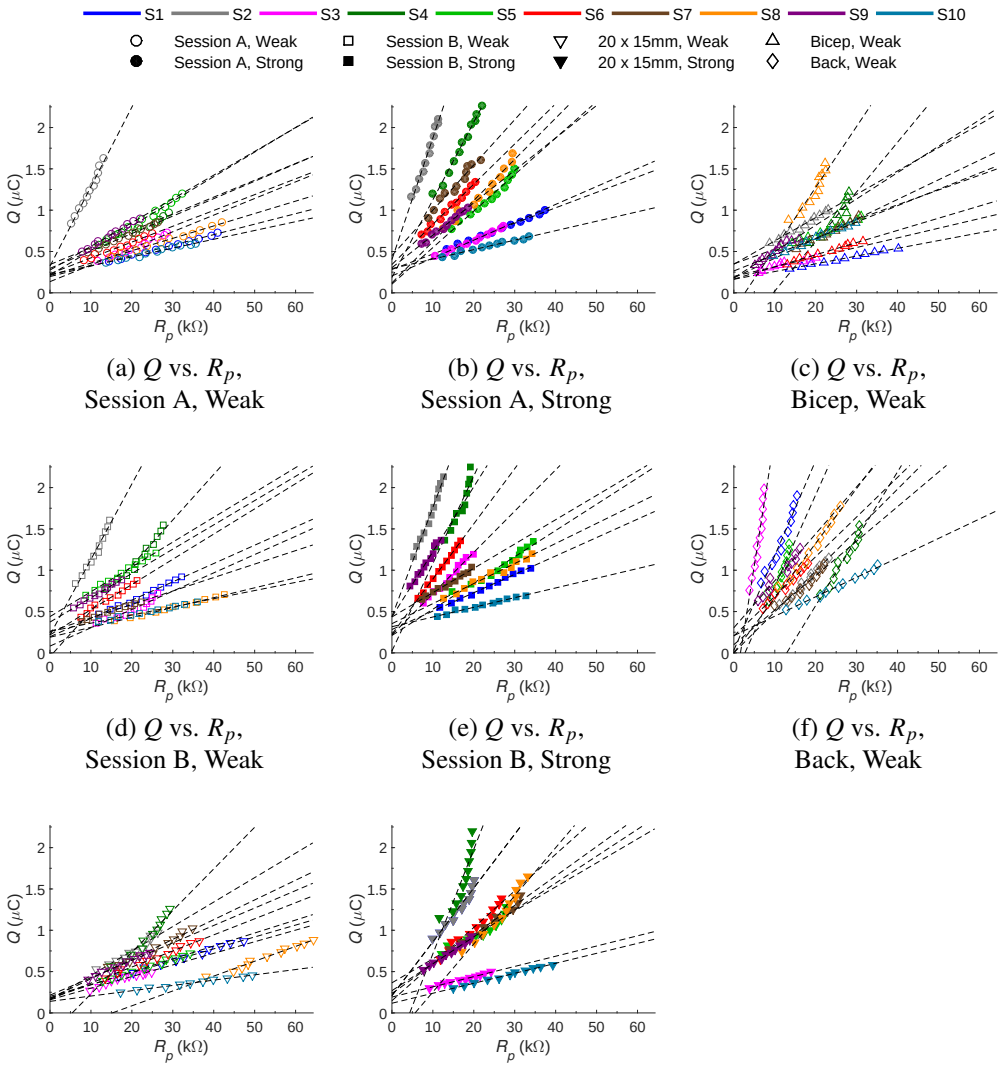

(a) Q vs. R_p, Session A, Weak

(b) Q vs. R_p, Session A, Strong

(c) Q vs. R_p, Bicep, Weak

(d) Q vs. R_p, Session B, Weak

(e) Q vs. R_p, Session B, Strong

(f) Q vs. R_p, Back, Weak

(g) Q vs. R_p, 20x15mm, Weak

(h) Q vs. R_p, 20x15mm, Strong

Figure 5.8: Phase charge (Q) vs. peak resistance (R_p) plots for all ten subjects showing linear trends across each of the eight conditions.

5.3.3 Aggregate results

The data for two of the ten subjects with all conditions combined are shown in Figs. 5.9-5.10. Based on the trends of the individual best fit lines converging to a common origin point, we determined values for the points of convergence for both E_p vs. R_p and Q vs. R_p.

Since $E_p = R_p I^2 T$ (Eq. 5.3), it holds that when $R_p = 0$, $E_p = 0$. Consequently, this dictates that all linear trends between the two variables should go through the origin. Furthermore, the slopes of these lines equal $I^2 T$.

Because the value of Q is not defined by R_p, we solved for the optimal point of convergence over all the trials. The problem can be modeled using the linear equation,

$$y_{ki} - y^* = m_k^*(x_{ki} - x^*) \ ,$$

where k is the trial (line) number, i is the i-th point within that trial, x_{ki} is the R_p value for a specific point in a trial, y_{ki} is the value of Q for a specific point in a trial, (x^*, y^*) is the ordered pair representing the point of convergence of all the lines, and m_k^* is the slope of the line for a specified trial. We solved for m_k^*, y^*, and x^*, such that the R^2 value for each trial is maximized,

$$\max_{m_k^*, y^*, x^*} \sum_k \mathrm{R}_k^2 \ ,$$

where

$$\mathrm{R}_k^2 = 1 - \frac{\sum_i (y_{ki} - y^* - m_k^*(x_{ki} - x^*))^2}{\sum_i (y_{ki} - \bar{y}_{ki})^2} \ . \tag{5.4}$$

The numerator in the second term of the equation above is the sum squared error determined by the linear model we are using, while the denominator is the total sum of squares. The $m_k^* x^*$ term makes the objective function nonlinear, and it can be shown that the Hessian of the objective function is not positive semidefinite, which means that the function is nonconvex. As a result, we used gradient ascent to find a locally optimal solution to the maximization problem. For our initial guess of x^*, a grid search was performed between $\pm 3\,\mathrm{k\Omega}$ and $\pm 3\,\mu\mathrm{C}$ in steps of 0.25. These limits were chosen since in our previous work, the locally optimal point was found to be (-0.81 kΩ, 0.21 μC). Step sizes for updating x^*, y^* and m_k^* on successive iterations were chosen to be 10^{-5}, 10^{-7}, and 10^{-6}, respectively. The algorithm ran for 10^6 iterations before stopping. Each initial guess converged to (-1.67 kΩ, 0.186 μC) for (x^*, y^*). Using this result, linear regression was applied

to each of the trials with the constraint that the line must go through this new point of convergence. The R^2 values from the constrained linear regression are reported in Table 5.2. The average value for E_p vs. R_p was 0.941 and for Q vs. R_p was 0.925, where an R^2 value of 1 denotes a perfect fit to the data.

5.4 Discussion

5.4.1 The linear relationship between E_p and R_p

Evidence for the linear relationship between E_p and R_p is provided both by our results and Tachi et al. [62]. The large average R^2 (0.941) for E_p vs. R_p strongly suggests that this relationship is consistent across all subjects, sessions, magnitudes of sensation, stimulation locations, and electrode sizes. Because $E_p = R_p I^2 T$ (Eq. 5.3), the slopes of the best fit lines in the E_p vs. R_p plot in Fig. 5.9 are equivalent to I^2T. This suggests that the value of I^2T is constant for constant sensation intensities, as determined by Tachi et al.

Though similar results were found by Tachi et al., an erroneous assumption led them to a different conclusion. As in our study, Tachi et al. adjusted pulse durations of monophasic square pulses and found the amount of current needed to reach stimulation threshold for three subjects. They reported that for pulse durations under 1 ms there was a logarithmic trend, that when plotted on a log-log scale resulted in a linear curve with slope -0.5. This is validated by our data as well, which when linearly fit with slopes of -0.5 achieved an R^2 of 0.956. For a specific waveform at a constant sensation intensity, the relationship between I and T can be written as $\log I = -0.5 \log T + c$, where c is a constant term. It follows that $I = c' T^{-0.5}$, and after squaring both sides and rearranging terms, we obtain $I^2T = c''$. This means that for a given magnitude of sensation, the value of I^2T always remains constant. Under the assumption that the impedance of the electrode-skin interface was constant over the course of an experimental trial, Tachi et al. reached the conclusion that the energy, $E = ZI^2T$, where Z is the impedance of the electrode-skin interface, is also constant for a constant sensation intensity. This assumption fails because it is well-studied that changing I, as Tachi et al. did, affects the impedance significantly [42, 67]. Therefore, for two different values of I, regardless of whether I^2T is constant, Z would not be the same. Furthermore, in his implementation of the constant energy controller, when

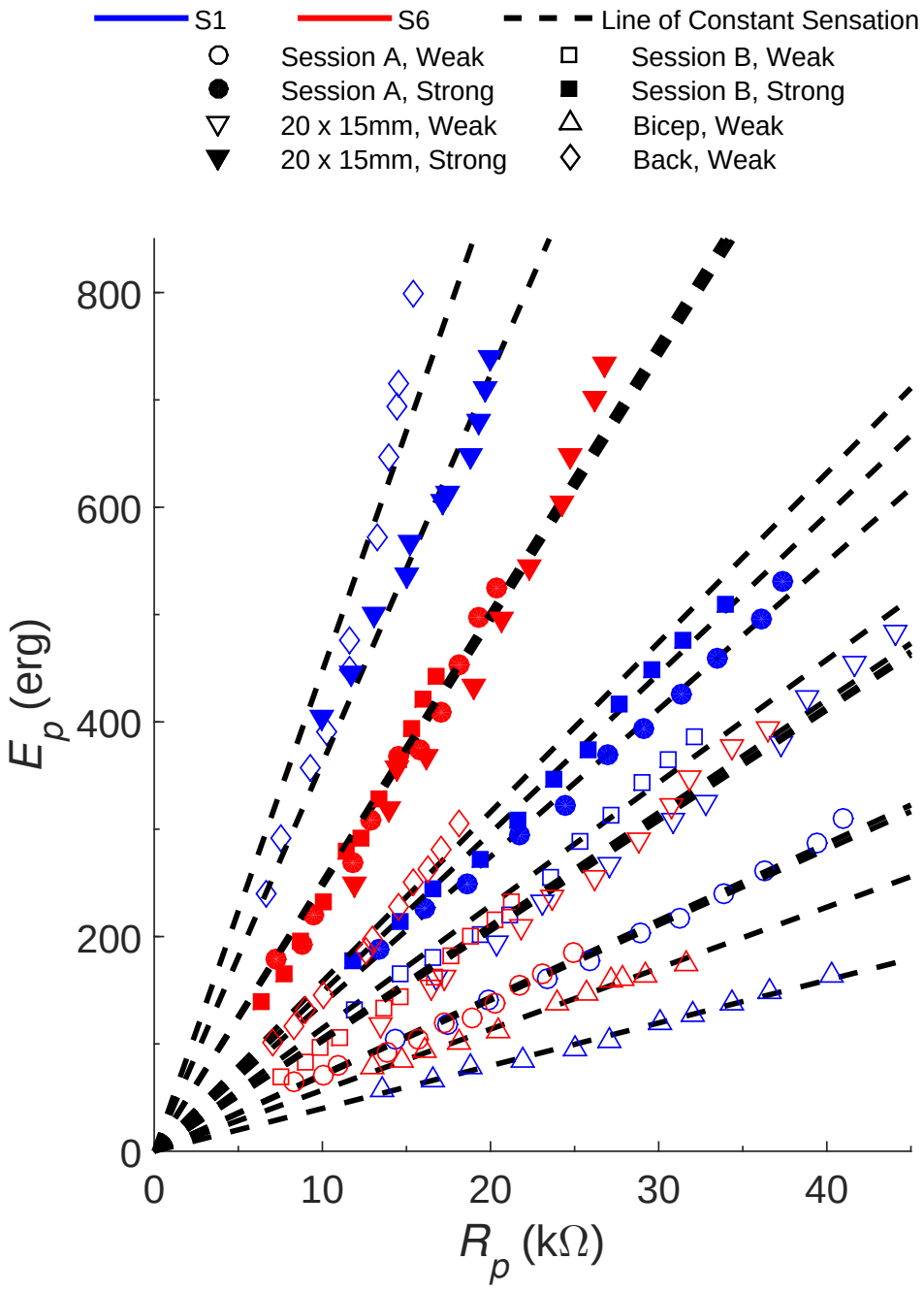

Figure 5.9: Peak pulse energy vs. peak resistance plots aggregating all trials from the two subjects in Fig. 5.5 across sessions, magnitudes of sensation, stimulation locations, and electrode sizes. Best fit lines were constrained to go through the origin. Each best fit line represents a line of constant sensation. The average R^2 values across all conditions for all ten subjects was 0.941 for E_p vs. R_p.

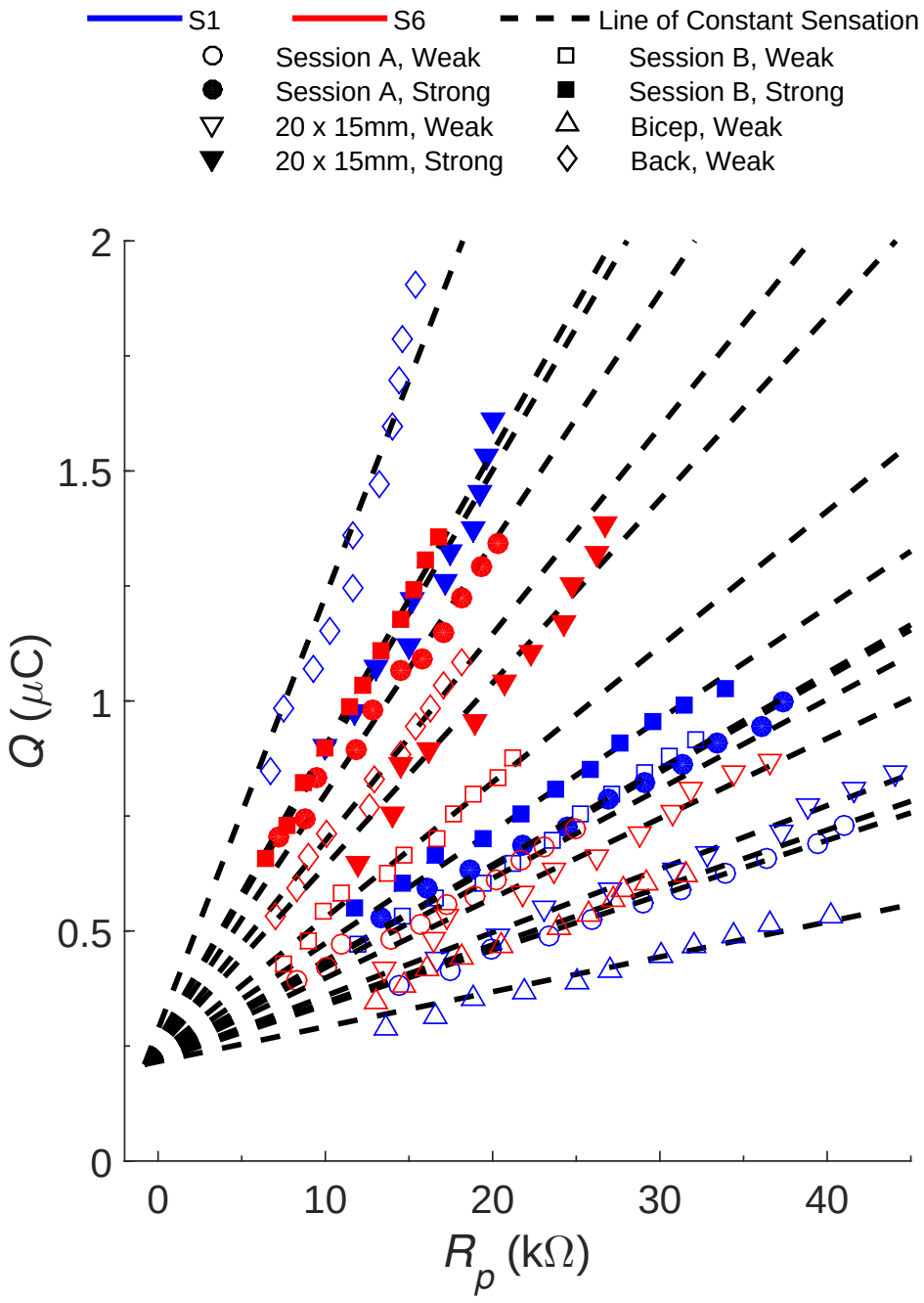

Figure 5.10: Phase charge vs. peak resistance plots aggregating all trials from the two subjects in Fig. 5.6 across sessions, magnitudes of sensation, stimulation locations, and electrode sizes. Best fit lines were constrained to go through an optimal point of convergence (-1.67 kΩ, 0.186 μC). Each best fit line represents a line of constant sensation. The average R^2 values across all conditions for all ten subjects was 0.925 for Q vs. R_p.

Table 5.2: R^2 regression statistics aggregated across all sessions, subjects, stimulations levels, locations, and electrode sizes.

Parameters	Mean	Std	Min	Max	Median
E_p vs. R_p	0.941	0.0580	0.764	0.995	0.965
Q vs. R_p	0.925	0.0876	0.606	0.996	0.956

the value of Z changed over time, I would be adjusted to maintain a constant E for a fixed T. Consequently, the value of I^2T will always be changing while trying to maintain a constant level of sensation. This contradicts the notion that I^2T must be held constant in order to maintain a constant level of sensation, as evidenced by the data of Tachi et al. as well as ours.

5.4.2 The linear relationship between Q and R_p

Similar to the relationship between E_p and R_p, the large average R^2 (0.925) for Q vs. R_p provides strong evidence of a linear relationship between the variables that is consistent across all subjects, sessions, magnitudes of sensation, stimulation locations, and electrode sizes. However, while the definition of E_p mandates that the point of convergence of the E_p vs. R_p constant sensation lines is at the origin, it is unknown why the point of convergence of the Q vs. R_p constant sensation lines is approximately (-1.67 kΩ, 0.186 μC). One possibility is that given a particular resistance, neurons require a specific amount of charge to accumulate before they will fire. This is not the case for the relationship between E_p and R_p since that relationship reduces to the value of I^2T being constant at a constant level of sensation, independent of the value of R_p. Future work will investigate a physiological model that may explain why the convergence point for Q vs. R_p is not at the origin.

The linear relationship we have found between Q and R_p is critical to computing stimulation parameters for constant sensation in response to impedance changes, though it has not been considered in previous studies. As previously mentioned, the value of I^2T should be constant in order to maintain a constant sensation intensity. However, simply holding this value constant is not sufficient because it does not account for changes in impedance. Recall the example in Fig. 5.3b and

Sec. 5.1. In this example, I and T were held fixed, thus making I^2T constant. Nevertheless, changes in sensation—corresponding to the changes in peak resistance shown—were still felt in light of I^2T being constant. Consequently, an additional relationship between the stimulation parameters I and T and peak resistance is necessary. Because $Q = IT$ (Eq. 5.2), the linear relationship between Q and R_p satisfies this requirement. We show how to compute I and T from the linear relationships between E_p, Q and R_p in Chapter 6.

5.5 Conclusion

The use of electrotactile stimulation is common in sensory substitution and haptic feedback applications. However, physiological and mechanical disturbances cause changes in the impedance of the electrode-skin interface, thereby causing variations in the perceived sensation level. Therefore, changes in impedance, which are reflected in the time domain by changes in R_p, must be accounted for in order to maintain a constant sensation level. In examining the effects of stimulation parameters on constant sensation, we found linear relationships between E_p and R_p, as well as Q and R_p. These linear relationships held across different subjects, sessions, magnitudes of sensation, stimulation locations, and electrode sizes. Furthermore, we determined that there is a common convergence point among all best fit lines of constant sensation in both E_p vs. R_p and Q vs. R_p. Fitting best fit lines constrained to these points resulted in average R^2 values of 0.941 and 0.925, respectively. From the relationship of E_p vs. R_p and I vs. T, we verified that I^2T is constant for constant levels of sensation, as previously determined by Tachi et al. However, we have shown that holding I^2T constant cannot alone account for changes in sensation due to varying R_p, but the linear relationship we present between Q vs. R_p can be used in conjunction to maintain a constant sensation level. In Chapter 6, we show how to use this information to compute the stimulation parameters I and T for a constant sensation level while taking impedance changes into account. We then develop and evaluate a controller to maintain constant sensation intensity based on these results.

CHAPTER 6

CONTROL OF ELECTROTACTILE SENSATION INTENSITY ENABLING LONG-TERM STIMULATION

In this chapter, we applied our model from Chapter 5 to implement a controller that holds perceived sensation intensity constant despite changes in impedance. This controller measures peak resistance and modulates stimulation parameters—the current amplitude and the pulse width—in order to keep the peak pulse energy and the phase charge on lines of constant sensation. For ten subjects, these lines of constant sensation strongly fit peak pulse energies ($\overline{R^2} = 0.941$) and phase charges ($\overline{R^2} = 0.917$) computed from subject-chosen stimulation parameters that felt constant across different peak resistance values. Extending our results to real-world activities of daily living, ten subjects were asked to ascend and descend stairs for five minutes, changing the electrode-skin interface impedance. Again, the lines of constant sensation computed pre-exercise strongly fit peak pulse energies ($\overline{R^2} = 0.950$) and phase charges ($\overline{R^2} = 0.918$) after impedance changes due to exercise. Finally, we show for a subject with a transradial amputation wearing a prosthesis that gives electrotactile feedback on fingertip contact that the controller is able to maintain constant sensation levels during activities of daily living. Furthermore, when the subject peeled off and reapplied an electrode during stimulation, the controller produced a constant perceived sensation intensity, while discomfort was felt when the controller was not used.

6.1 Introduction

In Chapter 5, we modeled the relationship between perceived sensation intensity during electrotactile stimulation and changes in the impedance of the electrode-skin interface, reflected by changes in measured peak resistance. In particular, we observed linear relationships between peak resistance and both peak pulse energy

($\overline{R^2} = 0.941$) and phase charge ($\overline{R^2} = 0.925$), when perceived sensation intensity was constant. These relationships held across different subjects, sessions, magnitudes of sensation, stimulation locations, and electrode sizes. We can use the linear relationships between E_p, Q and R_p to compute I and T to maintain a constant sensation intensity in response to changes in the electrode-skin interface impedance.

6.1.1 Computing I and T in response to changes in R_p for sensation intensity control

Using the linear relationships between E_p and R_p and Q and R_p, we can compute stimulation parameters I and T in response to changes in R_p. Fig. 6.1 shows a block diagram of this process. Suppose a subject is initially stimulated with a monophasic square pulse at some initial value of I_0 and T_0. Given these values of I_0 and T_0, we can measure R_{p0} after the initial pulse and compute the slopes of the constant sensation intensity lines using the following two equations,

$$m_E = I_0^2 T_0 \,, \tag{6.1}$$

where m_E is the slope of the constant sensation line from E_p vs. R_p and is independent of R_{p0}, and

$$m_Q = \frac{I_0 T_0 - y^*}{R_{p0} - x^*} \,, \tag{6.2}$$

where m_Q is the slope of the constant sensation line for Q vs. R_p and (x^*, y^*) is the point of convergence of all constant sensation lines for Q vs. R_p.

Now that we know the slopes of the constant sensation lines we want to stay on, suppose the peak resistance changes in response to a mechanical disturbance, such as an electrode peeling off. We can solve for the next I and T values using the equation $m_E = I_1^2 T_1$ and

$$\hat{Q} = m_Q(R_{p1} - x^*) + y^* = I_1 T_1 \,, \tag{6.3}$$

where $\hat{Q}$ is the desired Q determined from the Q vs. R_p constant sensation line. Rearranging these equations, we obtain

$$I_1 = \frac{m_E}{\hat{Q}} \,, \quad T_1 = \frac{\hat{Q}^2}{m_E} \,. \tag{6.4}$$

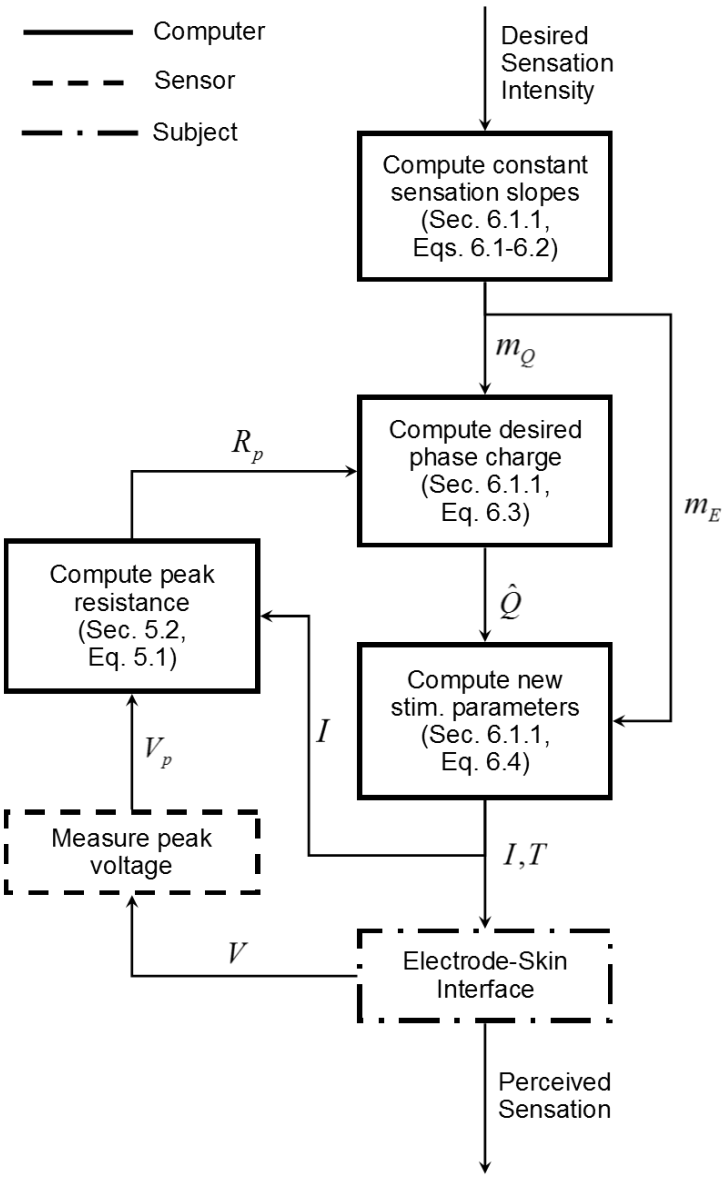

Figure 6.1: Block diagram for the control system to modulate sensation intensity. First, a sensation intensity is chosen that is mapped to m_E, equal to I^2T and the slope of the constant sensation line that relates E_p and R_p, and m_Q, the slope of the constant sensation line that relates Q and R_p. $\hat{Q}$ represents the desired value of Q from the constant sensation line of Q vs. R_p, and is determined by the value of R_p at the previous timestep. From m_E and $\hat{Q}$, the current (I) and pulse duration (T) used for stimulation are determined, and the appropriate waveform is delivered to the subject. The time-varying voltage (V) is measured across the electrodes by the sensor, whose peak value (V_p) is divided by I to obtain the peak resistance (R_p).

These values of I and T produce values of E_p and Q that are on the original lines of constant sensation for the measured value of R_p, and we would send these stimulation parameters to the subject.

6.1.2 Outline

The remainder of this chapter is organized as follows. In Section 6.2, we describe the methods for experiments to validate the linear relationships from Chapter 5 while manipulating the impedance of the electrode-skin interface through either the application or removal of electroconductive gel or exercise. The results of these experiments are described in Section 6.3. In Section 6.4, we discuss the performance of the controller in maintaining a constant sensation intensity as well as the limits of performance of the controller, followed by our conclusion in Section 6.5.

6.2 Methods

6.2.1 Electroconductive gel experiment

Ten subjects (five male, five female, ages: 20-30) without arm impairment volunteered to participate in the electroconductive gel experiment. Subjects were asked to participate in one session with five trials each testing a single condition. The five conditions tested were 1) weak and 2) strong stimulation using two large 20 x 25 mm electrodes (AMBU Neuroline 710) placed over glabrous skin on the proximal left forearm over the flexor carpi radialis muscle, 3) weak stimulation using two small 20 x 15 mm electrodes (AMBU Neuroline 700) placed in the same location, and weak stimulation using the large electrodes on 4) the skin lateral to the long head of the left biceps brachii muscle, and 5) the right lumbar paraspinal area of the back. The hardware setup was the same as the modeling experiments. All procedures and equipment were approved by the Institutional Review Board of the University of Illinois at Urbana-Champaign (#13920).

In all trials, two pairs of electrodes were used—a testing pair whose impedance was manipulated in order to test the controller, and a reference pair to provide a consistent reference sensation to compare against. For the testing electrodes,

Electro-Gel (Electro-Cap International, Eaton, OH) was either applied or removed between the electrodes and the skin in order to change the impedance. The reference electrodes were placed in the same location of the body on the contralateral side (e.g. right forearm corresponding to the location of the testing electrodes on the left forearm). The method of adjustments was used to match subject-chosen current amplitudes sent across the testing electrodes to the intensity of the reference sensation generated by the reference electrodes. Pulses were generated at a frequency of 50 Hz for each trial.

Each trial began by adjusting the current amplitude of a pulse with $T = 1000\,\mu s$ sent across the reference electrodes until the sensation intensity reached one of two specified magnitudes of sensation, weak or strong. These two magnitudes of sensation were chosen in the same manner as in the modeling experiments. Next, the current amplitude of a pulse sent across the testing pair of electrodes (again with $T = 1000\,\mu s$) was adjusted by the subject until the sensation intensity matched that of the reference electrodes. To ensure that each sensation intensity felt the same throughout each trial, a similar process to the modeling experiments was used. The reference sensation would be presented to the subject for two seconds, followed by a two second period of rest before presenting the new stimulation for two seconds across the other pair of electrodes. The subject would then make a decision on whether the new stimulation felt weaker, stronger, or the same as the reference stimulation. The subjects were allowed to repeat the presentation of stimulations as many times as they felt necessary to make a clear decision.

The values of I, T, and R_p for the initial sensation intensity from the testing electrodes that matched the reference were used to compute E_p and Q, corresponding to Label 1 in Fig. 6.2. Using Eqs. 6.1 and 6.2, we then determined the slopes of the lines of constant sensation for the controller to stay on for E_p and Q in response to changes in R_p (Label 2 in Fig. 6.2). When gel was applied or removed, R_p changed and the controller computed new values of I and T using Eq. 6.4. These new values of I, T, and R_p were used to derive new values of E_p and Q that stay on their respective lines of constant sensation. However, because changing I causes changes in the impedance of the electrode-skin interface (see Sec. 5.4.1), the actual R_p is different from the one used to compute the new stimulation parameters. Consequently, the controller must run for multiple iterations (i.e. multiple stimulation pulses) until the values for Q and R_p are back on the line of constant sensation (Fig. 6.2b)—in other words, when the actual value of m_Q approximates the original desired m_Q computed using Eq. 6.2. Fig. 6.2c

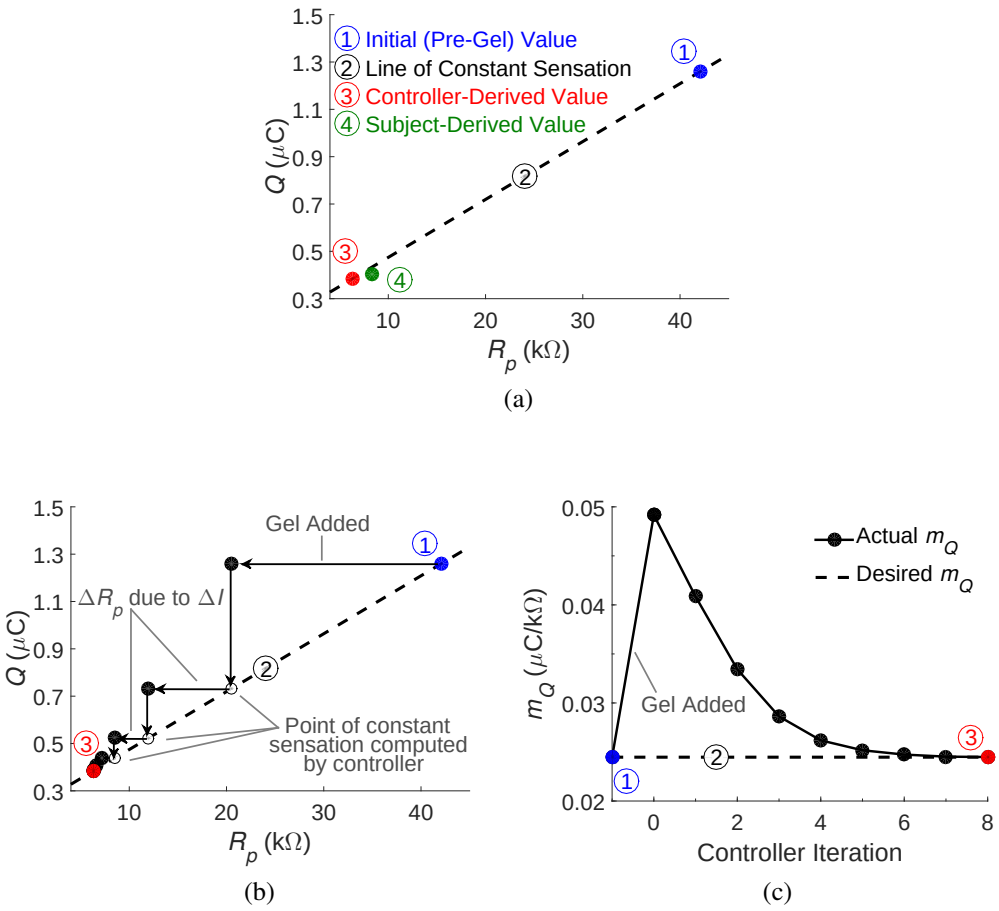

Figure 6.2: Convergence of controller. (a) 1. Initial stimulation parameters are chosen by the subject to match a reference sensation on the opposite arm before any gel is added. 2. The computer determines the line of constant sensation to stay on in response to changes in R_p. 3. Gel is applied to the electrode-skin interface, reducing R_p, and the controller computes new values for I and T to derive a value of Q that is on the line of constant sensation. 4. Fixing T to the controller-computed value, the subject then adjusts I until the sensation intensity matches the reference sensation. The subject's value of Q is derived and compared to the line of constant sensation. (b) The controller does not converge in a single iteration. When gel is added, R_p changes and the controller computes and sends new stimulation parameters. However, because changes in I induce changes in R_p, the controller requires more iterations in order for both R_p and Q to converge to the line of constant sensation. (c) In this example, nine iterations were required before the actual ratio of Q to R_p converged to the desired m_Q, representing the slope of the line of constant sensation.

shows an example of the change in m_Q after gel is added and the subsequent eight iterations of the controller to drive the actual m_Q towards the desired m_Q until their difference was within a heuristically-chosen threshold of 2.5×10^{-5} $\mu C/k\Omega$. In preliminary tests, at this threshold, subjects did not perceive a difference in sensation intensity between the converged stimulation parameters and the reference. It should be noted that the controller only acts on m_Q because its value depends on R_p—m_E will always remain constant on every iteration because I^2T will not change with R_p. Once the controller converges, I, T, and R_p are again used to compute the converged values of E_p and Q (Label 3 in Fig. 6.2). Finally, to test how well the subject would match the controller-generated line of constant sensation at the new value of R_p, we fixed T to the controller-computed value and asked the subject to adjust I until the sensation intensity from the testing electrodes matched that of the reference electrodes. We fixed T and adjusted I because, in general, when performing electrotactile stimulation, intensity changes are usually made by adjusting the current amplitude [42, 62]. This was also how we performed the modeling experiments in Chapter 5. The values of E_p and Q from the subject-chosen I and controller-computed T were determined, corresponding to Label 4 in Fig. 6.2a. In each trial, this process was repeated three times. This resulted in seven data points per trial, each consisting of an E_p, Q, and R_p value for 1) an initial subject-chosen sensation intensity that matched the reference, 2-4) the controller-computed sensation intensities after applying or removing gel three times, and 5-7) the subject-chosen sensation intensities at controller-computed pulse widths after applying or removing gel three times.

6.2.2 Activities of daily living experiments

In order to simulate real-world changes in electrode-skin interface impedance, we had nine subjects without impairment (four male, five female, ages: 18-29) and a subject with a right transradial amputation (male, age: 39) perform a similar experiment to the electroconductive gel experiment, replacing gel with exercise as the means to change the impedance. The subject with a transradial amputation was included to demonstrate a real-world application of electrotactile stimulation, which he could receive through fingertip contact from his prosthesis. Two large 20 x 25 mm electrodes (AMBU Neuroline 710) were placed over glabrous skin on the subject's right bicep. Monophasic positive square pulses were sent

across these electrodes at a frequency of 50 Hz. Because changes in impedance change perceived sensation (Fig. 5.3b), an electrotactile electrode reference could not be used, since exercise would change the impedance of the reference electrode. Instead, a vibrotactile motor (310-103, Precision Microdrives, London, UK) was used to provide a reference sensation intensity over the left bicep, under the assumption that changes in skin impedance have little to no effect vibrotactile stimulation intensity.

To verify that vibrotactile stimulation could be used as a reference to compare to the intensity of electrotactile stimulation, we first repeated the electroconductive gel experiment for all ten subjects. However, users adjusted current amplitudes to match a vibrotactile stimulation intensity instead. Only large 20 x 25 mm electrodes on the bicep were tested.

After completing the gel experiment, the subjects were asked to ascend and descend a flight of stairs for five minutes in order to reduce the electrode-skin impedance due to the accumulation of sweat. After the five minutes, the subjects were asked to adjust current amplitude at a controller-computed pulse duration to match the vibrotactile reference sensation intensity on the left bicep, similar to the electroconductive gel experiment. We recorded the value of the subject-chosen current amplitude I at the controller-computed pulse duration T, and the resulting peak resistance R_p. The subject would then rest for ten minutes to wait for his impedance to recover to a higher value before again trying to match the reference sensation, after which we recorded the second set of I, R_p, and T values that matched the reference. The subject was again asked to ascend and descend the flight of stairs for five minutes, reducing the impedance, and we recorded the third and final set of I, R_p, and T values.

To demonstrate the use of the controller in a real-world application, we asked the subject with a transradial amputation to wear a prosthesis that gave electrotactile feedback on contact [53]. When either the index, middle, or thumb digits touched an object, the subject would feel a monophasic square pulse with initial stimulation parameters of 1mA and 1000μs at 50Hz. While wearing the prosthesis, the subject was asked to perform three activities of daily living for five minutes each: stair ascent and descent, hammering nails into wood, and cross-training on an elliptical machine. For stair ascent and descent, the subject made contact with the handrail on every step in order to receive sensory feedback. When hammering nails into wood, the subject hammered with his unimpaired left arm and received sensory feedback from his prosthesis when guiding the nail or holding the board

in place. When using the elliptical machine, the subject kept his prosthesis gripping the handle for most of the activity. Two sets of electrodes were placed on the right bicep. The first set of electrodes was used to measure the peak resistance without the controller. The controller was used on the second set of electrodes, and the stimulation parameters and peak resistances were recorded.

In a final experiment, we asked the subject with an amputation to peel off and reapply electrotactile stimulation electrodes during stimulation in order to manipulate the impedance. Upon stimulation, after 5 s, the subject was asked to peel off and reapply the electrodes within 10 s by 25%, 50%, and 75%, pausing for 5 s in between. This was repeated for five trials using the controller and five trials without using the controller. The initial stimulation parameters (I=0.7 mA, T=1000 µs) were the same across all ten trials. The values of I, T, R_p, m_E, and m_Q throughout each trial were recorded. Finally, the subject was asked to report any changes in sensation throughout each trial.

6.3 Results

6.3.1 Electroconductive gel results

Data showing the results from the controller experiment using electrotactile stimulation as a reference for both E_p vs. R_p and Q vs. R_p are in Figs. 6.3-6.4. The figures show the results from Subject 10 across all five experimental conditions. The results from all ten subjects are shown in Figs. 6.5-6.6. To evaluate the effectiveness of the controller, the R^2 value was computed to determine how well the line of constant sensation for a single trial fit the three subject-derived values for both E_p vs. R_p and Q vs. R_p. The R^2 values from the linear regression are reported in Table 6.1. The average value for E_p vs. R_p was 0.941 and for Q vs. R_p was 0.917, where an R^2 value of 1 denotes a perfect fit to the data. As with the modeling results, these linear relationships held across ten different subjects, both magnitudes of sensation, both electrode sizes, and all three stimulation locations.

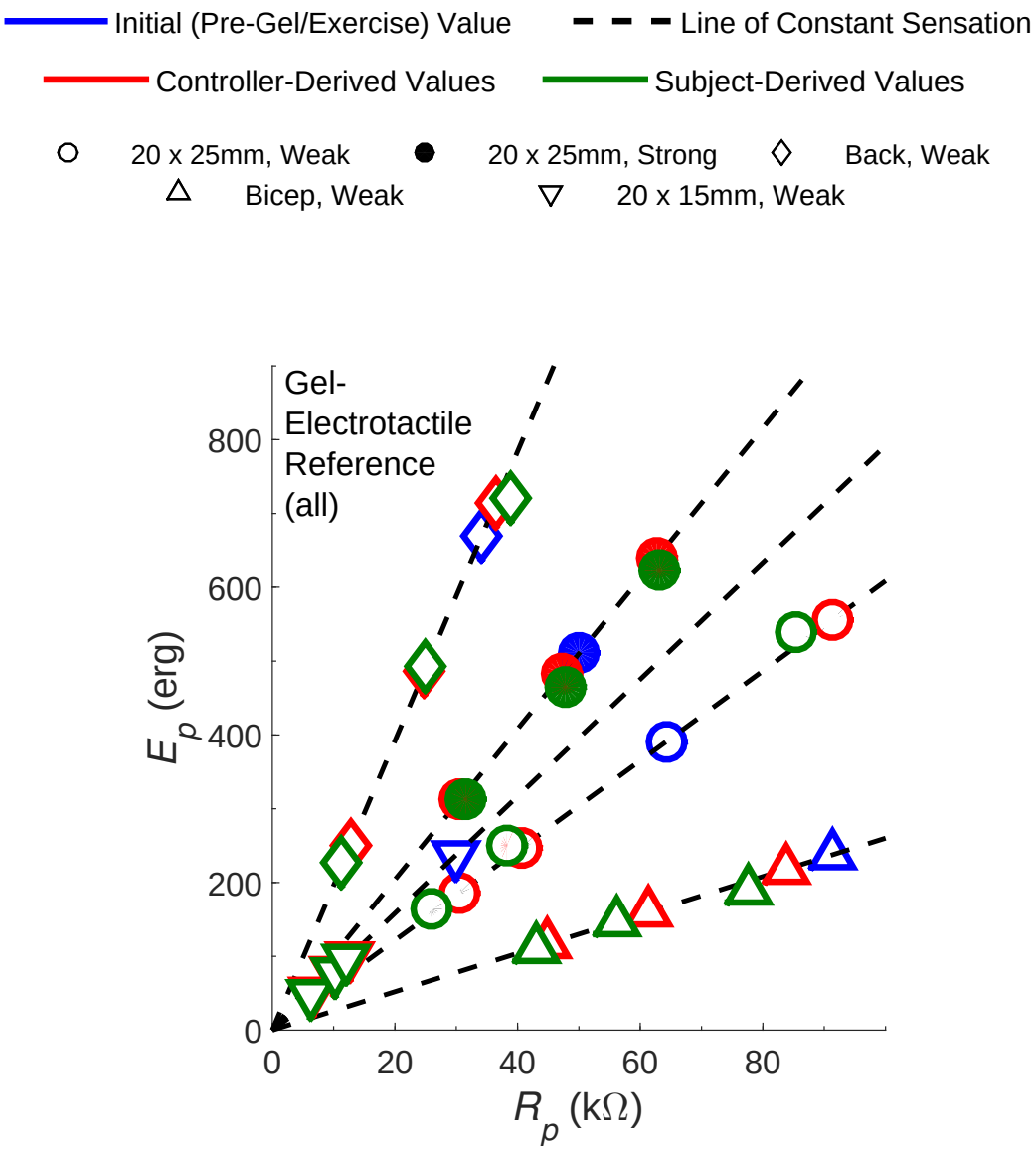

Figure 6.3: Quantitative controller experiment results validating the linear relationships at constant sensation for peak pulse energy in response to changes in peak resistance. For every condition, the subject was asked to match a reference sensation over three trials with differing values of R_p. Shown here is the peak pulse energy for a single subject across different sessions, magnitudes of sensation, stimulation locations, and electrode sizes matched to an electrotactile reference sensation intensity after using electroconductive gel to change R_p.

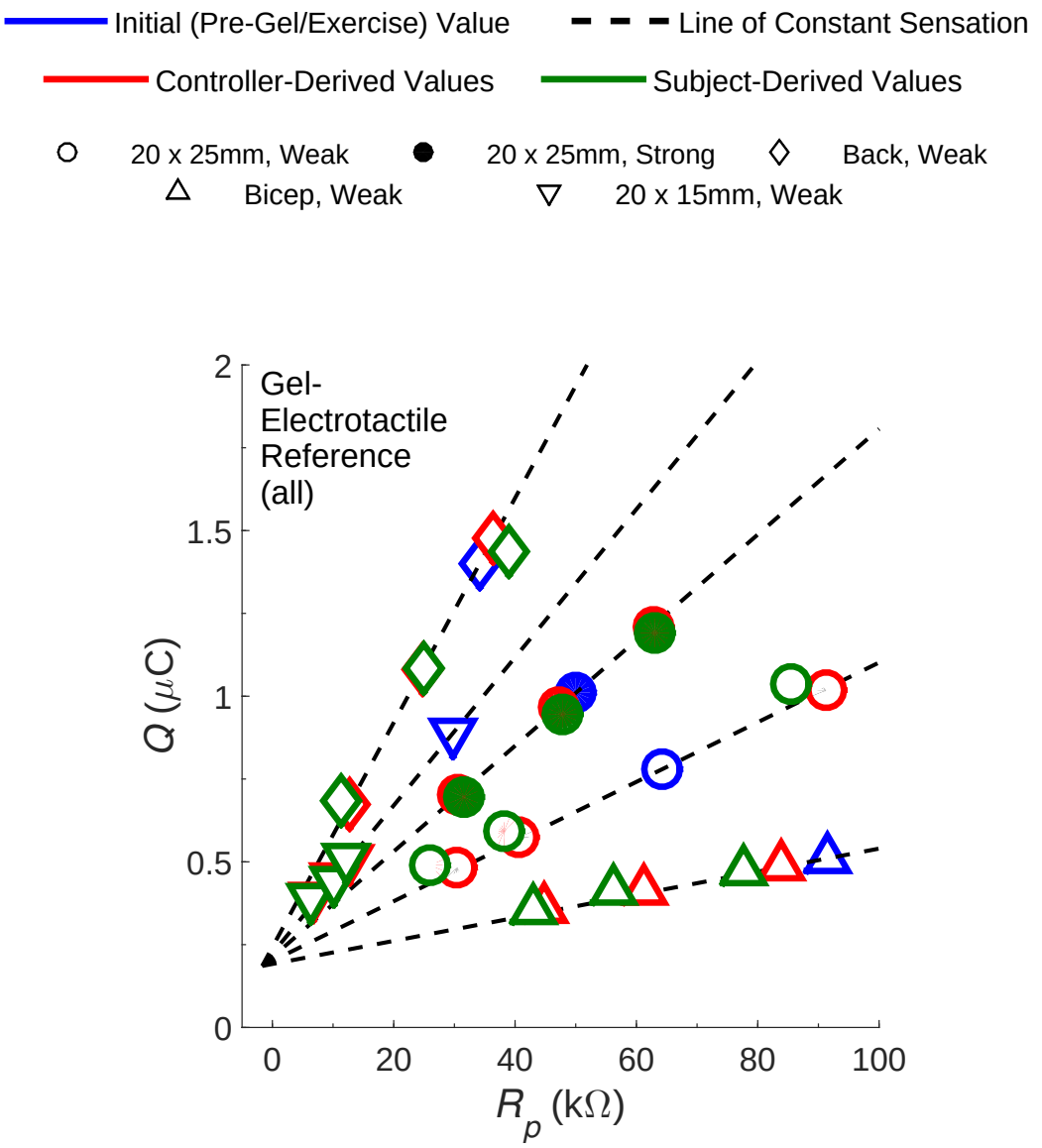

Figure 6.4: Quantitative controller experiment results validating the linear relationships at constant sensation for phase charge in response to changes in peak resistance. For every condition, the subject was asked to match a reference sensation over three trials with differing values of R_p. Shown here is the phase charge for a single subject across different sessions, magnitudes of sensation, stimulation locations, and electrode sizes matched to an electrotactile reference sensation intensity after using electroconductive gel to change R_p .

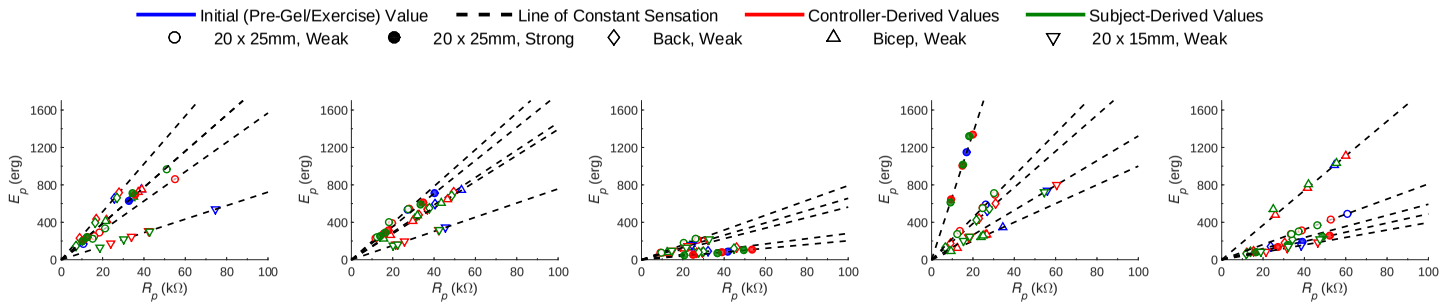

(a) E_p vs. R_p, Subject 1

(b) E_p vs. R_p, Subject 2

(c) E_p vs. R_p, Subject 3

(d) E_p vs. R_p, Subject 4

(e) E_p vs. R_p, Subject 5

(f) E_p vs. R_p, Subject 6

(g) E_p vs. R_p, Subject 7

(h) E_p vs. R_p, Subject 8

(i) E_p vs. R_p, Subject 9

(j) E_p vs. R_p, Subject 10

Figure 6.5: Controller experiment results for all ten subjects verifying the linear relationships at constant sensation for peak energy (E_p) in response to changes in peak resistance (R_p). For each of the five conditions, the subjects were asked to match a reference sensation over three trials with differing values of R_p.

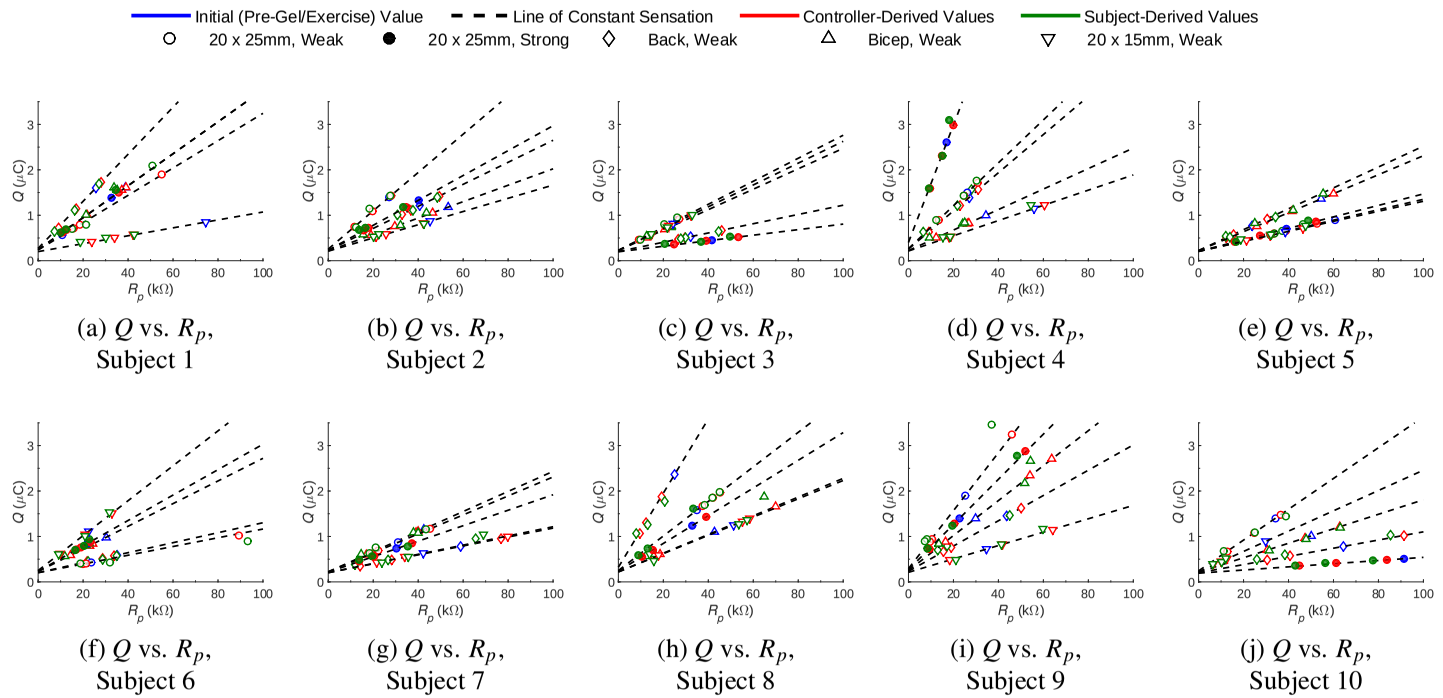

(a) Q vs. R_p, Subject 1 (b) Q vs. R_p, Subject 2 (c) Q vs. R_p, Subject 3 (d) Q vs. R_p, Subject 4 (e) Q vs. R_p, Subject 5

(f) Q vs. R_p, Subject 6 (g) Q vs. R_p, Subject 7 (h) Q vs. R_p, Subject 8 (i) Q vs. R_p, Subject 9 (j) Q vs. R_p, Subject 10

Figure 6.6: Controller experiment results for all ten subjects verifying the linear relationships at constant sensation for phase charge (Q) in response to changes in peak resistance (R_p). For each of the five conditions, the subjects were asked to match a reference sensation over three trials with differing values of R_p.

It should be noted that the reason we do not compute the R^2 between the subject-derived values and the controller-computed values used in the experiment is because of small fluctuations in R_p that occur throughout the experiment. Consequently, the subject-chosen value of I may not match the controller-computed value of I due to a discrepancy, albeit small, in R_p. However, when running the controller in realtime, these small fluctuations in R_p would be accounted for by adjusting I and T to the most recent measurement of R_p, staying on the lines of constant sensation. For this reason, it is more appropriate to compare the subject-derived values to the line of constant sensation, since the line of constant sensation more accurately reflects the values of I and T the controller would compute during practical use.

6.3.2 Activities of daily living results

Data showing the results from the controller experiment using vibrotactile stimulation as a reference for both E_p vs. R_p and Q vs. R_p are in Figs. 6.7-6.8. The figures show the results from the gel and exercise experiments for the subject with a transradial amputation using large 20 x 25 mm electrodes placed on the right bicep. The results from all ten subjects are shown in Figs. 6.9-6.10 for the tests using gel and in Figs. 6.11-6.12 for stair ascent and descent. As when using electrotactile stimulation as a reference, the R^2 value was computed to determine how well the line of constant sensation for a single trial fit the three subject-derived values for both E_p vs. R_p and Q vs. R_p. The R^2 values from the linear regression are reported in Table 6.1. The average value for E_p vs. R_p was 0.954 and for Q vs. R_p was 0.900 when using gel with a vibrotactile reference, and 0.950 and 0.918, respectively, after stair ascent and descent.

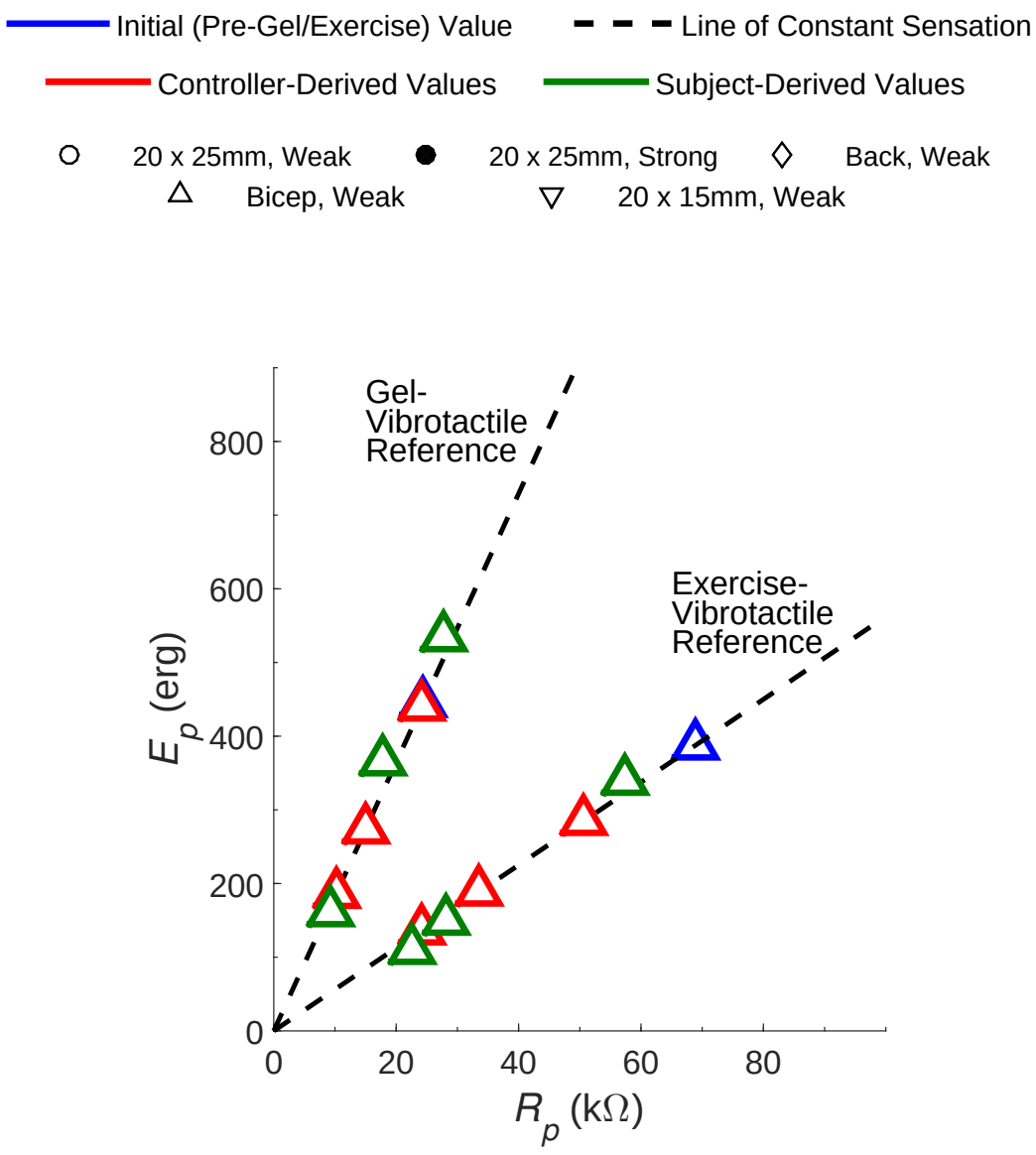

Figure 6.7: Peak pulse energy for a subject with a transradial amputation using either electroconductive gel or exercise to change R_p while comparing the sensation intensity to a vibrotactile reference.

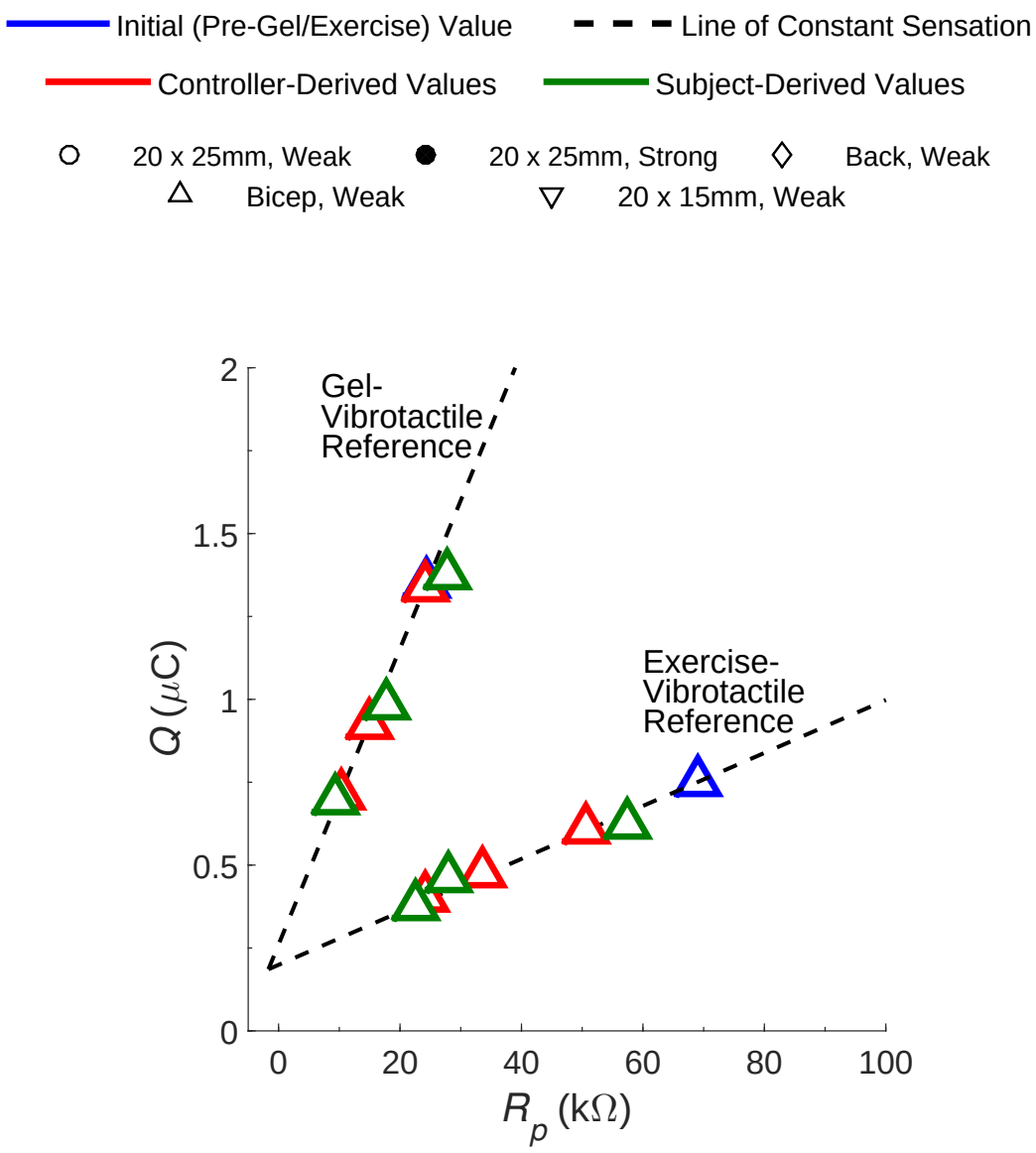

Figure 6.8: Phase charge for a subject with a transradial amputation using either electroconductive gel or exercise to change R_p while comparing the sensation intensity to a vibrotactile reference.

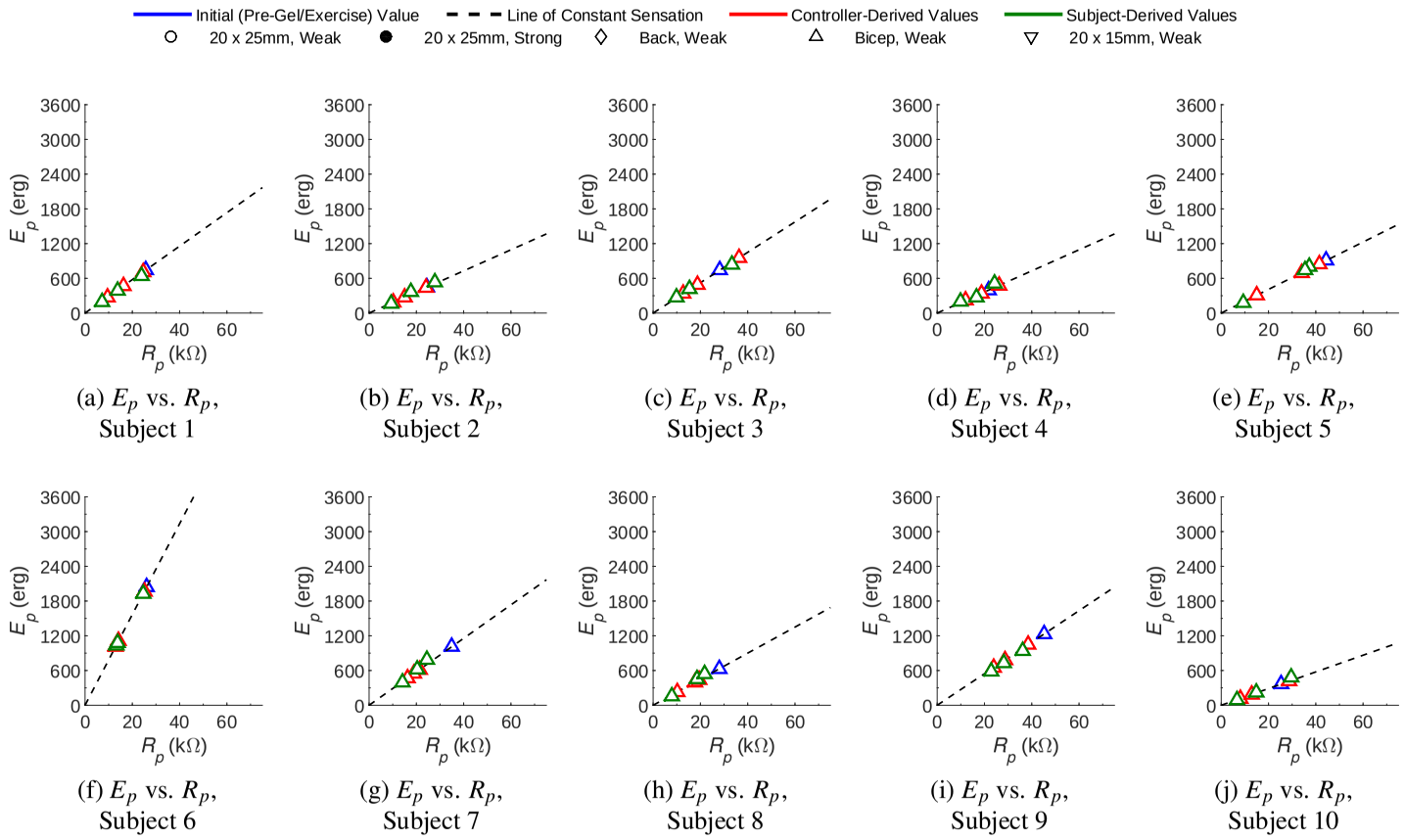

(a) E_p vs. R_p, Subject 1 (b) E_p vs. R_p, Subject 2 (c) E_p vs. R_p, Subject 3 (d) E_p vs. R_p, Subject 4 (e) E_p vs. R_p, Subject 5

(f) E_p vs. R_p, Subject 6 (g) E_p vs. R_p, Subject 7 (h) E_p vs. R_p, Subject 8 (i) E_p vs. R_p, Subject 9 (j) E_p vs. R_p, Subject 10

Figure 6.9: Controller experiment results for all ten subjects verifying the linear relationships at constant sensation for peak pulse energy (E_p) in response to changes in peak resistance (R_p) due to the addition and removal of gel. The subjects were asked to match an electrotactile sensation to a vibrotactile reference sensation over three trials with differing values of R_p.

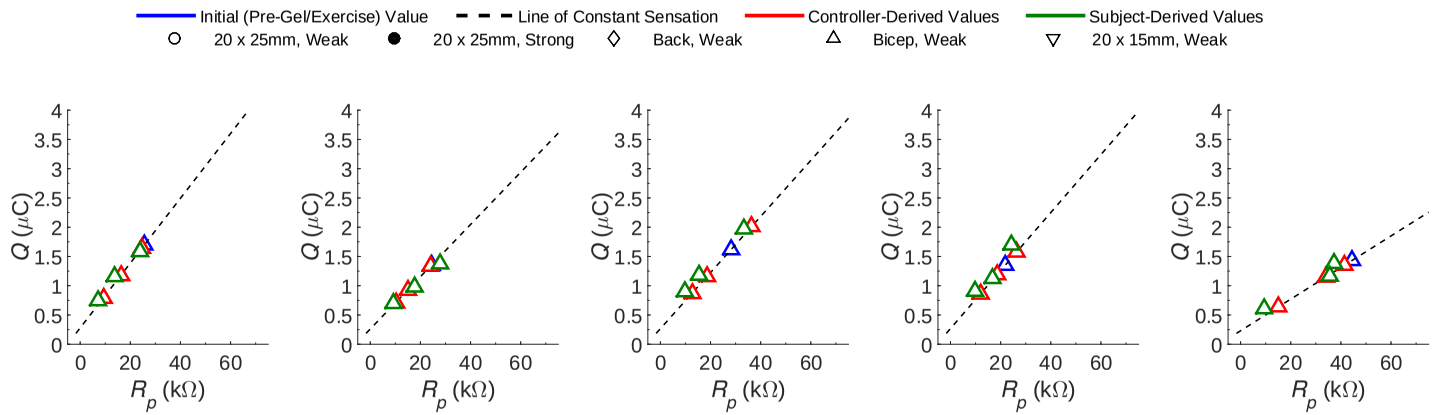

(a) Q vs. R_p, Subject 1 (b) Q vs. R_p, Subject 2 (c) Q vs. R_p, Subject 3 (d) Q vs. R_p, Subject 4 (e) Q vs. R_p, Subject 5

(f) Q vs. R_p, Subject 6 (g) Q vs. R_p, Subject 7 (h) Q vs. R_p, Subject 8 (i) Q vs. R_p, Subject 9 (j) Q vs. R_p, Subject 10

Figure 6.10: Controller experiment results for all ten subjects verifying the linear relationships at constant sensation for phase charge in response to changes in peak resistance due to the addition or removal of gel. The subjects were asked to match an electrotactile sensation to a vibrotactile reference sensation over three trials with differing values of R_p.

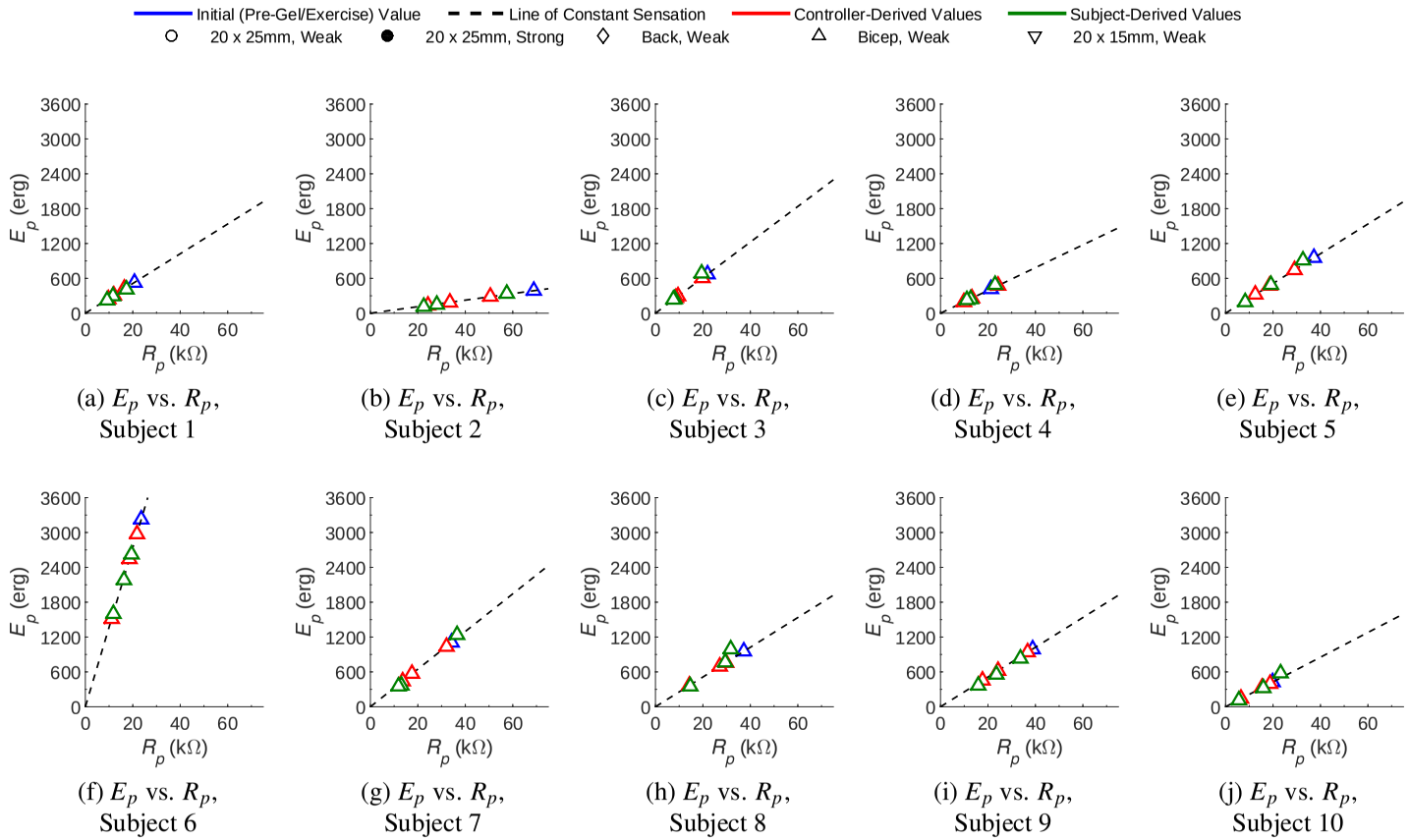

(a) E_p vs. R_p, Subject 1

(b) E_p vs. R_p, Subject 2

(c) E_p vs. R_p, Subject 3

(d) E_p vs. R_p, Subject 4

(e) E_p vs. R_p, Subject 5

(f) E_p vs. R_p, Subject 6

(g) E_p vs. R_p, Subject 7

(h) E_p vs. R_p, Subject 8

(i) E_p vs. R_p, Subject 9

(j) E_p vs. R_p, Subject 10

Figure 6.11: Controller experiment results for all ten subjects verifying the linear relationships at constant sensation for peak pulse energy in response to changes in peak resistance due to exercise. The subjects were asked to match an electrotactile sensation to a vibrotactile reference sensation over three trials with differing values of R_p due to exercise.

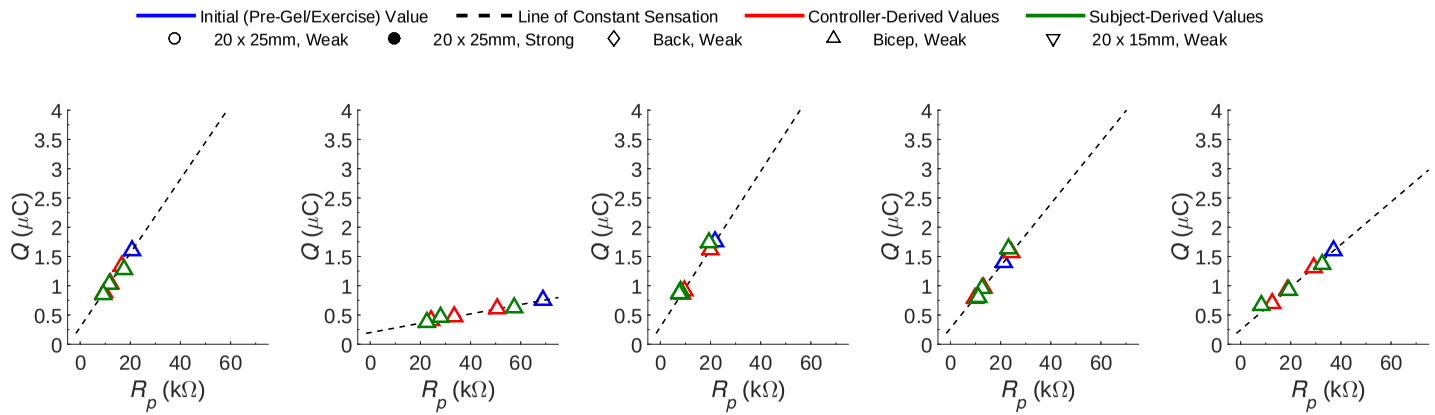

(a) Q vs. R_p, Subject 1 (b) Q vs. R_p, Subject 2 (c) Q vs. R_p, Subject 3 (d) Q vs. R_p, Subject 4 (e) Q vs. R_p, Subject 5

(f) Q vs. R_p, Subject 6 (g) Q vs. R_p, Subject 7 (h) Q vs. R_p, Subject 8 (i) Q vs. R_p, Subject 9 (j) Q vs. R_p, Subject 10

Figure 6.12: Controller experiment results for all ten subjects verifying the linear relationships at constant sensation for phase charge in response to changes in peak resistance due to exercise. The subjects were asked to match an electrotactile sensation to a vibrotactile reference sensation over three trials with differing values of R_p due to exercise.

Table 6.1: R^2 regression statistics across ten subjects under different experimental conditions.

Condition	Parameters	Mean	Std	Min	Max	Median
Gel-Electrotactile Reference	E_p vs. R_p	0.941	0.0800	0.684	1.00	0.973
	Q vs. R_p	0.917	0.0679	0.726	0.999	0.939
Gel-Vibrotactile Reference	E_p vs. R_p	0.954	0.0416	0.874	1.00	0.963
	Q vs. R_p	0.900	0.0871	0.744	0.993	0.915
Exercise-Vibrotactile Reference	E_p vs. R_p	0.950	0.0427	0.846	0.992	0.960
	Q vs. R_p	0.918	0.0423	0.838	0.981	0.916

For each of the three activities of daily living with the subject with a transradial amputation, Figs. 6.13-6.15 show the measured peak resistance (R_p) and computed slopes of the lines of constant sensation (m_E and m_Q) when the prosthesis came into contact with objects. The figures show a decrease in peak resistance ($\sim$5-15 kΩ) over the five minutes of activity measured without the controller running. This drop was within the range of peak resistances measured when using electroconductive gel. In response to changes in peak resistance, the controller is able to maintain constant values for m_E and m_Q, while the value of m_Q deviates greatly from its initial value when the controller is off. Supplementary Video 6.1 shows the response of the controller in real-time in these real-world examples.

Fig. 6.16 shows the values of I, T, R_p, m_E, and m_Q while the subject with a transradial amputation peeled and placed electrodes during stimulation. The mean and standard deviation over the five trials are shown both with and without the controller running. Real-time changes in these variables during peeling with and without the controller are shown in Supplementary Video 6.2. Similar to the example in Fig. 5.3b, when the controller was not in use, the subject reported increasing discomfort each time he peeled off the electrode by an increasing amount. However, when the controller was used, the subject reported no discomfort at all throughout all five trials. In addition, the subject reported no change in sensation intensity any time he peeled off the electrode by any amount.

(a)

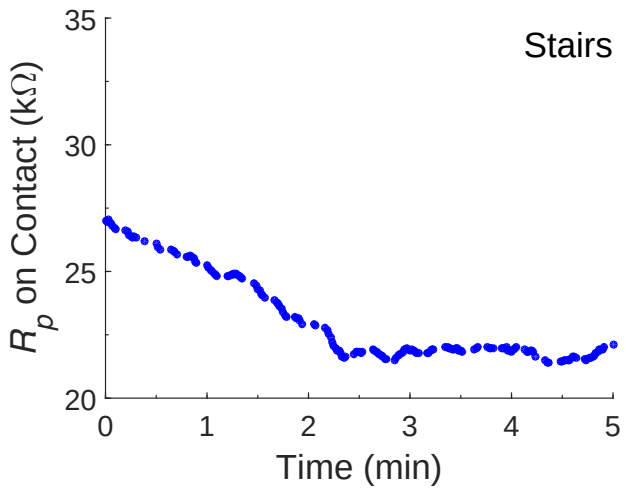

(b)

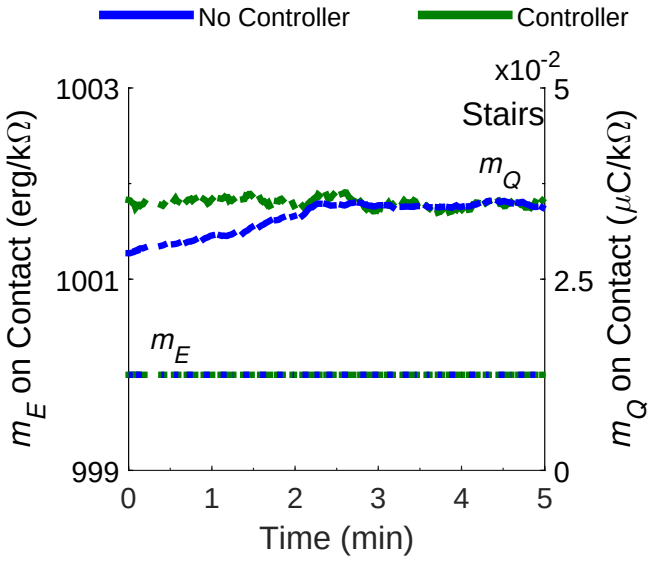

(c)

Figure 6.13: Realtime results from a subject with a transradial amputation during five minutes of ascending and descending stairs (a). The subject was provided electrotactile feedback, with and without the controller, via electrodes placed on the subject's right bicep. Electrotactile stimulation was only provided when the fingertips of the prosthetic hand made contact with an object. The R_p was recorded without the controller under constant stimulation parameters during contact (b). The controller modulates stimulation parameters to keep m_E and m_Q constant (c). Gaps in the plots correspond to times when the fingertips were not in contact with an object.

(a)

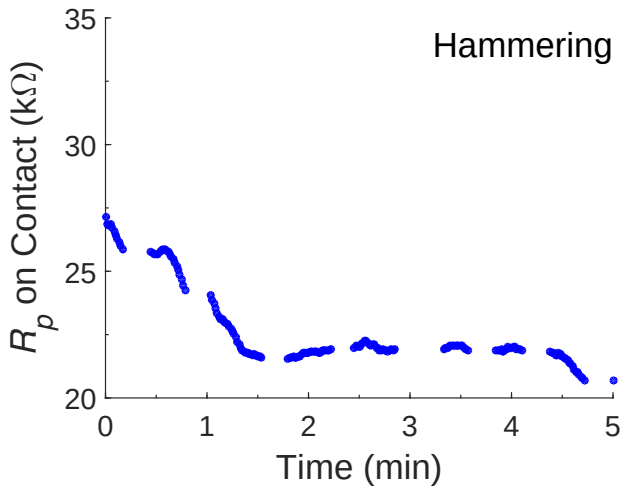

(b)

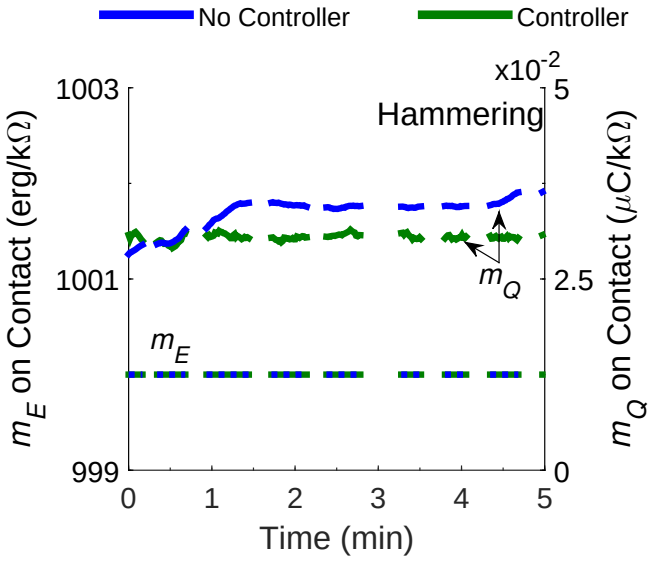

(c)

Figure 6.14: Realtime results from a subject with a transradial amputation during five minutes of hammering nails into wood (a). The subject was provided electrotactile feedback, with and without the controller, via electrodes placed on the subject's right bicep. Electrotactile stimulation was only provided when the fingertips of the prosthetic hand made contact with an object. The R_p was recorded without the controller under constant stimulation parameters during contact (b). The controller modulates stimulation parameters to keep m_E and m_Q constant (c). Gaps in the plots correspond to times when the fingertips were not in contact with an object.

(a)

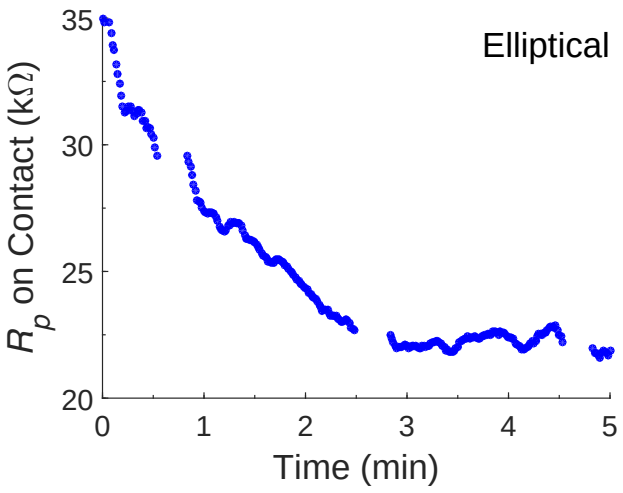

(b)

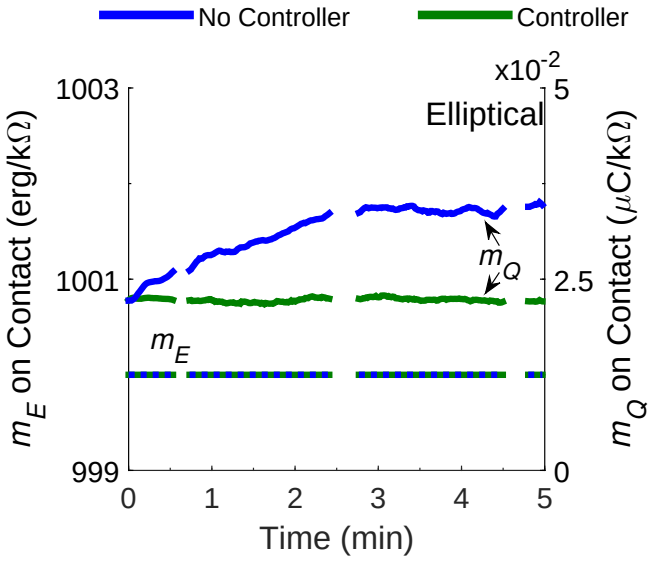

(c)

Figure 6.15: Realtime results from a subject with a transradial amputation during five minutes of using an elliptical cross-trainer (a). The subject was provided electrotactile feedback, with and without the controller, via electrodes placed on the subject's right bicep. Electrotactile stimulation was only provided when the fingertips of the prosthetic hand made contact with an object. The R_p was recorded without the controller under constant stimulation parameters during contact (b). The controller modulates stimulation parameters to keep m_E and m_Q constant (c). Gaps in the plots correspond to times when the fingertips were not in contact with an object.

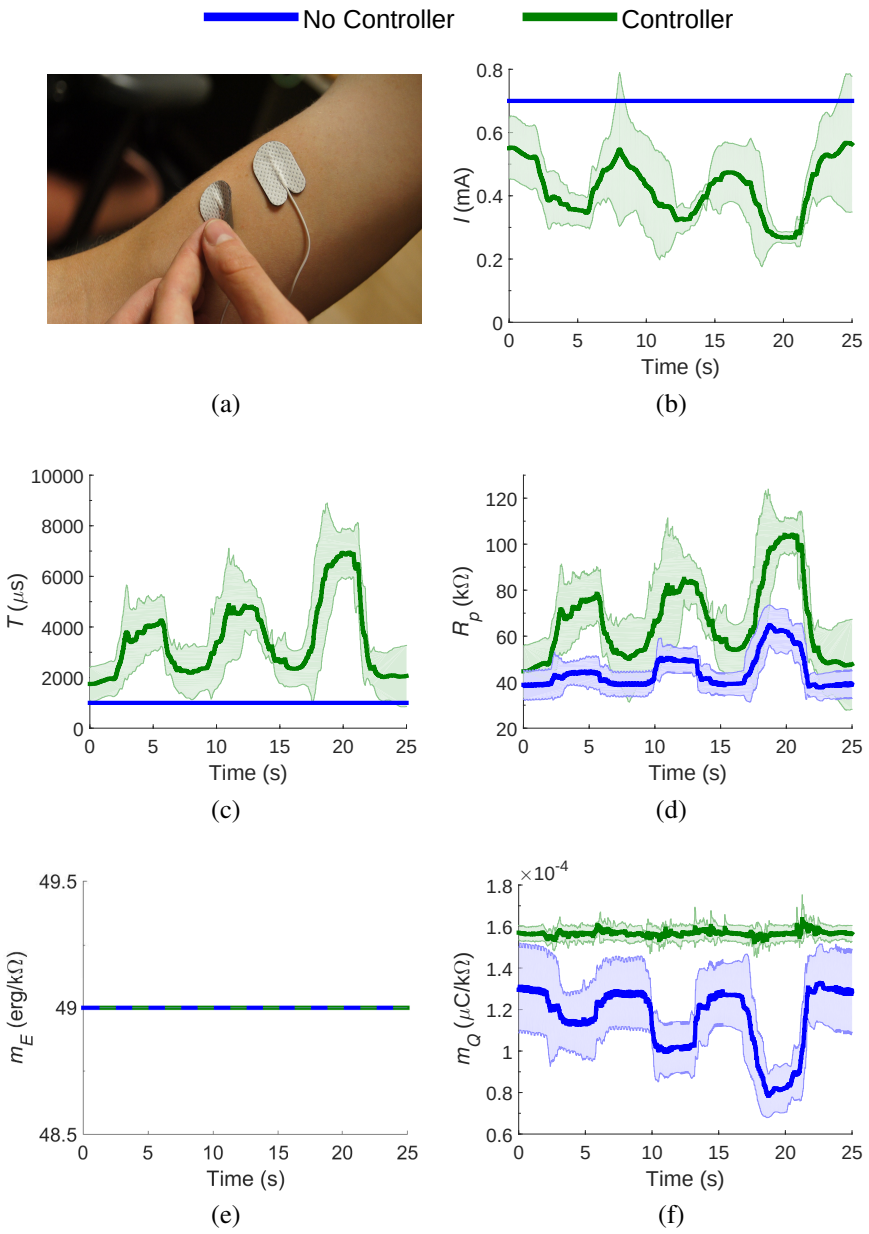

Figure 6.16: Realtime results from a subject with a transradial amputation peeling and reapplying electrodes by 25%, 50%, and 75%, every five seconds with and without the controller (a). The mean and standard deviation over five trials are shown. In (b) and (c), I and T remain constant when the controller is not used, but fluctuates in response to changes in (d) R_p, when the controller is used. In both cases, (e) m_E remains constant. In (f) m_Q varies greatly when the controller is not used, but is modulated to stay constant when the controller is used. The subject reported no change in sensation intensity when using the controller, but discomfort when peeling off the electrodes without the controller.

6.4 Discussion

6.4.1 Validation of linear relationships between E_p and R_p & Q and R_p

In the electroconductive gel experiment, the average R^2 values for evaluating how well the controller-computed line of constant sensation fits subject-derived values for both E_p vs. R_p and Q vs. R_p were greater than 0.9 (Table 6.1). These large values of R^2 strongly suggest that these lines computed by the controller represent constant sensation intensities, even when there are drastic changes in electrode-skin interface impedance. Furthermore, these results held across different subjects, magnitudes of sensation, stimulation locations, and electrode sizes.

Although in the example in Fig. 6.2c it took eight iterations for the controller to converge, it is unknown how quickly the controller needs to converge for a difference in sensation intensity to go unnoticed. If the controller takes too long to converge, the subject may be able to perceive all the variations in sensation intensity whenever R_p fluctuates. Recall that the reason it takes multiple iterations for the controller to converge is because every time I changes, R_p changes as well. Therefore, the number of iterations could potentially be reduced by modeling the relationship between changes in I and changes in R_p. If this relationship were known, then we could accurately predict what the new R_p value would be in response to a change in I, and compute stimulation parameters that would converge after a single pulse.

In addition, it is unknown how accurately the controller needs to converge to the desired m_Q for there to be no noticeable difference in sensation intensity. In order to find out, psychophysical experiments to determine the just-noticeable difference (JND) for m_Q would need to be performed. Knowing the JND could also reduce the number of iterations needed to converge, since our heuristically-chosen threshold is likely below the JND. Consequently, the controller could stop iterating once it is within one JND from the desired m_Q. Finally, determining the JND for both m_Q and m_E could serve as a guide to determine how to change the magnitude of the sensation during stimulation, since we know that increasing the values of either m_E or m_Q result in a stronger sensation. This would be useful in applications where the magnitude of sensation could be proportional to some varying input, for example, in relaying contact forces in a virtual reality setting.

6.4.2 Experiments using vibrotactile stimulation as a reference

The R^2 values for the gel controller experiment using vibrotactile stimulation as a reference were greater than 0.9, indicating a near perfect fit (Table 6.1). In fact, the results are very similar to the R^2 values when using electrotactile stimulation as a reference. These large values of R^2 suggest that vibrotactile stimulation can indeed be used as a reference, since poor comparisons between electrotactile and vibrotactile sensation intensities would have resulted in poor average R^2 values. The results after stair ascent and descent using vibrotactile stimulation as a reference produced similar R^2 values greater than 0.9 (Table 6.1). As a result, we can assume that the change in skin impedance after exercise did not have a large impact in perceiving vibrotactile sensation intensity, since changes in the reference sensation intensity would have resulted in poor R^2 values. However, further study is necessary to directly test how well subjects can compare vibrotactile and electrotactile sensation intensities, as well as the effect of skin impedance changes on vibrotactile sensation intensity. Nevertheless, our results imply that the controller will maintain constant sensation intensity even after changes in impedance due to activities of daily living.

6.4.3 Real-time control of sensation intensity during activities of daily living

The purpose of the exercise and electrode peeling tests on a subject with a transradial amputation was to evaluate the effectiveness of the controller in response to real-world examples of decreasing impedance (exercise) and increasing impedance (electrode peeling). For each of the exercises (stairs, hammering, and elliptical), the measured peak resistance decreased consistently throughout the activity, with the largest decrease corresponding to the heaviest exercise (elliptical, see Fig. 6.15b). These decreases in peak resistance result in lowered perceived sensation intensity, as reported by the subject. However, the controller was able to keep both m_E and m_Q constant, resulting in a constant perceived sensation.

The perception of constant sensation was much more apparent and immediate in the peeling test. When the controller was not in use, I (Fig. 6.16b) and T (Fig. 6.16c) were held constant at 0.7 mA and 1000 µs, respectively. R_p (Fig. 6.16d) varied in response to the electrode being peeled off and reapplied. The constant values of I and T resulted in a constant value of m_E (Fig. 6.16e), which is equal

to I^2T. However, because the controller was not in use, m_Q (Fig. 6.16f) varied, since it is equal to $\frac{IT-y^*}{R_p-x^*}$, and R_p was changing throughout each trial. When the controller was used, I (Fig. 6.16b) and T (Fig. 6.16c) were modulated in order to keep m_E and m_Q constant. Because changes in I result in changes in R_p, we see greater fluctuations in R_p (Fig. 6.16d) than when the controller was not in use. Again, m_E (Fig. 6.16e) was always constant since its value does not depend on R_p. However, because m_Q (Fig. 6.16f) depends on R_p, there are small fluctuations that are modulated by the controller to hold it constant. By keeping m_E and m_Q constant, E_p and Q always stayed on their lines of constant sensation, and the subject reported no change in sensation intensity while peeling off and reapplying the electrodes. In contrast, when m_Q fluctuated while the controller was not in use, the user reported discomfort proportional to the amount the electrode was peeled off.

6.4.4 Limits of performance of the controller

When the controller computes new stimulation parameters in response to changes in R_p, limitations in the rise time of our linear isolated stimulator require T to converge to a value above 200 µs. Otherwise, the subject will feel a diminished sensation because the current waveform will not reach the controller-computed current amplitude. Additionally, I must converge to a current amplitude that is higher than the sensation threshold. It may fall below the threshold if T converges to a large enough value, and the subject would not feel anything.

It should be noted that in daily activity, large sudden fluctuations in R_p are less likely to occur. In Kajimoto, et al. [66], subject resistances varied between 0-5 kΩ in multiple repeated stimulation trials. From our own observations, fluctuations in R_p were generally between 0-5 kΩ after periodic stimulation during hour-long sessions. Activities such as heavy exercise (Fig. 6.15b) and peeling the electrode (Fig. 6.16d) resulted in changes in R_p between 5-20 kΩ when measured without the controller, yet in these situations the controller was still able to maintain a constant perceived sensation intensity. However, studies over the period of days to weeks would need to be conducted to determine the variations in R_p over longer periods of use.

6.5 Conclusion

In Chapter 5, we modeled the relationship between perceived sensation intensity and changes in the impedance of the electrode-skin interface during electrotactile stimulation. We found linear relationships between E_p and R_p, as well as Q and R_p. Using this information we were able to compute stimulation parameters I and T to maintain a constant sensation intensity while taking impedance changes into account. We implemented a controller that uses the linear relationships presented in order to keep sensation intensity constant. This controller measures R_p and modulates I and T in order to keep E_p and Q on their respective lines of constant sensation. These lines of constant sensation strongly fit values of E_p and Q computed from subject-chosen stimulation parameters that felt constant across different peak resistance values, validating our linear models. These results also held across different subjects, magnitudes of sensation, stimulation locations, and electrode sizes. To highlight the real-world application of the controller, we verified that the controller maintains constant sensation intensity even after changes in impedance due to activities of daily living. We further tested the use of the controller in real-time experiments with a subject with a transradial amputation during activities of daily living and peeling electrodes during stimulation. In these cases, the controller produced a constant perceived sensation intensity, while a lack of sensation or discomfort was felt when the controller was not used.

In future work, we plan to extend our results to waveforms more complex than monophasic positive pulses. We can test different paradigms for providing force feedback to users, such as encoding the force signal (or changes in force) to a pulse train or a modulation in frequency over multiple channels of stimulation. Finally, to elucidate the physiology underlying perceived electrotactile sensation intensity as well as quality, we could use microneurography to find a relationship between stimulation parameters and nerve firing rates.

CHAPTER 7

CONCLUSION

7.1 Summary

In this dissertation, we described various mechanisms that enable closed-loop sensorimotor control of hand prostheses. Motor control was achieved using electromyography (EMG) and sensory feedback was achieved through the use of skin stretch for proprioception and electrotactile stimulation for both proprioception and touch/contact force. Chapter 2 described a passive skin stretch device that improved grip recognition and joint angle targeting using a hand prosthesis. Chapter 3 described a flexible, stretchable, epidermal electronic device that could simultaneously record EMG and provide sensory feedback through electrotactile stimulation electrodes. This device improved grasping control and joint angle targeting, and enabled a user to control a robot arm to grasp a bottle of water without crushing it, lift it, and place it back down while blindfolded. Chapter 4 described the development of a low-cost myoelectric prosthetic hand that could provide touch/pressure feedback through sensors in the fingertip. This pressure information was relayed to a person with a transradial amputation via electrotactile stimulation, enabling him to grasp eggshells and cups of water without crushing them. In Chapter 5 we focused on the development of a model for electrotactile stimulation that enables long-term wear of electrodes by characterizing the relationship between peak pulse energy, phase charge, and the impedance of the electrode-skin interface at constant sensation intensity. We used this model in Chapter 6 to implement and evaluate a controller that keeps sensation intensity constant despite changes in electrode-skin interface impedance that can occur during activities of daily living. We validated this controller by having a patient with a transradial amputation wear the prosthesis described in Chapter 4 and perform various exercises, including climbing stairs, hammering nails into wood, and using an elliptical machine. We also had the subject peel off and place down the

electrodes during stimulation. In each activity, the controller produced a constant perceived sensation intensity, while a lack of sensation or discomfort was felt when the controller was not used.

7.2 Future Work

The work presented in this dissertation lays the groundwork for future studies involving the combination of motor control and sensory feedback in upper limb prostheses. One potential study involves the use of the epidermal device described in Chapter 3 on a patient with targeted sensory reinnervation (TSR). In TSR, sensory nerves that normally carried touch information from skin from an amputated region of the body are transferred to intact skin. When the reinnervated intact skin receives a stimulus, it feels as though it originated from the amputated region [50]. These sensory reinnervated sites are collocated with motor reinnervated sites, however, where EMG sensors are normally placed. As a result, our epidermal device that integrates both EMG and stimulation electrodes could enable simultaneous sensorimotor control for the reinnervated patient. We could then evaluate improvements in prosthesis control using the epidermal device in standard occupational therapy tasks. Furthermore, we could test how well the user has embodied the prosthesis through surveys and measurements of residual limb temperature [61].

Another potential study would be in combining proprioceptive feedback with touch/pressure. The skin stretch device for proprioception from Chapter 2 can easily be integrated with electrotactile stimulation for touch/pressure. This combination could potentially enable a person with a transradial amputation to determine the softness of objects. When grasping a rigid object, the skin stretch would stop since the finger will not move, but the electrotactile stimulation would increase intensity as pressure on the object increases. When grasping a soft object, the user would simultaneously feel the skin stretch and electrotactile stimulation intensity increase.

The hand developed in Chapter 4 and the electrotactile sensation intensity controller from Chapter 6 open the door to long-term tests of touch/force feedback in a myoelectric prosthesis. We could have subjects with transradial amputations use the device for two weeks to a month and evaluate them on a weekly basis on tasks that require fine force control, such as the grasping experiments performed

in Chapter 4. We could also evaluate how well the subjects are learning to use the device through brain imaging of the sensorimotor cortex, looking for evidence of plasticity after having used the hand for an extended period of time.

All of these studies represent exciting avenues in sensorimotor prosthetic control research that have opened up from the work presented in this dissertation.

APPENDIX A

SUPPLEMENTARY VIDEOS

A.1 Supplementary Video 2.1

A video file named SupplementaryVideo2.1.mp4 demonstrates the passive linear skin stretch device and experiments described in Chapter 2.

A.2 Supplementary Video 3.1

A video file named SupplementaryVideo3.1.mp4 demonstrates control of a robot arm using the epidermal stimulation and sensing platform described in Chapter 3.

A.3 Supplementary Video 4.1

A video file named SupplementaryVideo4.1.mp4 shows a subject with a transradial amputation use the low-cost, open-source, compliant prosthetic hand described in Chapter 4.

A.4 Supplementary Video 6.1

A video file named SupplementaryVideo6.1.mp4 shows a subject with a transaradial amputation perform activities of daily living with and without the use of the electrotactile sensation intensity controller described in Chapter 6.

A.5 Supplementary Video 6.2

A video file named SupplementaryVideo6.2.mp4 shows a subject with a transaradial amputation peel and reapply electrodes with and without the use of the electrotactile sensation intensity controller described in Chapter 6.

REFERENCES

[1] D. Atkins, D. Heard, and W. Donovan, "Epidemiologic overview of individuals with upper-limb loss and their reported research priorities," *J. Prosthet. Orthot.*, 1996.

[2] B. Peerdeman, D. Boere, H. Witteveen, R. H. in 't Veld, H. Hermens, S. Stramigioli, H. Rietman, P. Veltink, and S. Misra, "Myoelectric forearm prostheses: State of the art from a user-centered perspective." *J. Rehabil. Res. Dev.*, vol. 48, no. 6, 2011.

[3] K. Ziegler-Graham, E. J. MacKenzie, P. L. Ephraim, T. G. Travison, and R. Brookmeyer, "Estimating the prevalence of limb loss in the united states: 2005 to 2050," *Arch. Phys. Med. Rehabil.*, vol. 89, no. 3, pp. 422–429, 2008.

[4] A. Akhtar, M. Nguyen, L. Wan, B. Boyce, P. Slade, and T. Bretl, *Passive Mechanical Skin Stretch for Multiple Degree-of-Freedom Proprioception in a Hand Prosthesis*. Berlin, Heidelberg: Springer Berlin Heidelberg, 2014, pp. 120–128. [Online]. Available: http://dx.doi.org/10.1007/978-3-662-44196-1_16

[5] H. Witteveen, E. Droog, J. Rietman, and P. Veltink, "Vibro- and electrotactile user feedback on hand opening for myoelectric forearm prostheses," *IEEE Trans. Biomed. Eng.*, vol. 59, no. 8, pp. 2219–2226, 2012.

[6] J. Wheeler, K. Bark, J. Savall, and M. Cutkosky, "Investigation of rotational skin stretch for proprioceptive feedback with application to myoelectric systems," *IEEE Trans. Neural Syst. Rehabil. Eng.*, vol. 18, no. 1, pp. 58–66, 2010.

[7] T. A. Kuiken, G. Li, B. A. Lock, R. D. Lipschutz, L. A. Miller, K. A. Stubblefield, and K. B. Englehart, "Targeted muscle reinnervation for real-time myoelectric control of multifunction artificial arms," *J Am Med Assoc*, vol. 301, no. 6, pp. 619–628, 2009.

[8] A. Cheng, K. A. Nichols, H. M. Weeks, N. Gurari, and A. M. Okamura, "Conveying the configuration of a virtual human hand using vibrotactile feedback," in *IEEE HAPTICS 2012*. IEEE, 2012, pp. 155–162.

[9] A. Blank, A. M. Okamura, and K. J. Kuchenbecker, "Identifying the role of proprioception in upper-limb prosthesis control: Studies on targeted motion," *ACM Trans. Appl. Percept.*, vol. 7, no. 3, p. 15, 2010.

[10] J.-W. Jeong, W.-H. Yeo, A. Akhtar, J. J. Norton, Y.-J. Kwack, S. Li, S.-Y. Jung, Y. Su, W. Lee, J. Xia et al., "Materials and optimized designs for human-machine interfaces via epidermal electronics," *Adv Mater*, vol. 25, no. 47, pp. 6839–6846, 2013.

[11] G. Langevin, "InMoov - Open source 3D printed life size robot," pp. URL: http://robohand.net, License: http://creativecommons.org/licenses/by–nc/3.0/legalcode, 2014.

[12] M. C. Jimenez and J. A. Fishel, "Evaulation of force, vibration and thermal tactile feedback in prosthetic limbs," in *IEEE HAPTICS 2014*. IEEE, 2014, pp. 437–441.

[13] B. Xu, A. Akhtar, Y. Liu, H. Chen, W.-H. Yeo, S. I. Park, B. Boyce, H. Kim, J. Yu, H.-Y. Lai, S. Jung, Y. Zhou, J. Kim, S. Cho, Y. Huang, T. Bretl, and J. A. Rogers, "An epidermal stimulation and sensing platform for sensorimotor prosthetic control, management of lower back exertion, and electrical muscle activation," *Adv. Mater.*, 2015. [Online]. Available: http://dx.doi.org/10.1002/adma.201504155

[14] C. Ramanathan, R. N. Ghanem, P. Jia, K. Ryu, and Y. Rudy, "Noninvasive electrocardiographic imaging for cardiac electrophysiology and arrhythmia," *Nat. Med.*, vol. 10, no. 4, pp. 422–428, 2004.

[15] S. Xu, Y. Zhang, L. Jia, K. E. Mathewson, K.-I. Jang, J. Kim, H. Fu, X. Huang, P. Chava, R. Wang, S. Bhole, L. Wang, Y. J. Na, Y. Guan, M. Flavin, Z. Han, Y. Huang, and J. A. Rogers, "Soft microfluidic assemblies of sensors, circuits, and radios for the skin," *Science*, vol. 344, no. 6179, pp. 70–74, 2014. [Online]. Available: http://science.sciencemag.org/content/344/6179/70

[16] T. F. Budinger, "Biomonitoring with wireless communications," *Annu. Rev. Biomed. Eng.*, vol. 5, no. 1, pp. 383–412, 2003.

[17] B. C. Tee, C. Wang, R. Allen, and Z. Bao, "An electrically and mechanically self-healing composite with pressure-and flexion-sensitive properties for electronic skin applications," *Nat. Nano.*, vol. 7, no. 12, pp. 825–832, 2012.

[18] M. A. Oskoei and H. Hu, "Myoelectric control systemsa survey," *Biomed. Sign. Proc. Control*, vol. 2, no. 4, pp. 275–294, 2007.

[19] D.-H. Kim, N. Lu, R. Ma, Y.-S. Kim, R.-H. Kim, S. Wang, J. Wu, S. M. Won, H. Tao, A. Islam, K. J. Yu, T.-i. Kim, R. Chowdhury, M. Ying, L. Xu, M. Li, H.-J. Chung, H. Keum, M. McCormick, P. Liu, Y.-W. Zhang, F. G. Omenetto, Y. Huang, T. Coleman, and J. A. Rogers, "Epidermal electronics," *Science*, vol. 333, no. 6044, pp. 838–843, 2011. [Online]. Available: http://science.sciencemag.org/content/333/6044/838

[20] D.-H. Kim, N. Lu, R. Ghaffari, Y.-S. Kim, S. P. Lee, L. Xu, J. Wu, R.-H. Kim, J. Song, Z. Liu, J. Viventi, B. de Graff, B. Elolampi, M. Mansour, M. J. Slepian, S. Hwang, J. D. Moss, S.-M. Won, Y. Huang, B. Litt, and J. A. Rogers, "Materials for multifunctional balloon catheters with capabilities in cardiac electrophysiological mapping and ablation therapy," *Nat. Mater.*, vol. 10, no. 4, pp. 316–323, 2011.

[21] D.-H. Kim, R. Ghaffari, N. Lu, S. Wang, S. P. Lee, H. Keum, R. DAngelo, L. Klinker, Y. Su, C. Lu, Y.-S. Kim, A. Ameen, Y. Li, Y. Zhang, B. de Graff, Y.-Y. Hsu, Z. Liu, J. Ruskin, L. Xu, C. Lu, F. G. Omenetto, Y. Huang, M. Mansour, M. J. Slepian, and J. A. Rogers, "Electronic sensor and actuator webs for large-area complex geometry cardiac mapping and therapy," *Proc. Natl. Acad. Sci. U.S.A.*, vol. 109, no. 49, pp. 19 910–19 915, 2012. [Online]. Available: http://www.pnas.org/content/109/49/19910.abstract

[22] M. Ramuz, B. C.-K. Tee, J. B.-H. Tok, and Z. Bao, "Transparent, optical, pressure-sensitive artificial skin for large-area stretchable electronics," *Adv. Mater.*, vol. 24, no. 24, pp. 3223–3227, 2012.

[23] D. Son, J. Lee, S. Qiao, R. Ghaffari, J. Kim, J. E. Lee, C. Song, S. J. Kim, D. J. Lee, S. W. Jun, S. Yang, M. Park, J. Shin, K. Do, M. Lee, K. Kang, C. S. Hwang, N. Lu, T. Hyeon, and D.-H. Kim, "Multifunctional wearable devices for diagnosis and therapy of movement disorders," *Nat. Nano.*, vol. 9, no. 5, pp. 397–404, 2014.

[24] G. S. Jeong, D.-H. Baek, H. C. Jung, J. H. Song, J. H. Moon, S. W. Hong, I. Y. Kim, and S.-H. Lee, "Solderable and electroplatable flexible electronic circuit on a porous stretchable elastomer," *Nat. Comm.*, vol. 3, p. 977, 2012.

[25] M. Kaltenbrunner, T. Sekitani, J. Reeder, T. Yokota, K. Kuribara, T. Tokuhara, M. Drack, R. Schwödiauer, I. Graz, S. Bauer-Gogonea, S. Bauer, and T. Someya, "An ultra-lightweight design for imperceptible plastic electronics," *Nature*, vol. 499, no. 7459, pp. 458–463, 2013.

[26] X. Huang, Y. Liu, H. Cheng, W.-J. Shin, J. A. Fan, Z. Liu, C.-J. Lu, G.-W. Kong, K. Chen, D. Patnaik, S.-H. Lee, S. Hage-Ali, Y. Huang, and J. A. Rogers, "Materials and designs for wireless epidermal sensors of hydration and strain," *Adv. Funct. Mater.*, vol. 24, no. 25, pp. 3846–3854, 2014. [Online]. Available: http://dx.doi.org/10.1002/adfm.201303886

[27] C. Pang, G.-Y. Lee, T.-i. Kim, S. M. Kim, H. N. Kim, S.-H. Ahn, and K.-Y. Suh, "A flexible and highly sensitive strain-gauge sensor using reversible interlocking of nanofibres," *Nat. Mater.*, vol. 11, no. 9, pp. 795–801, 2012.

[28] T. Yamada, Y. Hayamizu, Y. Yamamoto, Y. Yomogida, A. Izadi-Najafabadi, D. N. Futaba, and K. Hata, "A stretchable carbon nanotube strain sensor for human-motion detection," *Nat. Nano.*, vol. 6, no. 5, pp. 296–301, 2011.

[29] N. Lu, C. Lu, S. Yang, and J. Rogers, "Highly sensitive skin-mountable strain gauges based entirely on elastomers," *Adv. Funct. Mater.*, vol. 22, no. 19, pp. 4044–4050, 2012. [Online]. Available: http://dx.doi.org/10.1002/adfm.201200498

[30] C. Wang, D. Hwang, Z. Yu, K. Takei, J. Park, T. Chen, B. Ma, and A. Javey, "User-interactive electronic skin for instantaneous pressure visualization," *Nat. Mater.*, vol. 12, no. 10, pp. 899–904, 2013.

[31] D. J. Lipomi, M. Vosgueritchian, B. C. Tee, S. L. Hellstrom, J. A. Lee, C. H. Fox, and Z. Bao, "Skin-like pressure and strain sensors based on transparent elastic films of carbon nanotubes," *Nat. Nano.*, vol. 6, no. 12, pp. 788–792, 2011.

[32] R. C. Webb, A. P. Bonifas, A. Behnaz, Y. Zhang, K. J. Yu, H. Cheng, M. Shi, Z. Bian, Z. Liu, Y.-S. Kim, W.-H. Yeo, J. S. Park, J. Song, Y. Li, Y. Huang, A. M. Gorbach, and J. A. Rogers, "Ultrathin conformal devices for precise and continuous thermal characterization of human skin," *Nat. Mater.*, vol. 12, no. 10, pp. 938–944, 2013.

[33] M. Ying, A. P. Bonifas, N. Lu, Y. Su, R. Li, H. Cheng, A. Ameen, Y. Huang, and J. A. Rogers, "Silicon nanomembranes for fingertip electronics," *Nanotechnology*, vol. 23, no. 34, p. 344004, 2012.

[34] C. Frigo, M. Ferrarin, W. Frasson, E. Pavan, and R. Thorsen, "Emg signals detection and processing for on-line control of functional electrical stimulation," *J. Electromyogr. Kinesiol.*, vol. 10, no. 5, pp. 351–360, 2000.

[35] Y. Gerasimenko, R. Gorodnichev, T. Moshonkina, D. Sayenko, P. Gad, and V. R. Edgerton, "Transcutaneous electrical spinal-cord stimulation in humans," *Ann. Phys. Rehabil. Med.*, vol. 58, no. 4, pp. 225–231, 2015.

[36] J. D. Loeser, R. G. Black, and A. Christman, "Relief of pain by transcutaneous stimulation," *J. Neurosurg.*, vol. 42, no. 3, pp. 308–314, 1975.

[37] C. Antfolk, M. DAlonzo, B. Rosén, G. Lundborg, F. Sebelius, and C. Cipriani, "Sensory feedback in upper limb prosthetics," *Expert Rev. Med. Devices*, vol. 10, no. 1, pp. 45–54, 2013.

[38] C. Cipriani, C. Antfolk, C. Balkenius, B. Rosn, G. Lundborg, M. C. Carrozza, and F. Sebelius, "A novel concept for a prosthetic hand with a bidirectional interface: A feasibility study," *IEEE Trans. Biomed. Eng.*, vol. 56, no. 11, pp. 2739–2743, Nov 2009.

[39] C. Antfolk, C. Balkenius, B. Rosén, G. Lundborg, and F. Sebelius, "Smarthand tactile display: a new concept for providing sensory feedback in hand prostheses," *J. Plast. Surg. Hand. Surg.*, vol. 44, no. 1, pp. 50–53, 2010.

[40] K. Kim, J. E. Colgate, J. J. Santos-Munn, A. Makhlin, and M. A. Peshkin, "On the design of miniature haptic devices for upper extremity prosthetics," *IEEE/ASME Trans. Mechatronics*, vol. 15, no. 1, pp. 27–39, Feb 2010.

[41] P. D. Marasco, A. E. Schultz, and T. A. Kuiken, "Sensory capacity of reinnervated skin after redirection of amputated upper limb nerves to the chest," *Brain*, p. awp082, 2009.

[42] K. Kaczmarek, J. Webster, P. Bach-y Rita, and W. J. Tompkins, "Electrotactile and vibrotactile displays for sensory substitution systems," *IEEE Trans. Biomed. Eng.*, vol. 38, no. 1, pp. 1–16, 1991.

[43] H. Kajimoto, M. Suzuki, and Y. Kanno, "Hamsatouch: Tactile vision substitution with smartphone and electro-tactile display," in *ACM CHI 2014*, ser. CHI EA '14. New York, NY, USA: ACM, 2014. [Online]. Available: http://doi.acm.org/10.1145/2559206.2581164 pp. 1273–1278.

[44] E. Langzam, E. Isakov, and J. Mizrahi, "Evaluation of methods for extraction of the volitional emg in dynamic hybrid muscle activation," *J. Neuroeng. Rehabil.*, vol. 3, no. 1, p. 1, 2006.

[45] A. J. Young, L. J. Hargrove, and T. A. Kuiken, "The effects of electrode size and orientation on the sensitivity of myoelectric pattern recognition systems to electrode shift," *IEEE Trans. Biomed. Eng.*, vol. 58, no. 9, pp. 2537–2544, 2011.

[46] R. A. Green, S. Baek, L. A. Poole-Warren, and P. J. Martens, "Conducting polymer-hydrogels for medical electrode applications," *Sci. Tech. Adv. Mater.*, vol. 11, no. 1, p. 014107, 2010. [Online]. Available: http://stacks.iop.org/1468-6996/11/i=1/a=014107

[47] W.-H. Yeo, Y.-S. Kim, J. Lee, A. Ameen, L. Shi, M. Li, S. Wang, R. Ma, S. H. Jin, Z. Kang, Y. Huang, and J. A. Rogers, "Multifunctional epidermal electronics printed directly onto the skin," *Advanced Materials*, vol. 25, no. 20, pp. 2773–2778, 2013. [Online]. Available: http://dx.doi.org/10.1002/adma.201204426

[48] L.-F. Wang, J.-Q. Liu, B. Yang, and C.-S. Yang, "Pdms-based low cost flexible dry electrode for long-term eeg measurement," *IEEE Sensors J.*, vol. 12, no. 9, pp. 2898–2904, 2012.

[49] T. Keller and A. Kuhn, "Electrodes for transcutaneous (surface) electrical stimulation," *J. Autom. Control*, vol. 18, pp. 35–45, 2008.

[50] T. A. Kuiken, P. D. Marasco, B. A. Lock, R. N. Harden, and J. P. Dewald, "Redirection of cutaneous sensation from the hand to the chest skin of human amputees with targeted reinnervation," *Proc. Natl. Acad. Sci. U.S.A.*, vol. 104, no. 50, pp. 20 061–20 066, 2007.

[51] P. Nohama, A. V. Lopes, and A. Cliquet, "Electrotactile stimulator for artificial proprioception," *Artif. Organs*, vol. 19, no. 3, pp. 225–230, 1995.

[52] A. Akhtar, B. Boyce, and T. Bretl, "The relationship between energy, phase charge, impedance, and perceived sensation in electrotactile stimulation," in *Proceedings of the IEEE Haptics Symposium (HAPTICS)*, Feb 2014, pp. 69–74.

[53] A. Akhtar, K. Y. Choi, M. Fatina, J. Cornman, E. Wu, J. Sombeck, C. Yim, P. Slade, J. Lee, J. Moore, D. Gonzales, A. Wu, G. Anderson, D. Rotter, C. Shin, and T. Bretl, "A low-cost, open-source, compliant hand for enabling sensorimotor control for people with transradial amputations," in *IEEE EMBC 2016*, 2016.

[54] P. Slade, A. Akhtar, M. Nguyen, and T. Bretl, "Tact: Design and performance of an open-source, affordable, myoelectric prosthetic hand," in *IEEE Int. Conf. Robot. Autom. (ICRA)*, May 2015, pp. 6451–6456.

[55] W. H. O., *World Report on Disability*. New York, NY: World Health Organization, 2011.

[56] D. Cummings, "Prosthetics in the developing world: a review of the literature," ser. 20. Prosthet. Orthot. Int, 1996, pp. 51–60.

[57] E. Scheme, B. Lock, L. Hargrove, W. Hill, U. Kuruganti, and K. Englehart, "Motion normalized proportional control for improved pattern recognition-based myoelectric control," *IEEE Trans. Neural Syst. Rehabil. Eng.*, vol. 22, no. 1, pp. 149–157, Jan 2014.

[58] Y. Tenzer, L. P. Jentoft, and R. D. Howe, "Inexpensive and easily customized tactile array sensors using MEMS barometers chips," *IEEE R&A Magazine*, 2012. [Online]. Available: http://biorobotics.harvard.edu/pubs/2012/journal/2012_YTenzer_BarometricSensors.pdf

[59] B. Matulevich, G. E. Loeb, and J. A. Fishel, "Utility of contact detection reflexes in prosthetic hand control," in *IEEE Int. Conf. Int. Robot. Sys. (IROS)*, Nov 2013, pp. 4741–4746.

[60] M. D'Alonzo, S. Dosen, C. Cipriani, and D. Farina, "Hyve: Hybrid vibro-electrotactile stimulation for sensory feedback and substitution in rehabilitation," *IEEE Trans. Neural Syst. Rehabil. Eng.*, vol. 22, no. 2, pp. 290–301, March 2014.

[61] P. D. Marasco, K. Kim, J. E. Colgate, M. A. Peshkin, and T. A. Kuiken, "Robotic touch shifts perception of embodiment to a prosthesis in targeted reinnervation amputees," *Brain*, vol. 134, no. 3, pp. 747–758, 2011.

[62] S. Tachi, K. Tanie, K. Komoriya, and M. Abe, "Electrocutaneous communication in a guide dog robot (MELDOG)," *IEEE Trans. Biomed. Eng.*, vol. 32, no. 7, pp. 461–469, 1985.

[63] M. Altinsoy and S. Merchel, "Electrotactile feedback for handheld devices with touch screen and simulation of roughness," *IEEE Trans. Haptics*, vol. 5, no. 1, pp. 6–13, 2012.

[64] M. Kitagawa, D. Dokko, A. M. Okamura, and D. D. Yuh, "Effect of sensory substitution on suture-manipulation forces for robotic surgical systems," *J. Thorac. Cardiovasc. Surg.*, vol. 129, no. 1, pp. 151 – 158, 2005.

[65] C. Assambo, A. Baba, R. Dozio, and M. J. Burke, "Determination of the parameters of the skin-electrode impedance model for ECG measurement," in *Proceedings of the WSEAS International Conference on Electronics, Hardware, Wireless and Optical Communications*, 2007, pp. 90–95.

[66] H. Kajimoto, "Electrotactile display with real-time impedance feedback using pulse width modulation," *IEEE Trans. Haptics*, vol. 5, no. 2, pp. 184–188, 2012.

[67] A. Boxtel, "Skin resistance during square-wave electrical pulses of 1 to 10 mA," *Med. Biol. Eng. Comput.*, vol. 15, no. 6, pp. 679–687, 1977.

[68] G. Kantor, G. Alon, and H. S. Ho, "The effects of selected stimulus waveforms on pulse and phase characteristics at sensory and motor thresholds," *Phys. Ther.*, vol. 74, no. 10, pp. 951–962, 1994.

[69] B. R. Bowman and L. L. Baker, "Effects of waveform parameters on comfort during transcutaneous neuromuscular electrical stimulation," *Ann. Biomed. Eng.*, vol. 13, no. 1, pp. 59–74, 1985.

[70] R. Mann and S. Reimers, "Kinesthetic sensing for the EMG controlled "Boston Arm"," *IEEE Trans. Man-Mach. Syst.*, vol. 11, no. 1, pp. 110–115, 1970.

[71] A. Israr and I. Poupyrev, "Tactile brush: drawing on skin with a tactile grid display," in *Proceedings of the ACM SIGCHI Conference on Human Factors in Computing Systems*, 2011, pp. 2019–2028.

[72] M. Seps, K. Dermitzakis, and A. Hernandez-Arieta, "Study on lower back electrotactile stimulation characteristics for prosthetic sensory feedback," in *Proceedings of the IEEE/RSJ International Conference on Intelligent Robots and Systems (IROS)*, 2011, pp. 3454–3459.

[73] E. A. Pfeiffer, "Electrical stimulation of sensory nerves with skin electrodes for research, diagnosis, communication and behavioral conditioning: A survey," *Med. Biol. Eng.*, vol. 6, no. 6, pp. 637–651, 1968.